

**Universität  
Rostock**



Traditio et Innovatio

# **Environmentally friendly process for recovering cellulose from rice straw and for producing regenerated cellulose films**

## **Dissertation**

to obtain the academic degree

„*doctor rerum naturalium*“ (*Dr. rer. nat.*)

submitted at the

Faculty of Mathematics and Natural Sciences

University of Rostock

by

MSc. Nguyen Ngoc Mai

born on November 23<sup>rd</sup>, 1985 in Hanoi, Vietnam

**Rostock, July 2020**



Dieses Werk ist lizenziert unter einer  
Creative Commons Namensnennung 4.0 International Lizenz.

**Referees:**

1<sup>st</sup> Referee:

**Prof. Dr. Udo Kragl**

University of Rostock

Institute of Chemistry

Department of Analytical and Technical Chemistry

Albert-Einstein-Str. 3a

D-18059 Rostock, Germany

2<sup>nd</sup> Referee:

**Prof. Masahiro Yoshizawa-Fujita**

Sophia University

Department of Materials and Life Sciences

7-1 Kioi-cho, Chiyoda-ku

Tokyo 102-8554, Japan

Thesis submission:

20 July 2020

PhD Defense:

10 November 2020

The present work was conducted during the period from January 2018 until July 2020 under the supervision of Prof. Dr. Udo Kragl and Dr. Dirk Hollmann in the Institute of Chemistry at the University of Rostock.

## ACKNOWLEDGEMENTS

My PhD research would not be possible without the guidance, support and generous contribution of many. It is a pleasure to thank those who made this possible.

Firstly, I would like to thank my supervisor, Dr. Dirk Hollmann, for his tireless guidance, support and encouragement during my PhD research. It was a wonderful experience to work and learn from him. He inspired me to do scientific research, something I have never dreamed of in Vietnam. He has made a great time in my life.

I wish to thank my co-supervisor, Prof. Dr. Udo Kragl for giving me the opportunity to work in his research group as well as his suggestion, valuable discussions and comments.

Special thanks go to Dr. Michalik, Mrs. Borgwaldt, Prof. Ludwig, Dr. Lund, Dr. Barke, Mrs. Lange, Dr. Frank, Dr. Springer, Msc. Aladin, Prof. Corzilius, Dr. Nareyka and Dr. Rebl for analytical support; Dr. Oppermann and Dr. Mejia for discussion; Peter Kumm and Thomas Kröger-Badge for technical support.

I would like express gratitude to my present and former colleagues in Technische Chemie group at the Institute of Chemistry who were always there to advise me and support me, kind friendship.

I would like thanks to RoHan project for the sponsorship during my PhD studies. Hanoi university of Science and Technology is also appreciated for the support and permission to attend this doctoral program.

In Vietnam, I want to thank all my colleagues at the Department of Chemical Process Equipment, School of Chemical Engineering, Hanoi University of Science and Technology, especially, Assoc. Prof. Vu Dinh Tien for their support.

Thank my dear friends from Vietnam and Bangladesh for sharing of wonderful and precious moments. I have been very happy to meet you.

Foremost, I owe thanks from bottom of my heart to my family for their unconditional love and unlimited patience from the very beginning. Words cannot express how grateful I am to my beloved husband and our lovely daughter for their love, understanding and emotional support throughout my study for 3 years. I would not be able to achieve this without them.



---

List of Symbols and Abbreviations.....	III
List of Figures, Tables and Schemes.....	IV
ABSTRACT.....	IX
Zusammenfassung.....	X
<b>1. INTRODUCTION</b> .....	<b>1</b>
1.1 Green chemistry.....	1
1.2 Utilization of renewable raw materials .....	2
1.2.1 Raw biomass materials .....	2
1.2.2 Rice straw management in Vietnam .....	5
1.3 Composition of biomass .....	6
1.4 Cellulose and its application.....	7
1.5 Cellulose dissolution .....	10
1.5.1 Solvents.....	10
1.5.2 Electrolyte solutions.....	14
<b>2. RESEARCH OBJECTIVES</b> .....	<b>17</b>
<b>3. RESULTS AND DISCUSSION</b> .....	<b>19</b>
3.1 Selective isolation of cellulose from rice straw .....	19
3.1.1 A schematic diagram of cellulose isolation from rice straw .....	20
3.1.2 Structural characteristics and chemical composition of extracted cellulose .....	23
3.2 Dissolution of cellulose and the effect of additives .....	27
3.2.1 Dissolution of cellulose using TBPH with different solvents .....	27
3.2.2 Proposed dissolution mechanism with TBPH .....	34
3.3 MDCell methodology for the preparation of the regenerated cellulose films.....	38
3.3.1 Introduction of MDCell methodology.....	38
3.3.2 Investigation of the coagulation mechanism .....	39
3.3.3 Production of RC powder and films .....	47
3.3.3.1 Structural and chemical characterization of RC powder.....	47
3.3.3.2 Production, characterization and properties of RC films from microcrystalline cellulose.....	51
3.3.3.3 Application of the RS films as separation media .....	68
3.3.3.4 Production and characterization of RC films from extracted cellulose.....	73

3.3.4 Recycling of TBPH and PC.....	78
<b>4. SUMMARY AND OUTLOOK.....</b>	<b>81</b>
4.1 Summary.....	81
4.2 Outlook.....	82
<b>5. MATERIALS AND METHODS.....</b>	<b>85</b>
5.1 Materials.....	85
5.2 Preparation methods.....	85
5.2.1 Grinding rice straw to powder.....	85
5.2.2 Cellulose isolation from rice straw.....	85
5.2.3 Dissolution of cellulose in TBPH 50 wt.%.....	86
5.2.4 The viscosity of cellulose solution.....	86
5.2.5 Producing regenerated cellulose films from microcrystalline cellulose and extracted cellulose.....	88
5.2.6 Water flux.....	88
5.2.7 Determination of pore size distribution.....	88
5.2.8 Preparation of dyes solution.....	89
5.2.9 Online UV-Vis measurement with continues flow.....	89
5.2.10 Adsorption experiment.....	89
5.3 Characterization methods.....	90
<b>6. REFERENCES.....</b>	<b>95</b>
<b>7. APPENDIX.....</b>	<b>101</b>

### List of Symbols and Abbreviations

Ace	Acetone	MeCN	Acetone nitrile
AFM	Atomic force microscopy	MG	Malachite Green
AGU	Anhydroglucose unit	MO	Methylene orange
[AMIM][Cl]	1-allyl-3-methylimidazolium chloride	MWCO	Molecular weight cut-off
BC	Butylene carbonate	NMMO	N-methyl morpholine-N-oxide
[BMIM][Ac]	1-butyl-3-methylimidazolium acetate	NMR	Nuclear magnetic resonance
[BMIM][Cl]	1-butyl-3-methylimidazolium acetate	PC	Propylene carbonate
COSY	Homonuclear correlation spectroscopy	PEG	Polyethylene glycol
CR	Cresol red	PEO	Polyethylene oxide
CP	Cross polarization	PG	Propylene glycol
DEPT	Distortionless enhancement by polarization transfer	PMR	Photocatalytic membrane reactor
DMAc	Dimethylacetamide	ppm	Parts per million
DMSO	Dimethyl sulfoxide	RC	Regenerated cellulose
DNP	Dynamic nuclear polarization	RS	Rice straw
DP	Degree of polymerization	RT	Room temperature
EA	Ethyl acetate	SEM	Scanning electron microscopy
EC	Ethylene carbonate	SS	Solid state
[EMIM][Ac]	1-ethyl-3-methylimidazolium acetate	TB	Thymol blue
EtOH	Ethanol	TBAF	Tetrabutylammonium fluoride
ExtractC	Extracted cellulose	TBAH	Tetrabutylammonium hydroxide
EY	Eosin Y disodium salt	TBPH	Tetrabutylphosphonium hydroxide
FT-IR	Fourier transform infrared spectroscopy	TEM	Transmission electron microscopy
HC	Hydrogen carbonate	TGA	Thermogravimetric analysis
HMBC	Heteronuclear multiple bond coherence	THF	Tetrahydrofuran
HPLC	High performance liquid chromatography	UV	Ultra-Violet (Spectroscopy)
HSQC	Heteronuclear single quantum coherence	Vis	Visible
LS	Liquid state	VEC	Vinyl ethylene carbonate
MB	Methylene blue	wt. %	Weight percentage
MCC	Microcrystalline cellulose	XRD	X-ray diffraction

**List of Figures**

Figure 1. Management of rice straw in Vietnam .....	6
Figure 2. Chemical composition of rice straw .....	6
Figure 3. Cellulose structure .....	8
Figure 4. Intermolecular and intramolecular hydrogen bond in cellulose chains .....	8
Figure 5. The transformation of cellulose polymorphs.....	9
Figure 6. Supramolecular distinction between cellulose I and cellulose II based on inter- and intramolecular hydrogen bonds.....	9
Figure 7. Classification of cellulose solvents .....	11
Figure 8. Structure of cellulose xanthate and cellulose carbamate .....	12
Figure 9. Structure of non-derivatizing solvents .....	13
Figure 10. Structure of some ionic liquids .....	13
Figure 11. Structure of quaternary ammonium and phosphonium solvents .....	13
Figure 12. Selective isolation cellulose from rice straw .....	19
Figure 13. A schematic diagram of lignocellulosic compound extraction.....	20
Figure 14. Grinding rice straw in the ball mill with different conditions .....	21
Figure 15. Rice straw solution, supernatant and pellet.....	22
Figure 16. Isolation of cellulose from rice straw .....	23
Figure 17. LS- <sup>13</sup> C NMR spectra of supernatant before addition of water, extracted cellulose in TBPH 50 wt.% and remaining supernatant .....	23
Figure 18. SS- <sup>13</sup> C NMR (A) between rice straw powder and extracted cellulose; (B) between commercially available microcrystalline cellulose and extracted cellulose .....	24
Figure 19. FT-IR spectra of rice straw, extracted cellulose and microcrystalline cellulose ....	25
Figure 20. XRD patterns of rice straw, extracted cellulose and microcrystalline cellulose.....	26
Figure 21. Different amount of cellulose dissolved in TBPH 50 wt.%. .....	28
Figure 22. <sup>13</sup> C NMR spectra of different cellulose concentration in TBPH 50 wt.% .....	28
Figure 23. The viscosity of cellulose/TBPH solution depending on the molar ratio of additives and TBPH .....	30
Figure 24. The viscosity of cellulose/TBPH solution in terms of TBPH concentration after addition of solvents calculated from Figure 23 .....	31
Figure 25. TBPH/cellulose/solvents mixtures with molar ratio 4:1 between solvents and TBPH .....	31
Figure 26. a) Dissolution of 20 wt.% cellulose with TBPH 50 wt.% and then addition of water to decrease the concentration of TBPH 50 wt.% to 40 wt.%; b) Direct addition of 0.5 wt.% cellulose in TBPH 40 wt.% .....	32
Figure 27. Viscosity of the cellulose/TBPH solution as function of the cellulose concentration at different molar ratios of DMSO and H <sub>2</sub> O .....	32
Figure 28. Addition of 8 wt.% cellulose to different TBPH/cellulose/solvent mixtures.....	33
Figure 29. The effect of additives on the viscosity and dissolution of cellulose in TBPH.....	37
Figure 30. Preparation of regenerated cellulose by the MDCell process.....	38

Figure 31. LS- <sup>13</sup> C NMR spectra of the <i>in-situ</i> reaction mixture after addition of PC to the TBPH/cellulose solution .....	40
Figure 32. <sup>1</sup> H, <sup>13</sup> C, and <sup>31</sup> P NMR spectra of PC, TBPH and the reaction mixture of both.....	41
Figure 33. <sup>13</sup> C NMR spectra of the reaction mixture of PC and TBPH .....	42
Figure 34. <sup>13</sup> C DEPT NMR spectra of the reaction mixture of PC and TBPH.....	42
Figure 35. Comparison <sup>13</sup> C and <sup>13</sup> C DEPT NMR spectra of the reaction mixture of PC and TBPH .....	43
Figure 36. <sup>1</sup> H- <sup>13</sup> C HSQC NMR spectra of the reaction mixture of PC and TBPH .....	43
Figure 37. <sup>1</sup> H- <sup>1</sup> H COSY NMR spectra of the reaction mixture of PC and TBPH .....	44
Figure 38. <sup>1</sup> H- <sup>13</sup> C HMBC NMR spectra of the reaction mixture of PC and TBPH.....	45
Figure 39. Proposed mechanism for the reaction between cellulose and PC .....	46
Figure 40. FT-IR spectra of the microcrystalline cellulose, RC powder, and PC .....	47
Figure 41. LS- <sup>13</sup> C NMR of cellulose and RC powder dissolved in TBPH 50 wt.%.....	48
Figure 42. XRD patterns of commercially available microcrystalline cellulose (cellulose I) and RC powder (mainly cellulose II) .....	49
Figure 43. FT-IR spectra and XRD patterns of RC powder with different kind of organic carbonate.....	50
Figure 44. FT-IR spectra of RC powder with (A) different amount of cellulose; (B) different ratio of PC; (C) different kind of cellulose material .....	51
Figure 45. Casting machine with casting knife .....	52
Figure 46. Optimal coagulation conditions to form the RC film .....	53
Figure 47. RC film 1 (without DMSO), left and RC film 2 (with DMSO), right .....	54
Figure 48. Characterization the films by IR spectroscopy and XRD .....	55
Figure 49. Thermal gravimetric analysis of RC films and microcrystalline cellulose.....	55
Figure 50. <sup>1</sup> H- <sup>13</sup> C Cross Polarization (CP) MAS NMR spectra under DNP at 110 K.....	56
Figure 51. DNP enhancement spectra of RC film 1 (A) and RC film 2 (B) .....	57
Figure 52. <sup>1</sup> H- <sup>13</sup> C Cross Polarization (CP) MAS NMR spectra of RC film 1 and RC film 2 in wet (A) and dried phase (B).....	57
Figure 53. LS- <sup>13</sup> C NMR spectra of the produced RC films 1 and 2 and commercially microcrystalline cellulose .....	58
Figure 54. Light microscopic image of a semithin cross section .....	59
Figure 55. TEM analysis with uncontrasted films .....	60
Figure 56. High resolution TEM of cellulose microfibrillary after contrasting of thin sections (approx. 50 nm) contrasted with uranyl acetate and lead citrate .....	60
Figure 57. SEM analysis of top and bottom surface of the air-dried and freeze-dried films...	61
Figure 58. SEM cross section image of RC films .....	62
Figure 59. SEM analysis layer of freeze-dried film 2 .....	62
Figure 60. AFM of casted and spin coated RC film 1 and 2 .....	63
Figure 61. Home-made filtration system .....	64
Figure 62. Water flux through RC films as a function of water pressure .....	65

---

Figure 63. Apparatus used to measure PEG concentration after going through RC films .....	66
Figure 64. PEG retention of the films at a PEG concentration 2000 ppm.....	66
Figure 65. The stability test of the RC films.....	67
Figure 66. Zeta potential of regenerated cellulose film 2.....	68
Figure 67. Online UV-Vis measurement system with continues flow.....	70
Figure 68. Online continuous flow UV-Vis spectroscopy for charged dyes .....	71
Figure 69. Adsorption efficiency of RC film 1 and 2 .....	72
Figure 70. The degradation of organic dyes under UV-Vis light .....	73
Figure 71. The regenerated cellulose films from extracted cellulose.....	74
Figure 72. Characterization of the RC films from extracted cellulose and microcrystalline cellulose.....	74
Figure 73. SS - <sup>13</sup> C NMR of the RC film from extracted cellulose and MCC .....	75
Figure 74. Purification of the extracted cellulose .....	76
Figure 75. SS- <sup>13</sup> C NMR of extracted cellulose and purified extracted cellulose .....	77
Figure 76. The RC films from purified extracted cellulose .....	77
Figure 77. SS- <sup>13</sup> C NMR of RC films from extracted cellulose and purified ExtractC .....	78
Figure 78. A proposed process scheme for solvent extraction to separate mixture of PC, PG and [TBP] <sup>+</sup> [HCO <sub>3</sub> ] <sup>-</sup> .....	79
Figure 79. Synthesize cellulose-photocatalyst composite films.....	83
Figure 80. Cellulose-photocatalyst films.....	83
Figure 81. Grinding rice straw by the planetary ball mill with different time .....	85
Figure 82. Tetrabutylphosphonium hydroxide 40 wt.% and 50 wt.% .....	86
Figure 83. Viscosity equipment Rheo Stress 1 Thermo Scientific Haake.....	87

**List of Tables**

Table 1. Major categories of biomass feedstock .....	2
Table 2. Advantages and disadvantages of common lignocellulosic biomass pre-treatment methods.....	4
Table 3. The relative crystallinity index of samples .....	27
Table 4. The viscosity of TBPH solutions with different concentration as well as of selected TBPH/cellulose solutions .....	29
Table 5. Addition of cellulose to different TBPH/Cellulose/co-solvent mixtures.....	33
Table 6. The difference amount of cellulose and PC to produce the RC films .....	52
Table 7. Molecular weight and solutions diameter of the polyethylene glycol series.....	65
Table 8. Schematic structural illustration of the six organic dyes with different charges .....	69
Table 9. pH of organic dye solutions.....	69

**List of Schemes**

Scheme 1. Dissolution 20 wt.% cellulose in TBPH 60 wt.%.....	15
Scheme 2. Illustration of dissolving cellulose in traditional TBAF/DMSO/water and TBPH/water solutions .....	35
Scheme 3. A proposed simplified dissolution mechanism of cellulose in TBPH and after addition of protic and aprotic solvents.....	36
Scheme 4. The reaction between TPBH and PC .....	45



## ABSTRACT

Plant biomass, an attractive raw material, contains a high proportion of cellulose. The environmentally friendly utilization of cellulose from biomass, especially rice straw, is a very important topic for thinking about how we can change our lives and processes in a sustainable way. Thus, the aim of my PhD research was to recover cellulose from rice straw and to produce regenerated cellulose films by an environmentally friendly process. An electrolyte solution of tetrabutylphosphonium hydroxide (TBPH) in water can dissolve easily more than 20 wt.% cellulose or biomass at room temperature. The impact of different co-solvents as well as common anti-solvents on the advanced dissolution in TBPH was investigated. These results, especially the reduction of viscosity to achieve good processability and further dissolution, are important information towards a utilization of TBPH even in an industrial way. A quantitative amount of cellulose (25.9 % - 30.7 % w/w dry rice straw) was easily recovered from rice straw by dissolving rice straw in TBPH 50 wt.% at room temperature, followed by precipitation in water within a short period of time without heating or cooling. In addition, a process was developed that considers exactly this: simple, fast, non-toxic, not harmful to the environment and the use of aqueous solvents. With the so-called MDCell process, non-transparent and transparent regenerated cellulose (RC) powder and films of high quality can be produced. These RC powder and films were fully characterized with respect to structure, surface morphology, permeation and selectivity. Furthermore, the application in separation processes was demonstrated. This is a future-oriented green alternative to known industrial processes.

## ZUSAMMENFASSUNG

Die Nutzung von nachwachsenden Rohstoffen insbesondere aber von Biomasseabfall, wie zum Beispiel Reisstroh, ist von hoher Relevanz für die Menschheit. Daher ist es von essentieller Bedeutung über unser Leben und, im chemischen Sinne, über nachhaltige Prozesse nachzudenken. Ziel meiner Doktorarbeit war die Gewinnung von Cellulose aus Reisstroh, die Verarbeitung der gewonnenen Cellulose in einem möglichst umweltfreundlichen Verfahren und der Anwendung des Produktes. Dies wurde realisiert in der Herstellung von regenerierter Cellulosefolien und Celluloseverbundstoffen. Grundlage der vorgestellten Forschung ist die Nutzung einer Elektrolytlösung von Tetrabutylphosphoniumhydroxid (TBPH) in Wasser, welche bei Raumtemperatur mehr als 20 Gew.-% Cellulose oder Biomasse in kürzester Zeit bei Raumtemperatur auflösen kann. Im ersten Schritt wird ein Verfahren basierend auf TBPH vorgestellt, welches die selektive und quantitative Isolierung von Cellulose aus Reisstroh ermöglicht. Die wiederholte Lösung in TBPH ermöglicht eine Aufreinigung aber auch eine Weiternutzung. Die Lösung von Cellulose in TBPH weist eine hohe Viskosität auf. Daher erfolgt ein umfangreiches Studium der Auswirkungen verschiedener Co-Lösungsmittel sowie gebräuchlicher Anti-Lösungsmittel auf die Flieseigenschaften der Cellulose-Lösung. Die Viskosität kann wesentlich reduziert werden, was relevant für eine weitere Verarbeitung ist. Dies wurde realisiert in einem neuartigen Verfahren zur Herstellung von regenerierter Cellulose, welches schnell, ungiftig, unschädlich für die Umwelt ist und wässrige Lösungsmittel nutzt. Mit dem so genannten MDCell-Verfahren können nicht-transparente und transparente Pulver und Folien von hoher Qualität hergestellt werden. Diese RC-Pulver und -Filme wurden hinsichtlich Struktur, Oberflächenmorphologie, Permeation und Selektivität vollständig charakterisiert. Darüber hinaus wurde die Anwendbarkeit in Trennprozessen demonstriert. Das MDCell Verfahren stellt damit eine zukunftsorientierte grüne Alternative zu bekannten industriell genutzten Verfahren dar.

## 1. INTRODUCTION

### 1.1 Green chemistry

Since the start of the industrial revolution, human beings have been burning huge amounts of fossil fuels to supply our ever-increasing demand for energy. It is mainly through this activity that humans have increased the concentration of carbon dioxide (CO<sub>2</sub>) in the atmosphere over 400 ppm (the highest level in over 800,000 years).<sup>[1]</sup> The use of fossil fuels, industrial processes, deforestation, agriculture and population growth has resulted in continuous climate changes as well as increased pollution all over our planet. Therefore, we must ask ourselves the question: how can we manage, how can we change, or better, how can we prevent this major challenge for future generations? Green chemistry is the key to reducing waste and improving sustainability.<sup>[2]</sup>

Green chemistry is the sustainable approach in chemical sciences that makes efficient use of renewable resources, minimizes waste and avoids the use of toxic and hazardous reagents and solvents in the production and application of chemical compounds. It applies to the entire life cycle of a chemical product, including development, manufacture, application and final disposal. Green chemistry is also known as sustainable chemistry and is generally based on the 12 principles proposed by Anastas and Warner.<sup>[3]</sup> Nowadays, these 12 principles of green chemistry are regarded to be the fundamentals that contribute to sustainable development. The principles include instructions for the implementation of new chemical products, novel syntheses and new techniques.<sup>[4]</sup>

Due to the use of petrochemicals, most pollution consists of non-degradable materials that take hundreds of years to decompose. The rapid depletion of fossil fuels predictably with the expected increase of world populations and expanding energy intensive economies on several continents as well as the large impact of non-degradable material on the human health and the environment are significant and present major challenges for our scientists and leaders in the next 50 years. Therefore, biomass and renewable raw materials must be used as alternatives to fossil resources for energy production as well as feedstocks for industrial chemistry.

Indeed, principle 7 of the 12 Principles of Green Chemistry does state that “a raw material or feedstock should be renewable rather than depleting wherever technically and economically practicable”.<sup>[3a]</sup> Thus, the development of materials based on water, carbon dioxide and biomass are of essential interest. Biomass is one of the few resources that has the potential to deal with the challenges of sustainable and green energy systems. Biomass is already a modification of water and carbon dioxide, produced by plants, consisting of cellulose, hemicellulose and lignin.<sup>[5]</sup> Every plant, every natural bio resource and, therefore also bio waste consist of these major class of components but in different ratios. A lot of microorganisms are able to utilize cellulose for nutrition. Fungi or bacteria can use enzymes or radical generation for the degradation of the cellulose chain. Implying this biodegradability and biocompatibility cellulose and its modifications and derivatives are intensively employed in numerous fields such as textile, packaging, paper manufacturing or environmental, filtration and medical applications.<sup>[6]</sup>

## 1.2 Utilization of renewable raw materials

### 1.2.1 Raw biomass materials

Plant biomass is an attractive raw material produced by plants during the photosynthesis cycle, which convert carbon dioxide and water into sugar. They store this energy in the form of glucose or starch molecules, cellulose and lignocellulose. Selected categories of potential biomass feedstocks are displayed in Table 1.<sup>[7]</sup>

**Table 1.** Major categories of biomass feedstock

No.	Major category	Biomass feedstock
1	Forest by-products	Wood chips, logging residues, trees, shrubs and wood residues, bark, etc.
2	Agricultural residues	Straw (rice, wheat, maize), rice husk, corn stover, etc.
3	Energy crops	Short-rotation woody crops, herbaceous woody crops, grasses, forage crops
4	Food crops	Residue from grains and oil crops
5	Sugar crops	Sugar cane, sugar beets, molasses, sorghum
6	Landfill	Municipal solid wastes
7	Algae, kelps, lichens and mosses	Water hyacinth, mushrooms, etc.
8	Aquatic plants	Algae, water weed, water hyacinth, rushes

The use of biomass sources is attracting scientists due to three main advantages. Firstly, biomass is a renewable resource that could be sustainably developed in the future. Secondly, it has properties friendly to the environment due to consisting of carbon-neutral, which can reduce greenhouse gas at a level depending on its displacement to the fossil fuels. Thirdly, it has considerable economic potential if fossil fuel prices increase significantly in the future. The great versatility of biomass as a raw material is reflected in the range of materials that can be converted into various solid, liquid and gaseous fuels using biological and thermochemical conversion processes.

Biomass materials can be used for producing a wide range of value products, including biofuels (ethanol, hydrogen, etc.), bioproducts products (sugar and sugar alcohols, etc.), and industrially important chemicals (e.g., solvents).<sup>[8]</sup> The main component in biomass can be separated by the pre-treatment method such as thermo-chemical (pyrolysis, gasification), physical-chemical (pressing/extraction, chemical conversion) and biochemical (aerobic fermentation, alcoholic fermentation) processes (Table 2).<sup>[9]</sup> It is an essential step to increase the target component accessibility. Each method offers several advantages or disadvantages for high yielding of a certain product.

**Table 2.** Advantages and disadvantages of common lignocellulosic biomass pre-treatment methods

Category	Commonly used pretreatment	Advantages	Disadvantages
<b>Physical</b>	Milling-Mechanical disruption	<ul style="list-style-type: none"> <li>These treatments increase the available specific surface area, and reduce both the degree of polymerization (DP) and cellulose crystallinity<sup>[10]</sup></li> </ul>	<ul style="list-style-type: none"> <li>The power requirement of mechanical comminution of agricultural materials depends on the final particle size and the waste biomass characteristics<sup>[11]</sup></li> </ul>
<b>Chemical</b>	Acid hydrolysis	<ul style="list-style-type: none"> <li>Short reaction and residence time</li> <li>A part of lignin and hemicellulose are removed<sup>[12]</sup></li> </ul>	<ul style="list-style-type: none"> <li>Corrosion to reaction container</li> <li>Formation of inhibitory sugars degradation by products</li> </ul>
	Alkaline hydrolysis	<ul style="list-style-type: none"> <li>Increases the internal surface area</li> <li>Decrease both the degree of polymerization and cellulose crystallinity<sup>[13]</sup></li> </ul>	<ul style="list-style-type: none"> <li>Less effective with high lignin content biomass<sup>[14]</sup></li> </ul>
	High temperature organic solvents	<ul style="list-style-type: none"> <li>Removal of lignin is enhanced</li> <li>Organic solvents can be recovered by distillation</li> <li>High selective pretreatment method yielding<sup>[15]</sup></li> </ul>	<ul style="list-style-type: none"> <li>Organic solvents recovery requires energy consumption</li> <li>Fire and explosion hazard</li> <li>The cost of chemicals is expensive</li> </ul>
<b>Physicochemical</b>	Ammonia fiber expansion	<ul style="list-style-type: none"> <li>Short reaction time (15 min)</li> <li>Lignin is dislocated from cell wall structure</li> <li>The ability to reduce, recover, and recycle the ammonia used<sup>[16]</sup></li> <li>Compatible with fermentation organisms without the need for conditioning<sup>[17]</sup></li> </ul>	<ul style="list-style-type: none"> <li>Requires ammonia recycling system</li> <li>Low digestibility is generally reported for hard woods</li> </ul>
	Steam explosion	<ul style="list-style-type: none"> <li>Requires low energy input with no recycling or environmental cost<sup>[18]</sup></li> </ul>	<ul style="list-style-type: none"> <li>Incomplete destruction of lignin-carbohydrate matrix</li> </ul>
<b>Biological</b>	White rot and soft rot fungi	<ul style="list-style-type: none"> <li>Organisms will degrade lignin</li> <li>Energy requirement is low</li> <li>Mild reaction conditions</li> </ul>	<ul style="list-style-type: none"> <li>The slow rate of biological pretreatment for industrial purposes (10 to 14 days)<sup>[19]</sup></li> <li>The requirement of careful growth conditions<sup>[19]</sup></li> </ul>

Agricultural biomass wastes or residues are mainly cereal crops (rice straw), leaves, roots, husk, fruit peels and seed/nut shells which have a potential valuable supply of source material. In developing countries, especially in Vietnam, most biomass residues usually are burned or left in the field to decompose naturally. However, crop residues composition consists of cellulose, hemicellulose and lignin, which can be used to produce chemicals, resins and enzymes. Finding out an efficient process to recover carbohydrate from crop residues will have an impact on most of the Sustainable Development Goals.

### **1.2.2 Rice straw management in Vietnam**

Vietnam is the world's fifth-largest rice producer all over the world, meaning that it has a large amount of rice straw (RS).<sup>[20]</sup> Twenty years ago, Vietnamese farmers preferred to collect rice straw for animal feed and as a fuel for cooking. However, due to the increasing mechanization, the development of industrial cattle feed and the use of gas ovens, most modern farmers directly burn rice straw on the land. The latest research shows that in agricultural areas, 30 - 40 % of rice straw is burnt in the field, the proportion in suburban areas is 60 - 70 %.<sup>[21]</sup> Burning rice straw can make the soil harder and drier on the surface. The process of burning rice straw also emits a large amount of CO<sub>2</sub> along with CO, CH<sub>4</sub>, NO<sub>2</sub>, SO<sub>2</sub>, ... all these gases are very harmful to human health and cause environmental pollution, destroy public buildings and limit visibility. It especially causes an imbalance in the field ecosystem and increase greenhouse gas emissions.<sup>[22]</sup> Moreover, rice straw is a huge source of organic matter, which accounts for up to 80 % of the weight of rice plant, each hectare of rice cultivation contains 10 - 12 tons of straw. Therefore, it is highly necessary to avoid burning rice straw and to use it as a valuable source.

Nowadays, with the development of the technologies for collection and utilization, rice straw is increasingly removed from the fields to be used for better purposes. It can be utilized as cultivation substrate such as mushrooms,<sup>[23]</sup> for cattle feed,<sup>[24]</sup> compost,<sup>[25]</sup> and energy production<sup>[26]</sup> (Figure 1).

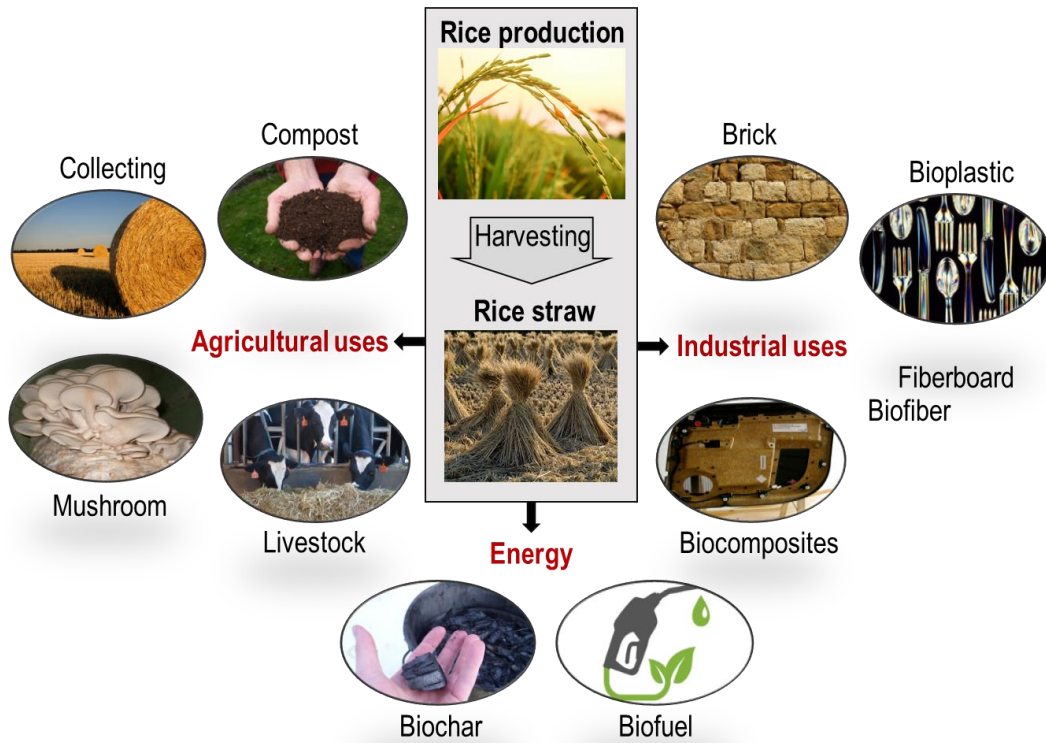


**Figure 1.** Management of rice straw in Vietnam (The composition pictures were downloaded from Pixabay, Pxfuel, Flickr and Wikimedia Commons)

Besides, rice straw also can be applied to produce high-end materials such as bioplastics, biofibers, and biocomposites. Thus, sustainable rice straw management is the key to avoid the negative effects to the environment and human health.

### 1.3 Composition of biomass

The general chemical composition of biomass can be characterized by five primary components: cellulose, hemicellulose, lignin, extractable compound and ash.<sup>[5]</sup>

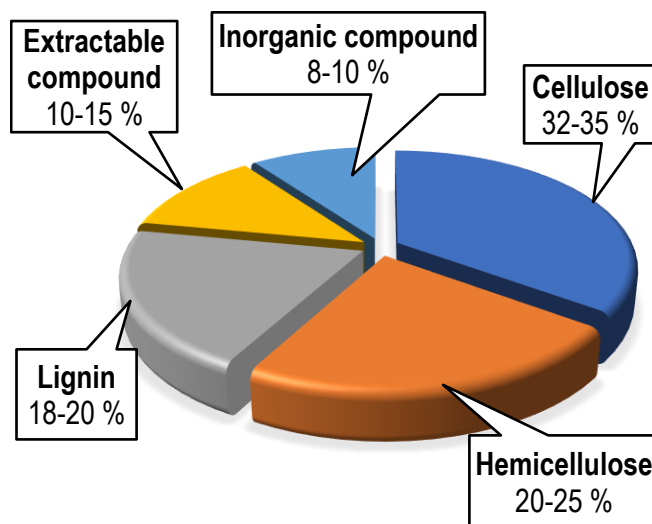


**Figure 2.** Chemical composition of rice straw

As seen in Figure 2, the major component in rice straw is cellulose. It is, by the way, the most abundant biopolymer on earth and consists of polysaccharide based on glucose monomers held together by  $\beta$  (1 $\rightarrow$ 4) links.<sup>[27]</sup>

The second main component of biomass, hemicellulose, is an amorphous polymer, whose major component is a xylose monomer unit heteropolymer. Because of its amorphous structure, hemicellulose is much more hydrolysis tolerant than crystalline cellulose.<sup>[28]</sup>

Lignin is a complex product of aromatic alcohols and is intertwined with cellulose and hemicellulose fraction of the biomass structure. This interlacing of lignin helps to provide rigidity to lignocellulosic materials such as trees. The lignin fraction consists of phenol-based molecules that act like an adhesive to hold the cellulose fibres together.<sup>[29]</sup>

Cellulose and hemicellulose together with lignin account for 80 % of lignocellulosic biomass. The other smaller components of the biomass are extractable matters and ash. Although these components make up a smaller part of the biomass composition, they still have an impact on the optimal conversion process. Extractable compounds are soluble in solvents such as hot and cold water, ethers or methanol. Water-soluble compounds include non-structural sugars and proteins, and the ethanol-soluble components are typically represented by chlorophyll and waxes.<sup>[30]</sup>

Inorganic materials, often referred to as ashes, are usually available in small quantities and contain elements that are essential for plant growth, such as calcium, potassium, silica...Rice straw has a high content of inorganic substances, ranging between 8 - 10 % w/w dry material. Several chemical analyzes of rice straw and rice husk from different rice varieties grown in Vietnam and other countries have confirmed the abundant presence of amorphous silica.<sup>[31]</sup>

#### **1.4 Cellulose and its application**

Cellulose is known as the largest source of biomass in the world, most of which is produced by plants. It is the major structural component in plant cells and tissues. Cellulose is a biosynthesized polymer in nature consisting of long chains of anhydroglucose units (AGU), each cellulose molecule having three hydroxyl groups per AGU except the end group<sup>[32]</sup> (Figure 3).

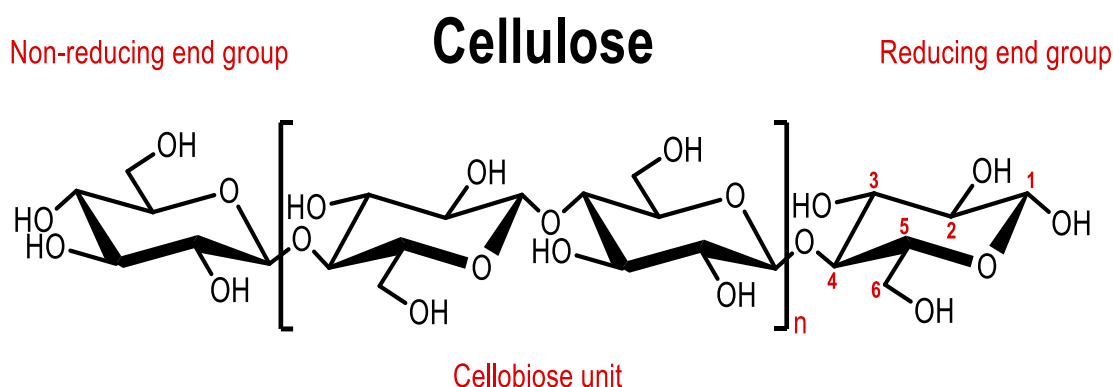


**Figure 3.** Cellulose structure

The size of the cellulose molecules can be defined by the average degree of polymerization. It may be stated that cellulose is a very insoluble substance with the following properties: insoluble in water and in typical organic solvents, partially soluble only in some solvents. The poor solubility can be explained by the strong intermolecular and intramolecular hydrogen bonds between the individual chains (Figure 4). Intermolecular hydrogen bond occurs between C3 and C6 OH in a laterally adjacent AGU within different chains. Intramolecular hydrogen bond normally occurs between C2 and C6 OH and C3 with oxygen hemiacetal on the same chain.<sup>[27]</sup> The presence of such a hydrogen bond network in cellulose results in rigid and stiff polymer chains. They are the reason for many observable physical properties such as solution viscosity, crystallinity, and the tendency to form fibrils, strands, and fibers.

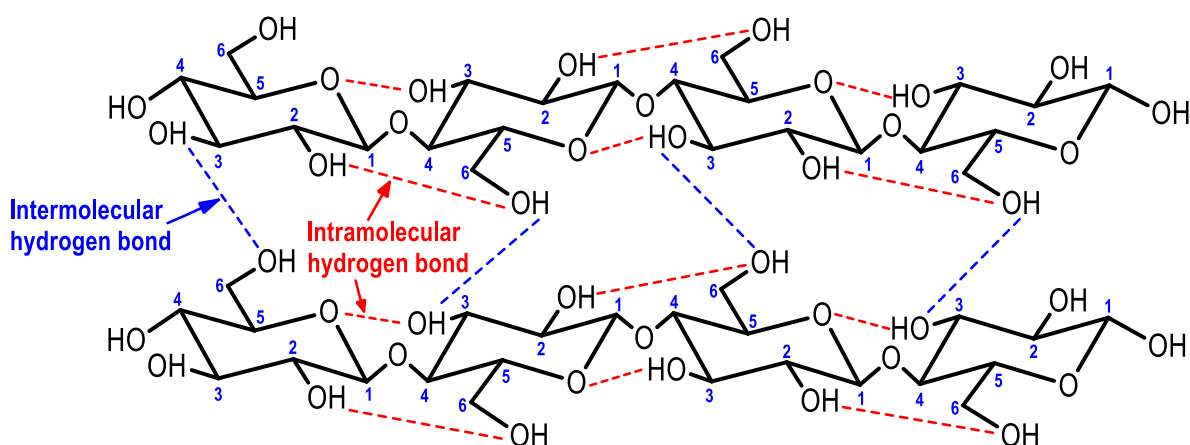


**Figure 4.** Intermolecular and intramolecular hydrogen bond in cellulose chains

Cellulose that is produced by plants is referred to as native cellulose, which is found in two crystalline forms,  $I_{\alpha}$  and  $I_{\beta}$ .<sup>[33]</sup> Native cellulose can be transformed into a new allomorph, namely cellulose II, by treatment in the alkaline solution.<sup>[34]</sup> Liquid ammonia treatment of cellulose I and cellulose II produces the crystalline form of cellulose III, and heating cellulose

III produces the crystalline form of cellulose IV.<sup>[35]</sup> Among the four different crystalline polymorphs, cellulose I is thermodynamically less stable while cellulose II is the most stable structure. Figure 5 shows the transformation of cellulose into its various polymorphs.

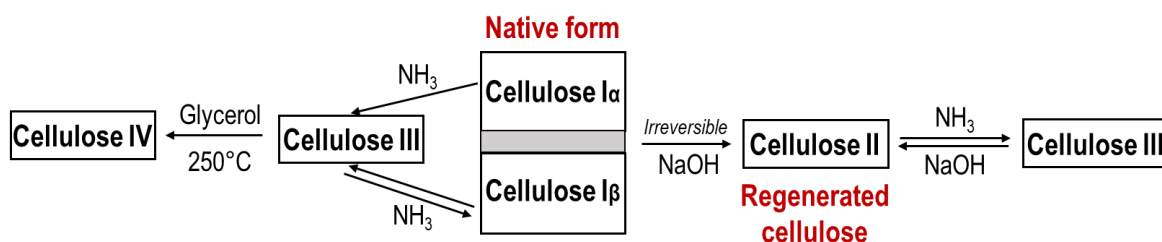


**Figure 5.** The transformation of cellulose polymorphs

Cellulose I and II differ in their inter- and intramolecular hydrogen bonds, which leads to different packings: parallel and antiparallel. Cellulose I is found in parallel arrangement of the cellulose chains but cellulose II arranged in antiparallel.<sup>[36]</sup> Cellulose I has C6-OH with C3-OH intermolecular hydrogen bonds whereas cellulose II has C2-OH with C6-OH intermolecular hydrogen bonds (Figure 6).<sup>[37]</sup>

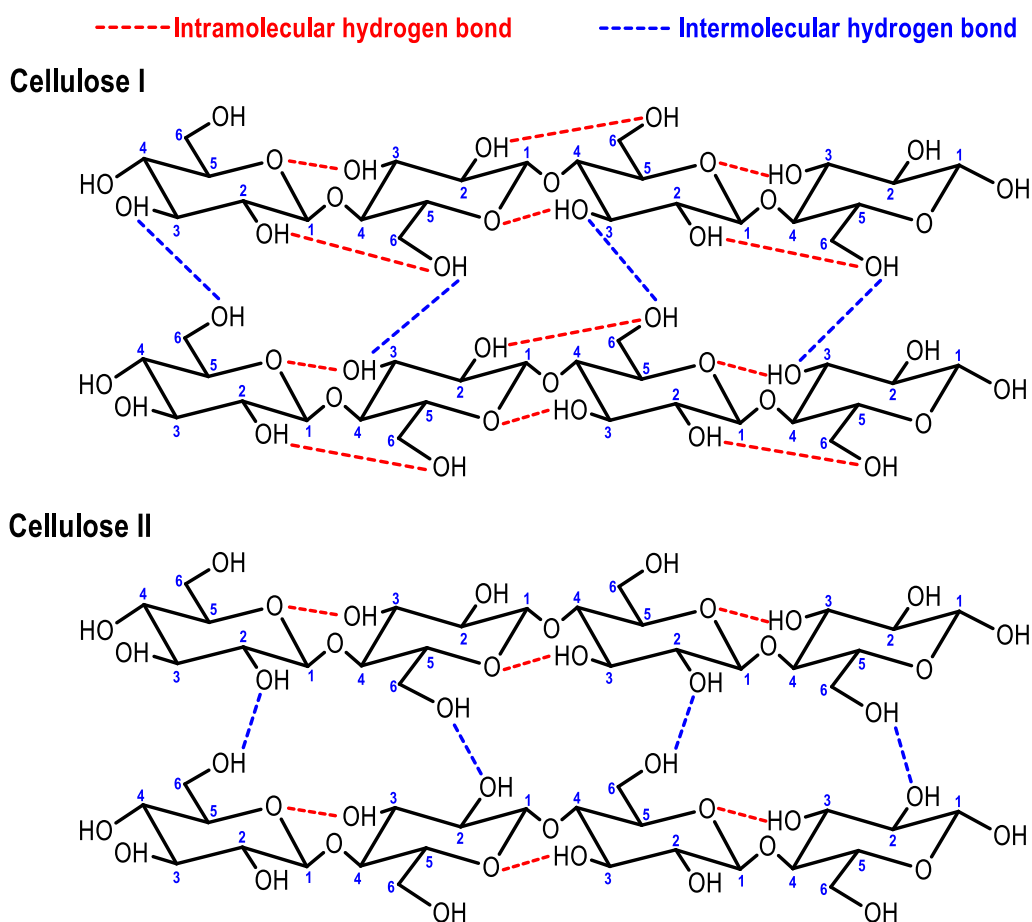


**Figure 6.** Supramolecular distinction between cellulose I and cellulose II based on inter- and intramolecular hydrogen bonds

Regenerated cellulose (cellulose II) is manufactured via the conversion of natural cellulose to a soluble cellulosic derivative and subsequent regeneration, typically forming either a fiber (via polymer spinning) or a film (via polymer casting).<sup>[38]</sup>

Cellulose and its chemical modifications are used in a wide range of applications:

- Cellulose is a main component of paperboard and paper products including new and advanced products with special properties, e.g. in the packaging industry.<sup>[39]</sup>
- Furthermore, cellulose is used in textile industry as main ingredient of textiles made from cotton, linen, and another plant fibers.<sup>[40]</sup>
- Cellulose ethers and cellulose esters are additives in pharmaceutical and cosmetic industries. They can be used as drug delivery systems by controlling the rate, time, and place of release of drugs,<sup>[41]</sup> extended and delayed release coated dosage forms, water conserving agent, osmotic, bio adhesives and mucoadhesive.<sup>[42]</sup>
- Science: Cellulose is employed in the laboratory as a stationary phase for thin layer chromatography.<sup>[43]</sup>
- Cellulose in filtration applications can greatly improve filtration performance.
- Cellulose composite materials are made of a polymer matrix and supporting fillers (often a fibrous material), resulting in materials with high strength and light weight. These properties enable composite materials to be used for a wide range of applications, such as in the construction or automotive industries. Nanofibers from cellulose have both high strength and stiffness, and have at the same time low weight, as well as the advantage of being renewable. This makes them interesting as reinforcing material in composites and this has been investigated extensively.<sup>[44]</sup>

## 1.5 Cellulose dissolution

### 1.5.1 Solvents

Nowadays, cellulose is employed in many applications. Nevertheless, in order to produce most of these end products, the cellulose needs to be dissolved. The dissolution is a very challenging process because cellulose presents one of the most insoluble substances. Most common solvents, including water cannot break the strong intramolecular and intermolecular hydrogen bonds. The research to develop the cellulose solvents has attracted much consideration of many scientists. In recent years, several suggestions have been made to

classify the cellulose solvents, displayed in Figure 7. They can be divided into two categories: derivatizing and non-derivatizing solvents.<sup>[45]</sup>

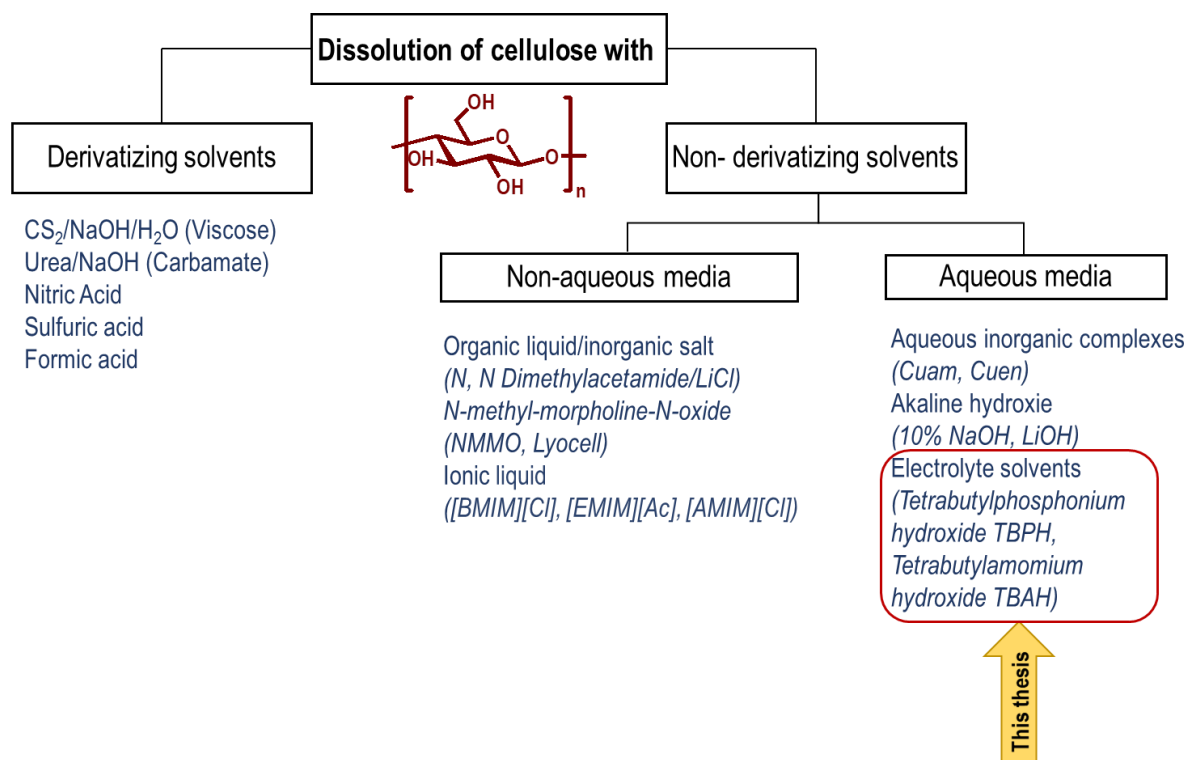
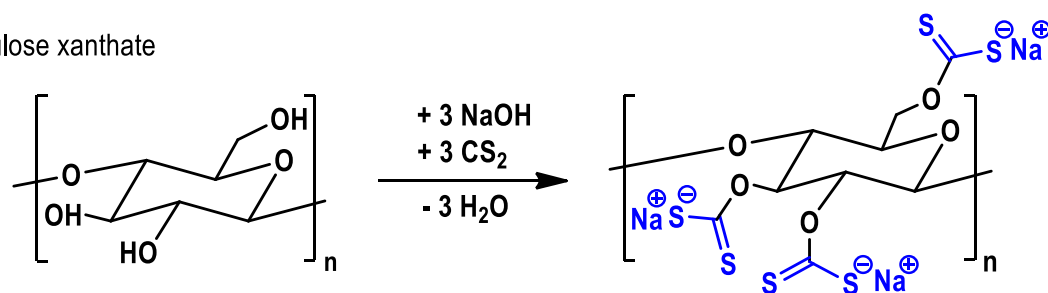


**Figure 7.** Classification of cellulose solvents

“Derivatizing” solvents include all systems involve the formation of water-soluble “unstable” ether, ester or acetal derivatives. “Non-derivatizing” solvents systems dissolve cellulose without change the modification.

The most prominent “derivatizing” method is the viscose process (cellulose xanthate in alkali solution).<sup>[46]</sup> Regenerated cellulose fibers are produced in large scale. An alternative to the viscose process is the formation of cellulose carbamate intermediate with urea, which is soluble in an aqueous sodium hydroxide solution.<sup>[47]</sup> Both processes require prior chemical modification of the macromolecule, which results in severe environmental pollution and poor health of the human body (Figure 8).

## A, Cellulose xanthate



## B, Cellulose carbamate

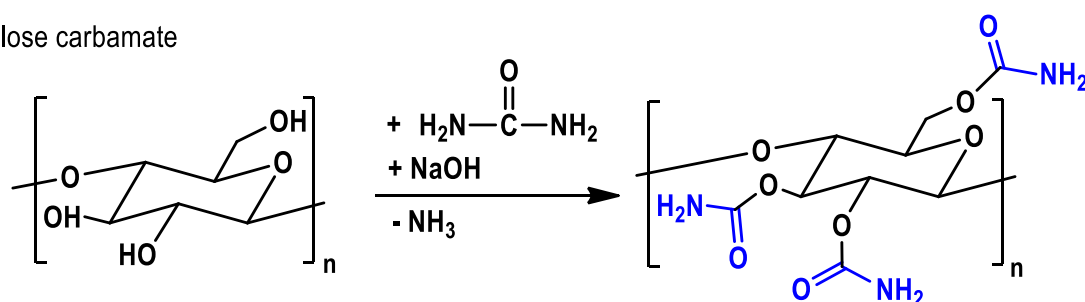


**Figure 8.** Structure of cellulose xanthate and cellulose carbamate

Thus, due to these drawbacks more acceptable non-derivatizing solvent systems have been developed. The best-known solvents are cuprammonium hydroxide [Cu(NH<sub>3</sub>)<sub>4</sub>](OH)<sub>2</sub> (Cuam) and cupriethylenediamine hydroxide [Cu(H<sub>2</sub>N(CH<sub>2</sub>)<sub>2</sub>NH<sub>2</sub>)<sub>2</sub>](OH)<sub>2</sub> (Cuen).<sup>[48]</sup> The regeneration of membranes from Cuam solution provides high quality membranes for hemodialysis.<sup>[49]</sup>

In addition, cellulose can be dissolved in approx. 10 % aqueous NaOH solution, however, the solubility is limited to cellulose of comparatively low degree of polymerization of up to 200.<sup>[50]</sup> Non-aqueous systems are also suitable for dissolving cellulose including N,N-dimethylacetamide/lithium chloride (DMAc/LiCl),<sup>[51]</sup> N-methyl-morpholine-N-oxide (NMMO, Lyocell Process) (Figure 9).<sup>[52]</sup> These “non-derivatizing” amide and amine solvents dissolve the cellulose without breaking any existing chemical bonds. Among these cellulose solvents, only NMMO is used on an industrial scale as a solvent for cellulose processing. However, NMMO also has some disadvantages, such as the occurrence of oxidative side reactions, thermal instability or quite high temperatures, which are necessary for the dissolution process. Most of the current systems have undesired properties, such as high toxicity, thermal instability, volatility, and high costs, thus, have initiated the search for alternative greener substitutes with increased impact on sustainability.

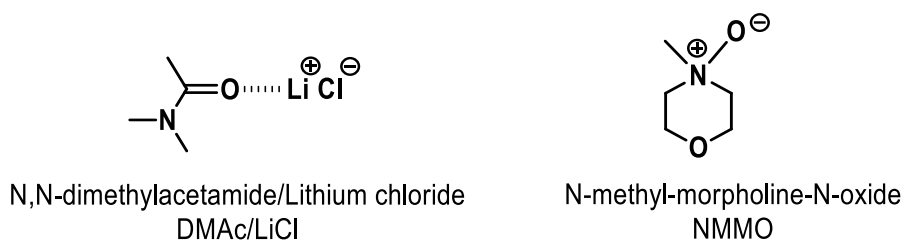


**Figure 9.** Structure of non-derivatizing solvents

In the last decades, ionic liquids (ILs) have been proven as promising solvents for cellulose (Figure 10). ILs have attracted significant attention due to their special physicochemical properties, low melting point, high thermal stability, low flammability and negligible vapor pressure.<sup>[53]</sup> The organic cation and an inorganic anion of the ILs can break the strong hydrogen bonds and, thus, facilitate the dissolution of cellulose.<sup>[54]</sup> In 2002, Swatloski et al. reported the efficient application of ILs based on 1-butyl-3-methylimidazolium cation.<sup>[55]</sup> Since then, a range of 1,3-dialkylimidazolium cations ILs has been demonstrated as effective cellulose solvents at elevated temperature.

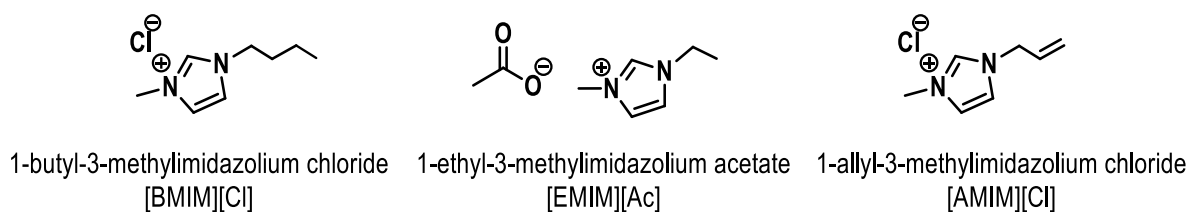


**Figure 10.** Structure of some ionic liquids

However, during and after the dissolution process no or only a low amount of water is tolerated. Compared to the imidazolium cation, quaternary ammonium<sup>[56]</sup> as well as phosphonium cations<sup>[57]</sup> have been recently employed as mild and highly efficient dissolution system e.g. tetrabutylphosphonium hydroxide (TBPH) and tetrabutylammonium hydroxide (TBAH) as shown in Figure 11.<sup>[58]</sup>

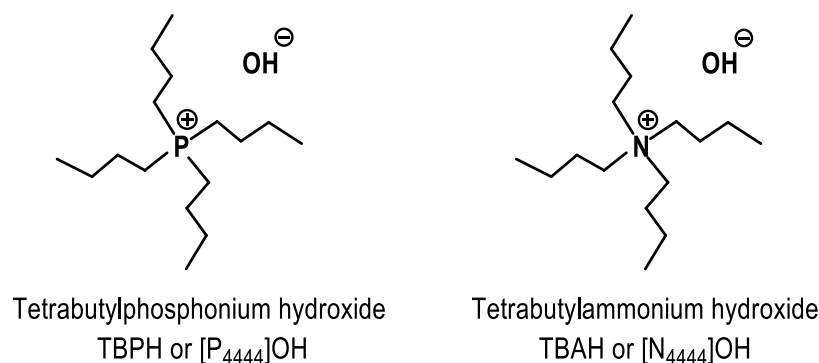


**Figure 11.** Structure of quaternary ammonium and phosphonium solvents

### 1.5.2 Electrolyte solutions

Although some polar ILs have been recognized as effective solvents for cellulose, they still have a serious problem as adding water significantly reduces the solubility of cellulose in the ILs. Since ILs highly absorb water from the atmosphere, drying processes of ILs under vacuum as well as manufacture under protective gases are required. It is therefore of great importance to develop alternative solvents capable of dissolving cellulose at room temperature even in the presence of water.

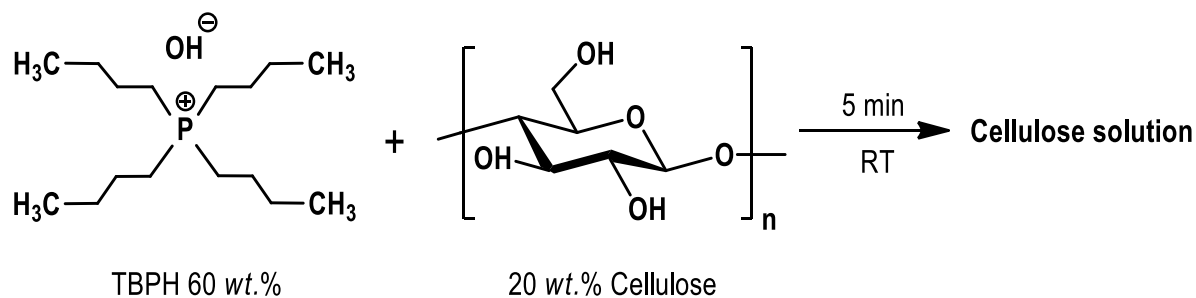
Tetraalkyl onium hydroxide aqueous has been a potential solvent for dissolution for many decades. It has been known at least since the 1930s that tetraalkylammonium hydroxide solutions can dissolve cellulose at room temperature if the water content falls below a certain value.<sup>[59]</sup> Tetraethylammonium hydroxide,  $[N_{2222}]OH$ , was first discovered in 1954 by Krässig<sup>[60]</sup> as a solvent for cellulose. In 1956, Strepikheev et al. deployed other ammonium hydroxide bases in aqueous solutions that dissolved relatively pure cellulose (DP = 860 with a 91.2 % content of  $\alpha$ -cellulose) namely dimethylphenylbenzylammonium hydroxide, triethylbenzylammonium hydroxide and triethylfurylammonium hydroxide.<sup>[61]</sup>

However, this was forgotten until Abe et al. (2012) demonstrated that both tetrabutylammonium hydroxide (TBAH) and tetrabutylphosphonium hydroxide (TBPH) 60 wt.% in water can dissolve up to 20 wt.% cellulose at room temperature.<sup>[58]</sup> After that, Ema et al. (2014) demonstrated that a 40 wt.% solution of tetrabutylammonium hydroxide in water with crown ether (18-crown-6) could also dissolve 10 wt.% cellulose at room temperature.<sup>[62]</sup> Wei et al. (2015) recently pointed out that lower temperatures (i.e. 16 °C) have a much more beneficial effect on cellulose dissolution than higher temperatures (i.e. 28 °C).<sup>[63]</sup>

Also, some recent reports showed that the biomass,<sup>[64]</sup> wheat straw,<sup>[65]</sup> and rice husks<sup>[46]</sup> can be simply and directly dissolved by quaternary ammonium hydroxide or quaternary phosphonium hydroxide indicating its great potential in applications of processing cellulose and related materials.

From this overview, therefore, the dissolution of cellulose is very important for further applications. In my PhD research, I focused on tetra-n-butylphosphonium hydroxide ( $[P_{4444}]OH$ , TBPH, an organic base) which can be regarded as a significantly 'greener' solvent system. Phosphonium salts have several advantages compare to ammonium salts in terms of

thermal and chemical stability.<sup>[66]</sup> As reported, it can dissolve a high amount of microcrystalline cellulose at room temperature<sup>[58]</sup> (Scheme 1).



**Scheme 1.** Dissolution 20 wt.% cellulose in TBPH 60 wt.%

In aqueous TBPH 50 wt.%, positive charged phosphonium cations  $[\text{TBP}]^+$  and hydroxide anions  $[\text{OH}]^-$  are present. The reason for the excellent dissolution behavior is still an open discussion. During the research, important factors are investigated and will be discussed in more detail (section 3.2.2).



## 2. RESEARCH OBJECTIVES

Green chemistry and sustainable processing have been paid attention to by scientists in many fields, in terms of reducing the consumption of depleting resources and protecting the environment. With the aim of developing chemistry towards sustainability, the study of the utilization of biomass such as rice straw is practical meaningful, especially for an agricultural country like Vietnam. Rice straw is a nutritious raw material with a high content of cellulose that has some advantages, such as renewability, biodegradability, and environmental friendliness.

At the beginning of my study, commercial microcrystalline cellulose was used to test its properties and applications. In order to modify the cellulose efficiently, cellulose needs to be dissolved. Cellulose solubility has been studied for a long time but keeps going to develop. Abe et al. (2012) reported that tetrabutylphosphonium hydroxide has superior properties which can dissolve a large amount of cellulose in a short time under mild conditions.<sup>[58]</sup> TBPH constitutes a non-toxic<sup>[67]</sup> and recyclable solvent that can tolerate even large amounts of water and other standard solvents<sup>[68]</sup> without losing dissolution capacity. Due to the investigation in the direct application and modification of cellulose, the resulting solution was found to be highly viscous. Stirring of the solution to improve the homogeneous environment was still difficult limiting the further processing and application. Therefore, it is necessary to reduce the viscosity of cellulose solution without changing its properties. The utilization of solvents can enable adjustment of the viscosity, by using high viscose to low viscose cellulose solution (presented in section 3.2). These are the studies shown in the first publication<sup>[68]</sup> (**Publication 1:** *“The Effect of Additives on the Viscosity and Dissolution of Cellulose in Tetrabutylphosphonium Hydroxide”*).

The search for non-toxic and renewable co-solvents to decrease the viscosity of the TBPH-cellulose solution and, thus, to increase the processability has been continued. Surprisingly, organic carbonates such as propylene carbonate - in principle formed by the reaction of CO<sub>2</sub> with diols or epoxides<sup>[69]</sup> - did not decrease the viscosity. Instead of dissolution, spontaneous solidification occurred within seconds. Thus, in two simple and fast steps, microcrystalline cellulose can be transformed into highly pure cellulose powders and films under mild conditions. This developed method (so called MDCell) was the subject of a **patent**

**application.**<sup>[70]</sup> This methodology is easy to handle, fast, without need for inert gas, feasible at room temperature and environmentally friendly. All chemicals are non-toxic and can be partially produced via utilization of CO<sub>2</sub> (organic carbonate) or are recyclable ([TBP]<sup>+</sup>). Water is tolerated in any step. The resulting cellulose films have excellent properties that can be applied in the filtration process. The RC films are stable in water and can be stored for several months. Recycling of the membrane can be done easily via another dissolution step in TBPH. The characterizations and properties of the films were clarified, as presented in section 3.3 and shown in the **publication 2** as well “*Coagulation using organic carbonates opens up a sustainable route towards regenerated cellulose films*” (Communications Chemistry).

During my recent research, I recognized the usage of some polar protic solvents results in a precipitation of cellulose. Interestingly, precipitation did not occur with hemicellulose and lignin in these solvents. Therefore, a simple, fast and selective method was proposed, using only one solvent (TBPH 50 wt.%) to dissolve rice straw, followed by easily precipitation in water (section 3.1). The cellulose obtained can be utilized again in the MDCell process to produce the regenerated cellulose films.

### 3. RESULTS AND DISCUSSION

#### 3.1 Selective isolation of cellulose from rice straw

Plant biomass (rice straw) has been recognized as a potential alternative for a sustainable, biodegradable and renewable resource. Finding out an efficient process to convert biomass into useful materials and products without generating pollutants will have an impact on most of the Sustainable Development Goals. In recent years, researchers have focused more on the separation of cellulose from plant biomass, which has a wide application in green chemistry. The isolation of cellulose can be achieved by various methods, which have some disadvantages in terms of final composition and structural characteristics as shown in Table 2 (section 1.2.1). During the investigations on the solubility of cellulose (section 3.2.1), it was found that after dissolving a large amount of cellulose into TBPH 50 wt.% at room temperature, if some polar solvents were added in the cellulose solution, cellulose will be precipitated easily. It was noteworthy that it did not happen with hemicellulose and lignin. Thus, a simple and easy isolation method of cellulose directly from rice straw is obtained (Figure 12). Indeed, this can enable a selective isolation cellulose from rice straw by dissolving in only one non-derivatizing electrolyte solvent TBPH 50 wt.% at room temperature. The extracted cellulose was separated out by adding rice straw solution in water. A quantitative amount of cellulose was recovered (25.9 % - 30.7 % w/w dry rice straw) within a short period of time without heating or cooling. The structure and chemical composition of extracted cellulose was investigated by using liquid state nuclear magnetic resonance (LS-NMR), Fourier transform infrared (FT-IR) spectroscopy, X-ray diffraction (XRD) and solid-state nuclear magnetic resonance spectroscopy (SS-NMR).

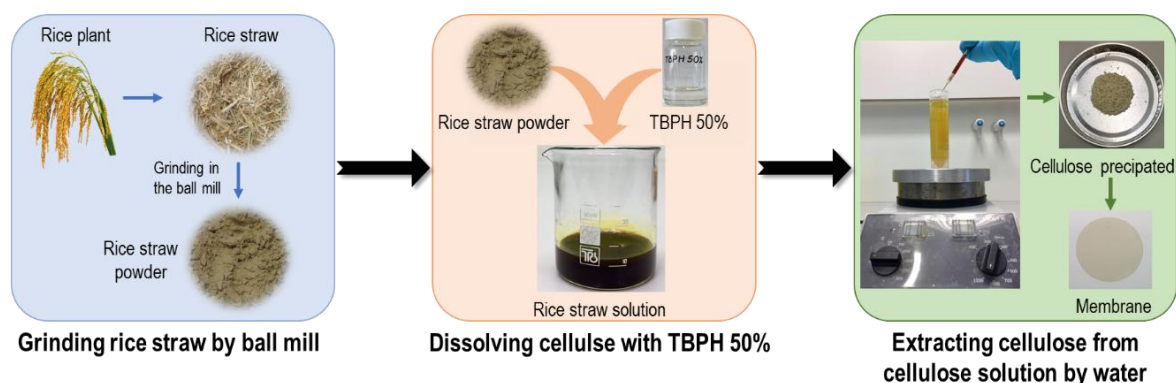


**Figure 12.** Selective isolation cellulose from rice straw

### 3.1.1 A schematic diagram of cellulose isolation from rice straw

The procedure for isolation of cellulose using electrolyte solution is illustrated in Figure 13 according to the following 3 steps: Grinding, dissolving, and extracting.

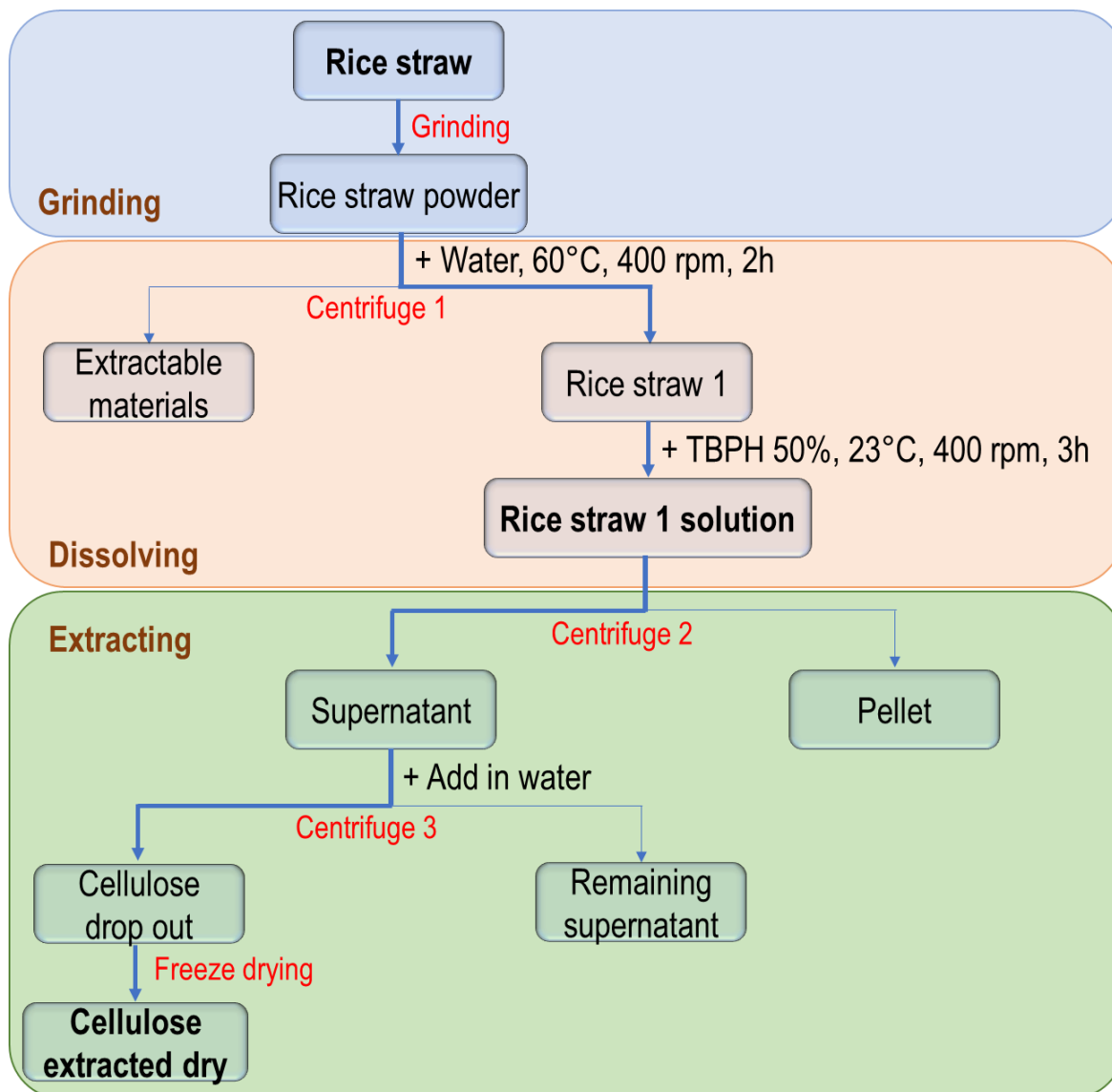


**Figure 13.** A schematic diagram of lignocellulosic compound extraction

Firstly, to increase the accessible surface between rice straw with solvents, rice straw was ground in a planetary ball mill. Mechanochemistry (using ball mill) is considered as a promising method, easy to perform and environmentally friendly. It can reduce the particle size, increase the contact surface, reduce time for solving, and decrease the degree of crystallinity.<sup>[71]</sup> In order to produce ultrafine powders, suitable grinding conditions were obtained by carrying out an evaluation of grinding process (more detail information please refer to section 5.2.1). The

operating conditions involve milling time, milling speed, ball and material load (Figure 14). Good distribution and homogeneous powder were found by using pre-cut rice straw (size 0.5 cm in lengths) under grinding conditions: 400 rpm, 180 min in agate material with 15 balls.



**Figure 14.** Grinding rice straw in the ball mill with different conditions

To remove water-soluble extractable materials such as non-structural sugars and proteins, different conditions such as microwave extraction as well as water extraction were tested. Focusing on the most simple, non-time consuming and effective extraction, the water extraction was used. For this, the finely ground rice straw was washed in hot distilled water at 60 °C followed by drying at 60 °C in the oven. The amount of extractable materials accounted for 12.8 % to 15.7 % of rice straw's mass which corresponds to the values reported in literature (Figure 2).

The dried powder was then typically dissolved in TBPH 50 wt.% at room temperature to get the homogeneous rice straw solution. It has been reported that lignin, hemicellulose as well as cellulose can be dissolved by TBPH.<sup>[58, 65, 72]</sup> This was confirmed during my research. The power of the TBPH solutions to dissolve all components is a function of the water content of the TBPH.<sup>[64]</sup> After testing of different TBPH concentration regarding dissolution and viscosity, the best concentration of TBPH in the presence of water for dissolving all compounds was found to be 50 wt.% of TBPH at room temperature.

To separate the insoluble compounds from the dissolved cellulose, hemicellulose and lignin, rice straw solution was centrifuged at high speed 14000 rpm for 1 hour (Figure 15). Separation via filtration was not efficient due to the viscosity of this solution ( $\eta = 1954 \text{ mPa s}$ ). The pellet contained mainly inorganic compounds. Note, with the alkaline method such as using sodium hydroxide, the removal of silica is inefficient and affects the purity and quality of cellulose.<sup>[73]</sup>

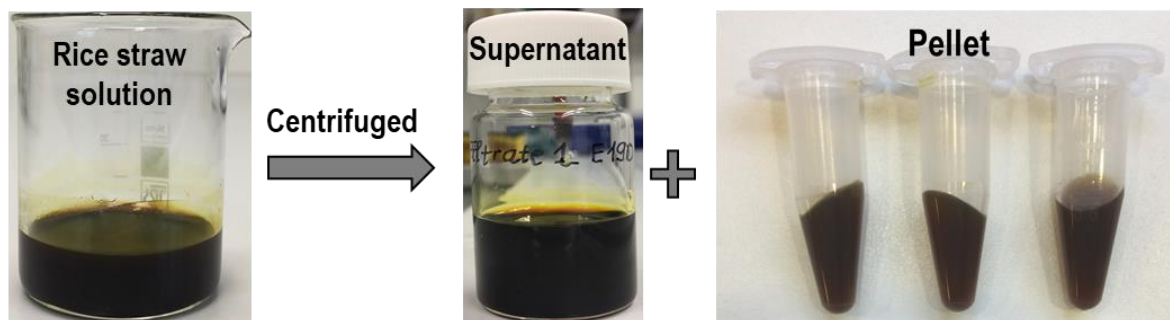


**Figure 15.** Rice straw solution, supernatant and pellet

Two common solvents, water and methanol, which are known and tested for their ability to precipitate cellulose from its solution were investigated.<sup>[68, 74]</sup> Water was chosen as a solvent to precipitate cellulose due to the non-toxicity for human. The supernatant (containing dissolved cellulose, hemicellulose and lignin) was added into a large amount of water resulting in the selective precipitation of cellulose as fine fiber sheet (Figure 16). Water reacts as an anti-solvent for cellulose solution which will weaken and even destroy the hydrogen bonds formed between cellulose and TBPH.<sup>[68]</sup> The precipitated cellulose can be isolated by centrifugation and washing with water (4 times with 50 ml water).

The selectivity was proven by a study of the precipitation behavior of dissolved cellulose, hemicellulose and lignin from aqueous TBPH 50 wt.% solution. If these solutions are added to an excess of water, only cellulose is precipitated from the solution. This result can be explained by their structure. In contrast to cellulose, which is made only from glucose, hemicellulose is an amorphous heteropolymer consisting of several different carbohydrates, including xylose, mannose, glucose and galactose in the main chain and arabinose, galactose and 4-O-methyl-d-glucuronic acid in the side chain. They are water-soluble due to their branched structure.<sup>[75]</sup> Lignin is a three-dimensional amorphous polymer containing ionized phenolic groups making the lignin soluble in a water solution. Lignin precipitation is usually carried out by acidification due to the protonation of the ionized phenolic groups on the lignin molecules.<sup>[76]</sup>

Thus, with a simple process of dissolving rice straw into TBPH 50 wt.% and then adding it to water, the cellulose was precipitated easily and selectively. Extracted cellulose contents range from 25.9 wt.% to 30.7 wt.% of rice straw. It corresponds nicely to the reported literature data (see section 1.4).

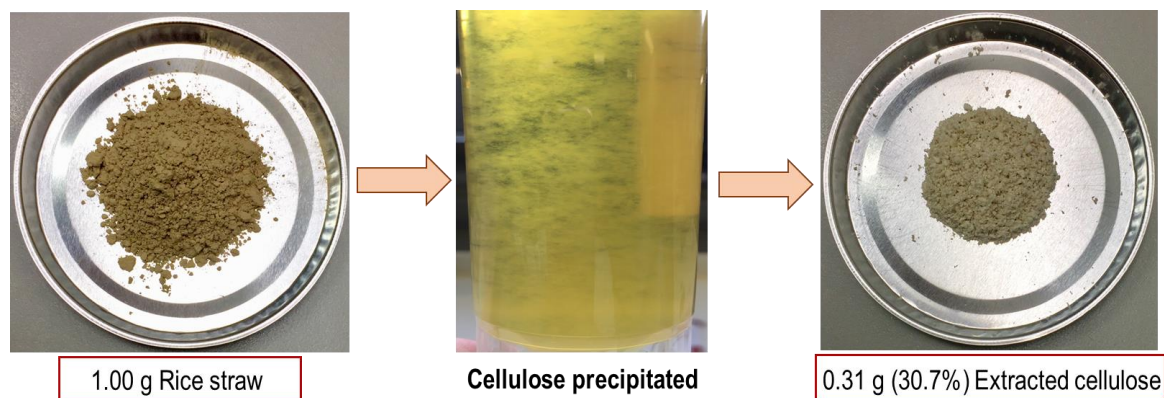


**Figure 16.** Isolation of cellulose from rice straw

### 3.1.2 Structural characteristics and chemical composition of extracted cellulose

To demonstrate the efficiency of the extraction cellulose from rice straw, the supernatant before addition of water (the rice straw solution after removing insoluble compounds), extracted cellulose dissolved in TBPH 50 wt.% and the remaining supernatant (the supernatant left after precipitating cellulose) were analyzed by the liquid state  $^{13}\text{C}$  NMR spectra (Figure 17).

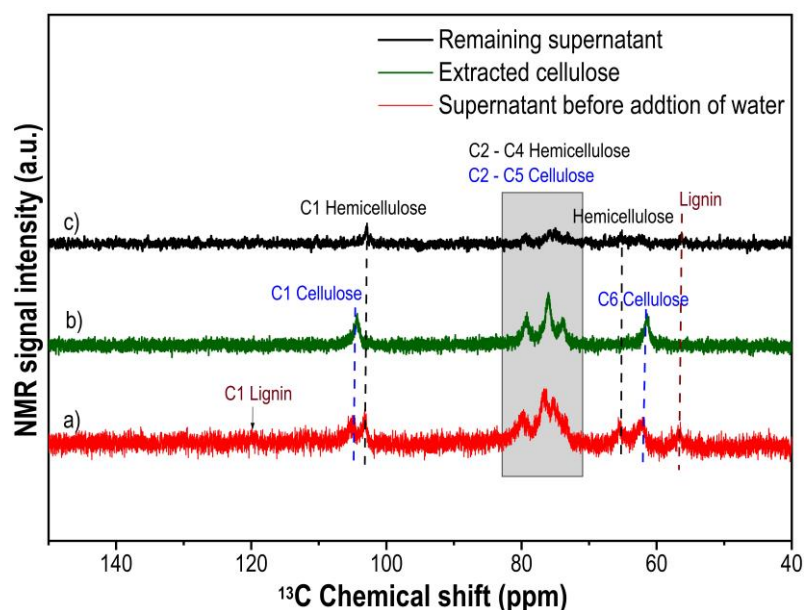


**Figure 17.** LS- $^{13}\text{C}$  NMR spectra of supernatant before addition of water, extracted cellulose in TBPH 50 wt.% and remaining supernatant

The supernatant before addition of water spectra shows the signal of cellulose, hemicellulose and lignin as expected (Figure 17a). However, the intensity of C1 lignin is very weak due to the small amount of lignin. After separation, cellulose with distinct characteristic signals is obtained (Figure 17b). The signal at 104.9 ppm (C1), 70 ppm to 80 ppm (a cluster of signals from C2-C5), and 63 ppm (C6) is related to cellulose. The remaining supernatant features only the signals of hemicellulose and lignin at 103.3 ppm, 65.8 ppm and 56.6 ppm, respectively (Figure 17c).

As the second method, the solid state  $^{13}\text{C}$  NMR was applied (Figure 18). The main aim was a more sensitive detection of lignin. However, even with this method only small traces of lignin and hemicellulose are detected (Figure 18A). Notably, the signals from 180 ppm to 120 ppm are attributed to the aromatic carbons of lignin, from 58 ppm to 50 ppm are related to methoxy groups (-O-CH<sub>3</sub>) of lignin,<sup>[77]</sup> from 30 ppm to 20 ppm are assigned to acetyl groups (-CO-CH<sub>3</sub>) of hemicellulose.<sup>[77a, 78]</sup> These results indicate the purity of the precipitated cellulose.

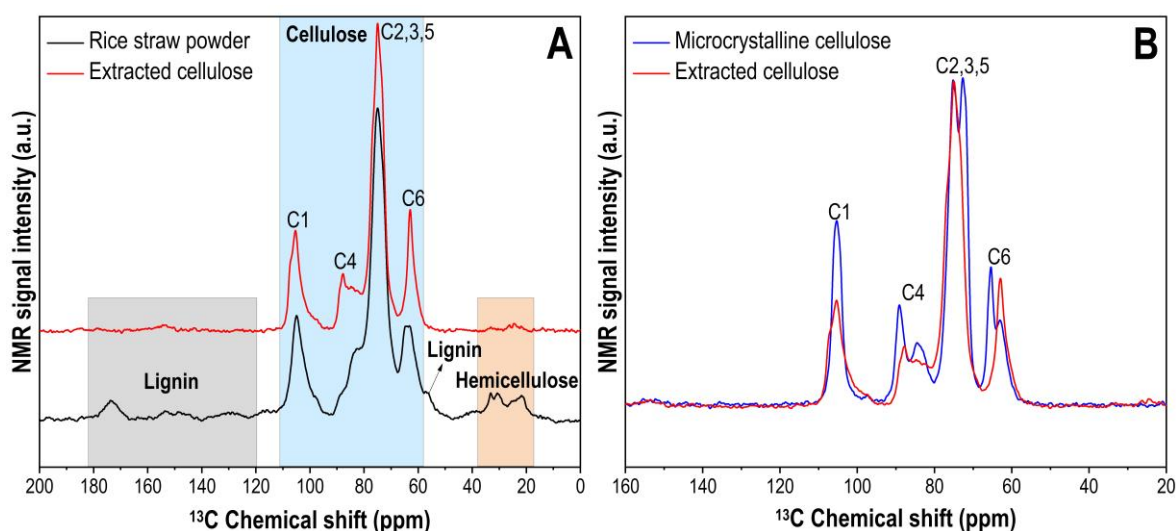


**Figure 18.** SS- $^{13}\text{C}$  NMR (A) between rice straw powder and extracted cellulose; (B) between commercially available microcrystalline cellulose and extracted cellulose

To get a more comprehensive idea of the structure of extracted cellulose, the SS- $^{13}\text{C}$  NMR signals of the extracted cellulose were compared with commercially available microcrystalline cellulose from cotton linters (Sigma Aldrich) (Figure 18B). According to previous studies,<sup>[79]</sup> in microcrystalline cellulose spectra, the two signals at 83 ppm and 88 ppm are respectively attributed to C4 of amorphous and crystalline cellulose and the chemical shifts at 62 ppm and 64 ppm are assigned to C6 of the primary alcohol group of amorphous and crystalline

cellulose, respectively.<sup>[78]</sup> The sharper and higher signal of C4 at 88 ppm and C6 at 64 ppm implies higher crystallinity of microcrystalline cellulose. The chemical shift of C4 in extracted cellulose appears at 88 ppm. The result suggests that hydrogen bonds in amorphous structure of rice straw was disrupted to some extent, resulting an increase of cellulose crystallinity of extracted cellulose during the treatment. However, the signals of C6 from extracted cellulose shifted to 62 ppm (C6 amorphous) show the existence of an amorphous part.

The cellulose materials were compared by FT-IR and XRD (Figure 19 and Figure 20). Figure 19 shows the FT-IR spectra of rice straw, cellulose isolated from rice straw and microcrystalline cellulose. The bands at  $3334\text{ cm}^{-1}$  correspond to the O–H stretching band. The absorption band at  $2888\text{ cm}^{-1}$  is due to stretching of C–H stretching vibrations in cellulose. This result suggest that the main component of the precipitated material is cellulose. This was demonstrated more clearly when the spectra of extracted cellulose and microcrystalline cellulose are compared. The FT-IR spectra of extracted cellulose and rice straw shows several differences. The band at  $1728\text{ cm}^{-1}$  (position 1) is assigned to aliphatic esters in lignin and/or hemicellulose in rice straw.<sup>[80]</sup> Besides, the band at  $1640\text{ cm}^{-1}$  (position 2) can be attributed to the bending mode of the absorbed water and also to carbonyl groups of hemicelluloses.<sup>[81]</sup> The decrease of the intensity of this band after fiber treatment is attributed to the partial removal of hemicelluloses. The bands at  $1512\text{ cm}^{-1}$  and  $1460\text{ cm}^{-1}$  in rice straw are indicative of the aromatic C=C stretch in bound lignin (position 3 and 4).<sup>[82]</sup> The disappearance of these bands in extracted cellulose spectra indicates the nearly complete cleavage of both lignin and hemicellulose after treatment.

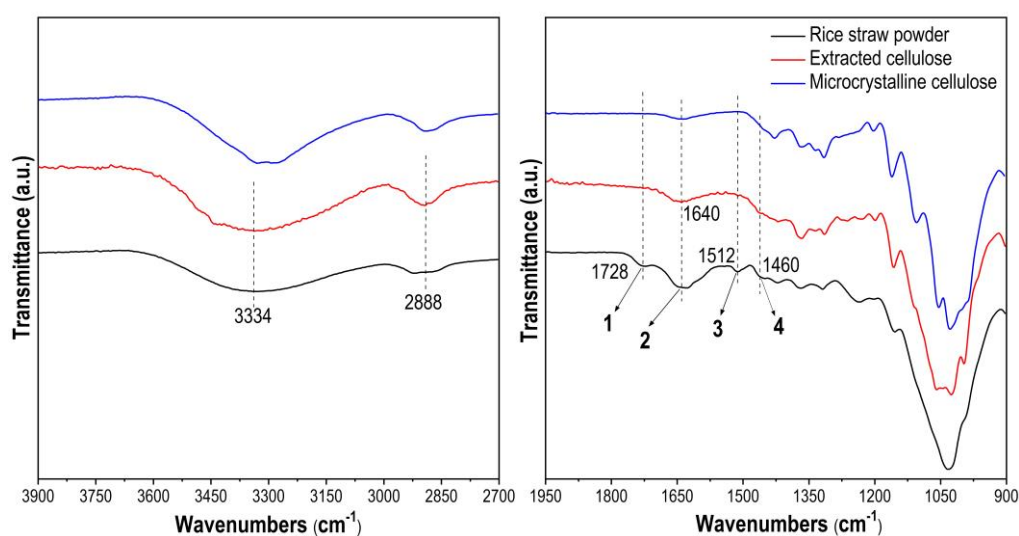


**Figure 19.** FT-IR spectra of rice straw, extracted cellulose and microcrystalline cellulose

To obtain further information, the XRD patterns of rice straw powder, cellulose isolated from rice straw and microcrystalline cellulose were analyzed (Figure 20). Rice straw composes of crystalline and amorphous regions.<sup>[83]</sup> After grinding rice straw in the ball mill, rice straw powder's spectrum shows a broad distribution, indicating that it consists of a large amount of amorphous substances. No distinct of polymorph can be observed. This could be due to the effect of ball mill which changed the morphological and structural features of cellulose has been changed. Ago et al. (2007) reported a similar observation.<sup>[84]</sup>

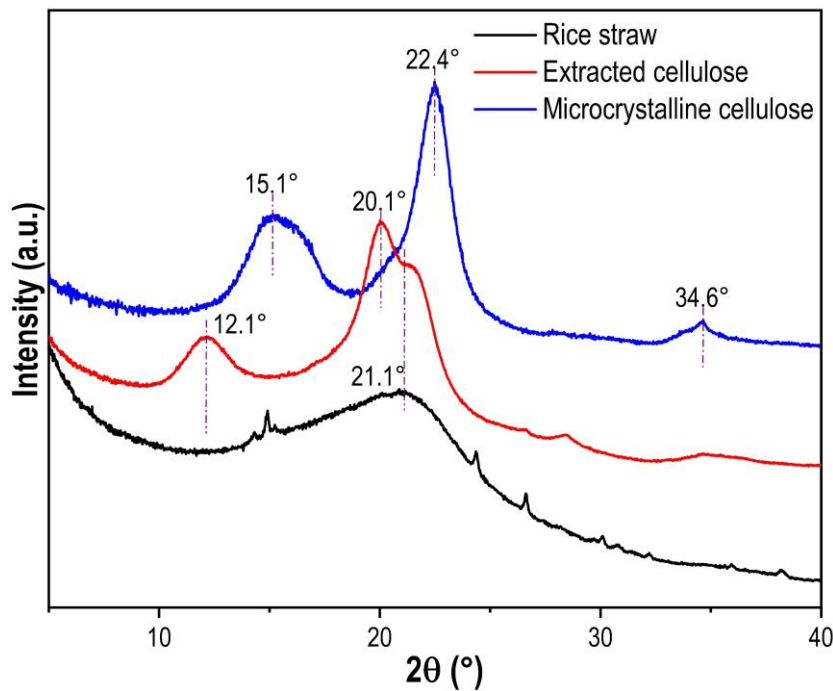


**Figure 20.** XRD patterns of rice straw, extracted cellulose and microcrystalline cellulose. Analyzing the extracted cellulose samples revealed the presence of reflections ( $2\theta = 12.1^\circ$  (101);  $20.1^\circ$  ( $10\bar{1}$ )) which can be assigned to cellulose II. However, the sharper and narrower diffraction reflection at ( $10\bar{1}$ ) clearly demonstrated the increase in the crystallinity of extracted cellulose. During the extraction process, amorphous hemicellulose and lignin were readily dissolved, while leaving the remaining cellulose of a higher degree of crystallinity.<sup>[80a]</sup> For references as native cellulose, microcrystalline cellulose was analyzed which is composed of cellulose I with three characteristic diffraction reflections ( $2\theta = 15^\circ$ ,  $22.4^\circ$ , and  $34.2^\circ$ ).

To illustrate this, the percent crystalline material in the total biomass (Table 3) was expressed by the relative “crystallinity index”, which was suggested by Segal et al. (1959)<sup>[85]</sup> as follows:

$$\text{CrI} = \frac{I_{002} - I_{\text{am}}}{I_{002}} \times 100 (\%) \quad (1)$$

Where:

- CrI: The relative degree of crystallinity, %
- $I_{002}$ : The intensity at (002) reflection of the crystalline contribution
- $I_{am}$ : The intensity of the amorphous diffraction (the minimum intensity between 002 reflection and 101 reflection)

**Table 3.** The relative crystallinity index of samples

Entry	Sample	Relative crystalline index (%)
1	Rice straw powder	23.34
2	Extracted cellulose	77.5
3	Microcrystalline cellulose	78.8

### 3.2 Dissolution of cellulose and the effect of additives <sup>1)</sup>

The utilization of cellulose even directly from biomass requires first the dissolution of it. Here an efficient and, nowadays more important, a green solvent is needed. Indeed, as reported by Abe et.al in 2012,<sup>[58]</sup> an aqueous electrolyte solution of TBPH is an excellent solvent to dissolve up to 20 wt.% of cellulose. Therefore, this system is applied as starting point for the dissolution, followed by further utilization/application. However, the reported system showed a high viscosity which limits the processability. It is therefore of significant interest to find solutions to enhance the processability and overcome this disadvantage.

#### 3.2.1 Dissolution of cellulose using TBPH with different solvents

After dissolution of cellulose in TBPH, a honey-like solution was obtained. This cellulose solution is difficult to centrifuge e.g. to separate the undissolved fragments or stir to improve a homogeneous distribution. Thus, a detailed research on the viscosity and the additional dissolution of cellulose was performed with different solvents such as dimethyl sulfoxide (DMSO), acetone (Ace), acetonitrile (MeCN), tetrahydrofuran (THF), ethanol (EtOH) and water (H<sub>2</sub>O).

First, different concentrations of cellulose were dissolved in TBPH 50 wt.% (Figure 21). To ensure complete dissolution, clear cellulose solutions were obtained and determined with the solubility test.

<sup>1)</sup>Parts of these results have been published in *ChemSusChem* **12**, 3458-3462 (2019).

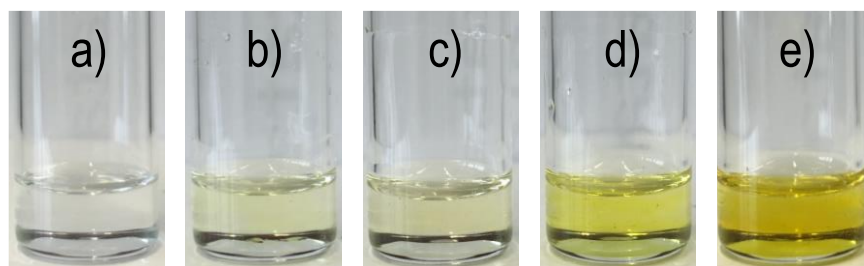


**Figure 21.** Different amount of cellulose dissolved in TBPH 50 wt.%.  
(a) TBPH 50 wt.%, (b) with 5 wt.% cellulose, (c) with 10 wt.% cellulose,  
(d) with 15 wt.% cellulose, (e) with 20 wt.% cellulose

The determination of a precise amount of cellulose in TBPH was investigated by LS- $^{13}\text{C}$  NMR spectroscopy.<sup>[86]</sup> Many studies have focused on dissolving cellulose, however the investigations on cellulose solubility are mostly semi-quantitative. Herein, series of four different concentrations of cellulose (5, 10, 15, 20 wt.%) were measured by a simple LS-NMR without using deuterated solvents (Figure 21). 1,4-dioxane was added as internal standard for quantification. The ratio of intensities between the signals of dioxane (67.19 ppm) and the anomeric sugar carbon C1 (104.9 ppm) of cellulose was used to determine the concentration of cellulose. The results are shown in Figure 22.

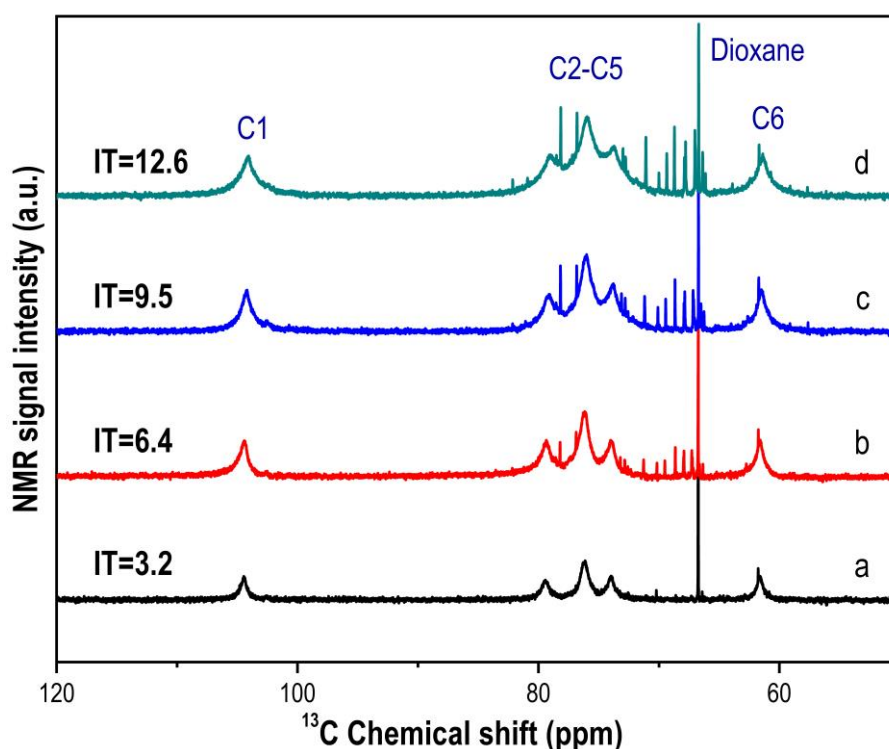


**Figure 22.**  $^{13}\text{C}$  NMR spectra of different cellulose concentration in TBPH 50 wt.%. a) 5 wt.% cellulose, b) with 10 wt.% cellulose, c) 15 wt.% cellulose, d) with 20 wt.% cellulose

The relative intensity between the C1 of the glucose unit in cellulose and dioxane is 3.2 to 1 for 5 wt.% cellulose. Every increase of 5 wt.% results in a relative increase in the intensity of about 3.2. The experimental data on the relative intensity are approximated by a linear dependence of the concentration of cellulose. Only at very high cellulose concentration (20 wt.%), the intensity is no longer linear. The error is less than 0.5 %. The viscosities of the cellulose solutions are shown in Table 4.

**Table 4.** The viscosity of TBPH solutions with different concentration as well as of selected TBPH/cellulose solutions

Entry	Solutions	Viscosity $\eta$ (mPa s)
1	TBPH 40 wt. %	4.9±0.4
2	TBPH 50 wt. %	11±1.0
3	TBPH 60 wt. %	17.2±0.5
4	TBPH 50 wt. % + 5 wt. % cellulose	143±11.3
5	TBPH 50 wt. % + 10 wt. % cellulose	826±23.8
6	TBPH 50 wt. % + 15 wt. % cellulose	3338±16.7
7	TBPH 50 wt. % + 20 wt. % cellulose	9610±20.8
8	TBPH 60 wt. % + 20 wt. % cellulose	12638±31.7

At 25 °C, TBPH is a transparent solvent with the viscosity depending on the concentration of TBPH. TBPH 40 wt.% has a viscosity of 4.9±0.4 mPa s which is much higher than water (0.9 mPa s). With higher concentration, the viscosities of the solutions increase slightly (TBPH 50 wt.% - 11±1.0 mPa s and TBPH 60 wt.% - 17.2±0.5 mPa s) (Table 4, entries 2 and 3). However, adding cellulose results in a significant increase of the viscosity (Table 4, entries 4-8) and the color changed to a pale yellow (Figure 21). The viscosity behavior of TBPH 50 wt.% with cellulose as a function of shear rate is strongly dependent on the concentration of cellulose (Table 4, entries 4-7). Even at low concentrations, the viscosity with 5 wt.% cellulose and 10 wt.% cellulose increase to 143±11.3 mPa s and 826±23.8 mPa s, respectively. Increasing the concentration up to 20 wt.% of cellulose results in a drastic increase of the viscosity (3338±16.7 mPa s for 15 wt.% cellulose and 9610±20.8 mPa s for 20 wt.% cellulose). However, dissolving 20 wt.% of cellulose in TBPH 60 wt.% results in a

dramatic increase of the viscosity to  $12638 \pm 31.7$  mPa s (Table 4, entry 8). The solution has a honey like-character. Mixing to create a homogeneous environment for subsequent processes is difficult. Therefore, as optimal conditions, a mixture of TBPH 50 wt.% and 20 wt.% cellulose was applied for further investigations.

To decrease the high viscosity and to enable further applications, different common anti- and co-solvents were tested. To compare the different effect on the viscosity, molar ratios between co-solvent and TBPH were applied (Figure 23 and Figure 24).

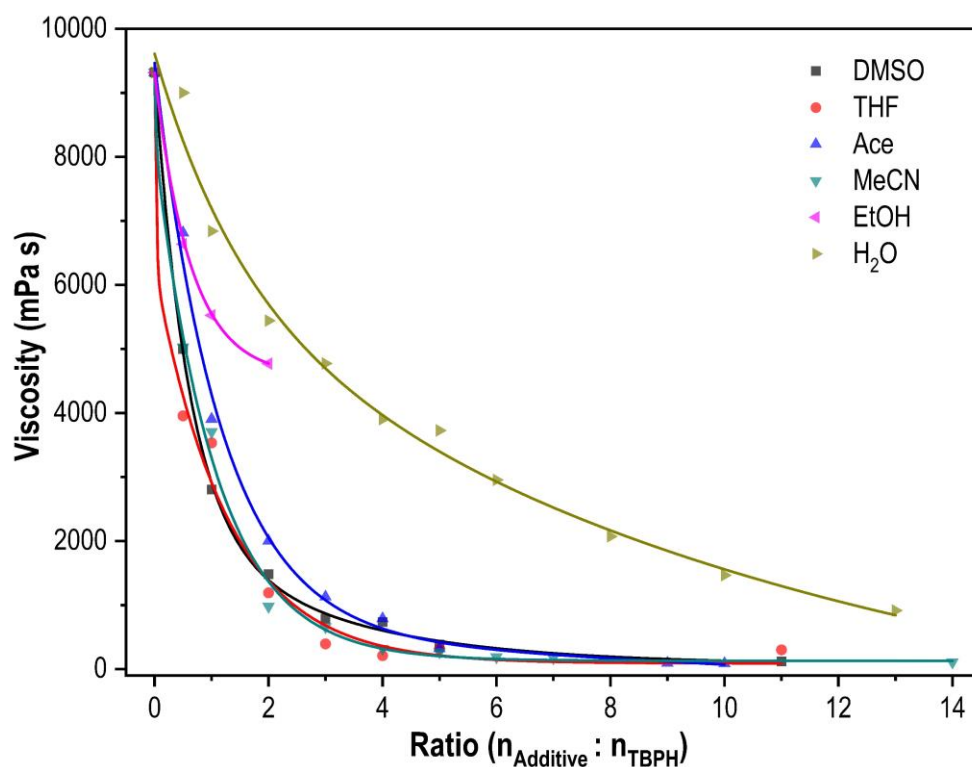


**Figure 23.** The viscosity of cellulose/TBPH solution depending on the molar ratio of additives and TBPH

The aprotic polar solvent dimethyl sulfoxide (DMSO), which is a common co-solvent for dissolution of cellulose with ILs showed promising results with TBPH.<sup>[87]</sup> If DMSO is added at a molar ratio of 1:2, the viscosity of the solution drops from 9610 mPa s to 5001 mPa s. At a molar ratio of 1:1, the viscosity is reduced again to 2806 mPa s. Note that at this ratio the concentration of TBPH is reduced to 40 wt.%, but still all cellulose is dissolved in the solution. Continued addition of DMSO with the ratio of 2:1, 3:1, 4:1, 5:1 result in a fast reduction of the viscosity to below 400 mPa s. The same behavior was determined for acetone, tetrahydrofuran and acetonitrile. At the molar ratio of 1:2 and 1:1, the viscosity of these solutions decreases

rapidly. Increasing the ratio results only to a slight decrease in viscosity. Especially for acetonitrile, the viscosity of the solution reduces significantly below 30 mPa s. It is remarkable that in all cases, even at low concentration of TBPH 20 wt.% (Figure 24), no cellulose precipitates out of solution.

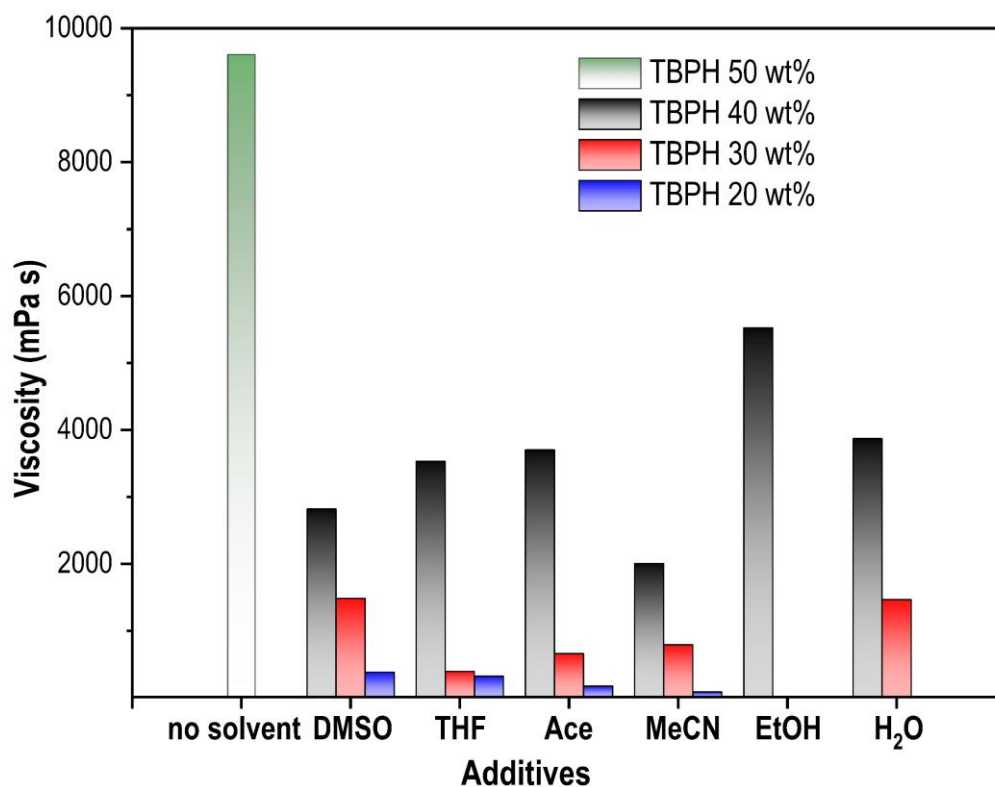


**Figure 24.** The viscosity of cellulose/TBPH solution in terms of TBPH concentration after addition of solvents calculated from Figure 23

Furthermore, even polar protic solvents such as ethanol and water were partially tolerated (up to molar ratio of 2:1). In the case of ethanol, an increased excess led to a precipitation of cellulose (Figure 25).<sup>[88]</sup>

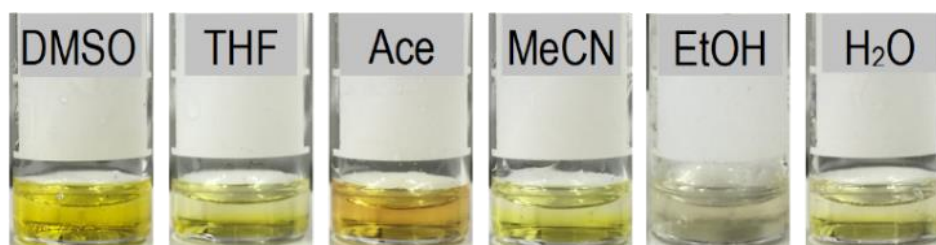


**Figure 25.** TBPH/cellulose/solvents mixtures with molar ratio 4:1 between solvents and TBPH

Finally, the effect of the most protic solvent water was investigated, since this solvent is already chosen for TBPH.<sup>[57]</sup> As expected, the viscosity decreases gradually with the molar amount. Surprisingly, addition of water did not lead to the precipitation of cellulose. Even the reduction to 40 wt.% (Figure 26a) and later to 30 wt.% of TBPH is still possible. The viscosity drops half to 3728 mPa s (40 wt.%) and 1467 mPa s (30 wt.%). This is quite surprising since TBPH 40 wt.% cannot dissolve even 0.5 wt.% cellulose (Figure 26b). However, a large excess of water still results in the precipitation of cellulose which is in an agreement with the precipitation obtained during the selective isolation from rice straw (section 3.1).

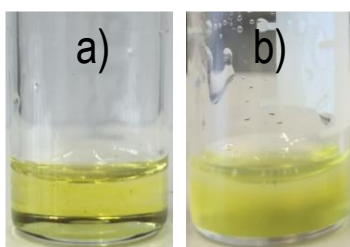


**Figure 26.** a) Dissolution of 20 wt.% cellulose with TBPH 50 wt.% and then addition of water to decrease the concentration of TBPH 50 wt.% to 40 wt.%; b) Direct addition of 0.5 wt.% cellulose in TBPH 40 wt.%

Furthermore, getting an improved insight into the change of the viscosity, the most important co-solvents (DMSO and H<sub>2</sub>O) were measured with different cellulose concentrations (Figure 27). Even small amounts of DMSO showed a large influence of the viscosity. This effect was much smaller with H<sub>2</sub>O, thus, enabling a flexible adjustment of the viscosity.

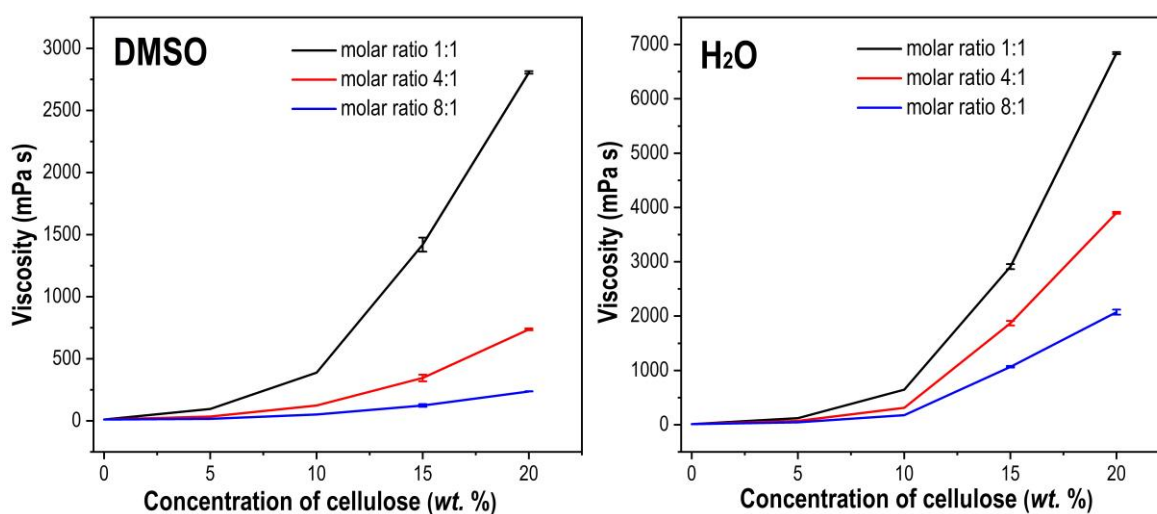


**Figure 27.** Viscosity of the cellulose/TBPH solution as function of the cellulose concentration at different molar ratios of DMSO and H<sub>2</sub>O

The reproducibility standard deviations of the viscosity of the cellulose solution at different molar ratios of DMSO and H<sub>2</sub>O was investigated as shown in Figure 27.

In general, during these experiments the total amount of cellulose did not change while the viscosity of the solution decreased. The influence of the co-solvent became interesting for the additional dissolution of the cellulose. Therefore, certain amounts of cellulose were added to the cellulose solution (Figure 28).

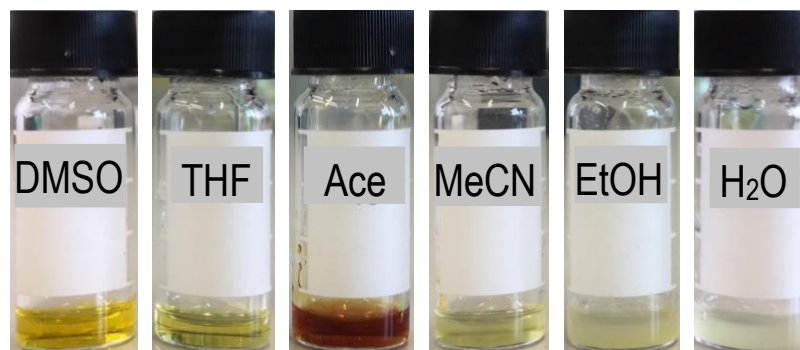


**Figure 28.** Addition of 8 wt.% cellulose to different TBPH/cellulose/solvent mixtures

Interestingly, additionally 6 wt.% of cellulose can be dissolved in acetonitrile (Table 5, entry 4), 8 wt.% cellulose in acetone and THF (Table 5, entry 2 and 3). Only with DMSO more than extra 10 wt.% can be dissolved (Table 5, entry 1). Note, DMSO can enhance the cellulose dissolution in ILs.<sup>[89]</sup>

**Table 5.** Addition of cellulose to different TBPH/Cellulose/co-solvent mixtures

Entry	Additive	Ratio	Amount of cellulose					Colour
			2 wt.%	4 wt.%	6 wt.%	8 wt.%	10 wt.%	
1	DMSO	1:1	Yes	Yes	Yes	Yes	Yes	Yellow
2	THF	1:1	Yes	Yes	Yes	Yes	No	Yellow
3	Ace	1:1	Yes	Yes	Yes	Yes	No	Orange
4	MeCN	2:1	Yes	Yes	Yes	No	No	Yellow
5	EtOH	1:1	No	No	No	No	No	White
6	H <sub>2</sub> O	4:1	No	No	No	No	No	White

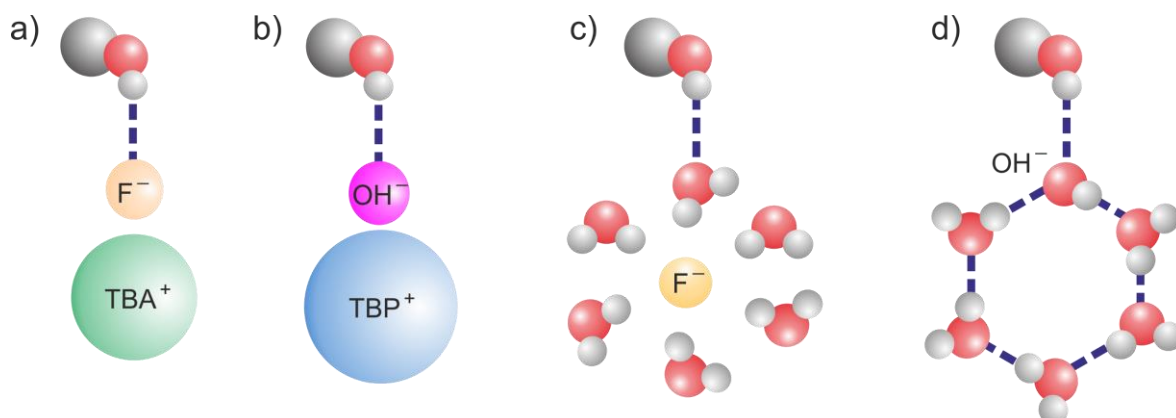
### 3.2.2 Proposed dissolution mechanism with TBPH

The addition of solvents such as DMSO, MeCN, Ace, H<sub>2</sub>O, and THF strongly decreases the viscosity without precipitation of cellulose. Only the addition of EtOH and large amounts of H<sub>2</sub>O force the precipitation of cellulose. Interestingly the addition of solvents does not influence the further dissolution of cellulose. These surprising results raised the question on the effect of the solvent for dissolution of cellulose. Thus, in cooperation with Prof. Ludwig, University of Rostock, the dissolution mechanism was investigated.

These results are of high impact for the processability since MeCN, Ace, H<sub>2</sub>O, EtOH are well known as anti-solvent for dissolved cellulose in ILs such as 1-n-butyl-3-methylimidazolium acetate ([BMIM][Ac]), 1-n-butyl-3-methylimidazolium acetate ([BMIM][Cl]), 1-allyl-3-methylimidazolium chloride ([AMIM][Cl]).<sup>[55, 90]</sup> Among the four solvents, water is the most effective substance to regenerate cellulose by breaking and destructing the hydrogen bonds between cellulose and ILs.<sup>[91]</sup> It can be emphasized by the exchange of cellulose – bonded anion Cl<sup>-</sup> and Ac<sup>-</sup> induced by the strong attraction of water and polar solvents.<sup>[92]</sup> However, it is not the same behavior with aqueous TBPH solution. Therefore, a detailed density functional theory study was performed to explain the high dissolution power of TBPH.

In TBPH 50 wt.%, positive charged phosphonium cations [TBP]<sup>+</sup> and hydroxide anions [OH]<sup>-</sup> as well as a high access of water (50 wt.%) are presented. In this electrolyte solution, the dissolving power mainly depends on the following factors: the disruption power of the anion, the hydrogen bonding capacity, the choice of the counter ion and, especially in these electrolyte solutions, the presence of water.<sup>[93]</sup> Without water, ILs are capable to dissolve cellulose easily (Scheme 2a). It is reported that the interaction between ILs and cellulose was stronger than the intermolecular interaction of cellulose.<sup>[94]</sup> The anion is the electron donor, e.g. [F]<sup>-</sup>, which can form strong hydrogen bonds with cellulose.<sup>[95]</sup> Besides, the cation also has a significant impact on the dissolving power of ILs due to their size.<sup>[96]</sup> If the cation is sufficiently large such as in tetrabutylammonium [TBA]<sup>+</sup>, the large cation interacts only weakly with the anion, e.g. [F]<sup>-</sup>. Therefore, it maintains its disruption power for the strong cellulose hydrogen-bond network. This was demonstrated for related polyols.<sup>[93, 97]</sup> In theory, in neat TBPH, the situation might be similar. The hydroxide anion [OH]<sup>-</sup> is strongly disruptive and the counter

cation  $[\text{TBP}]^+$  is large enough for not reducing the disruptive power and stabilizes the anionic cellulose- $\text{OH}^-$  complex (Scheme 2b).

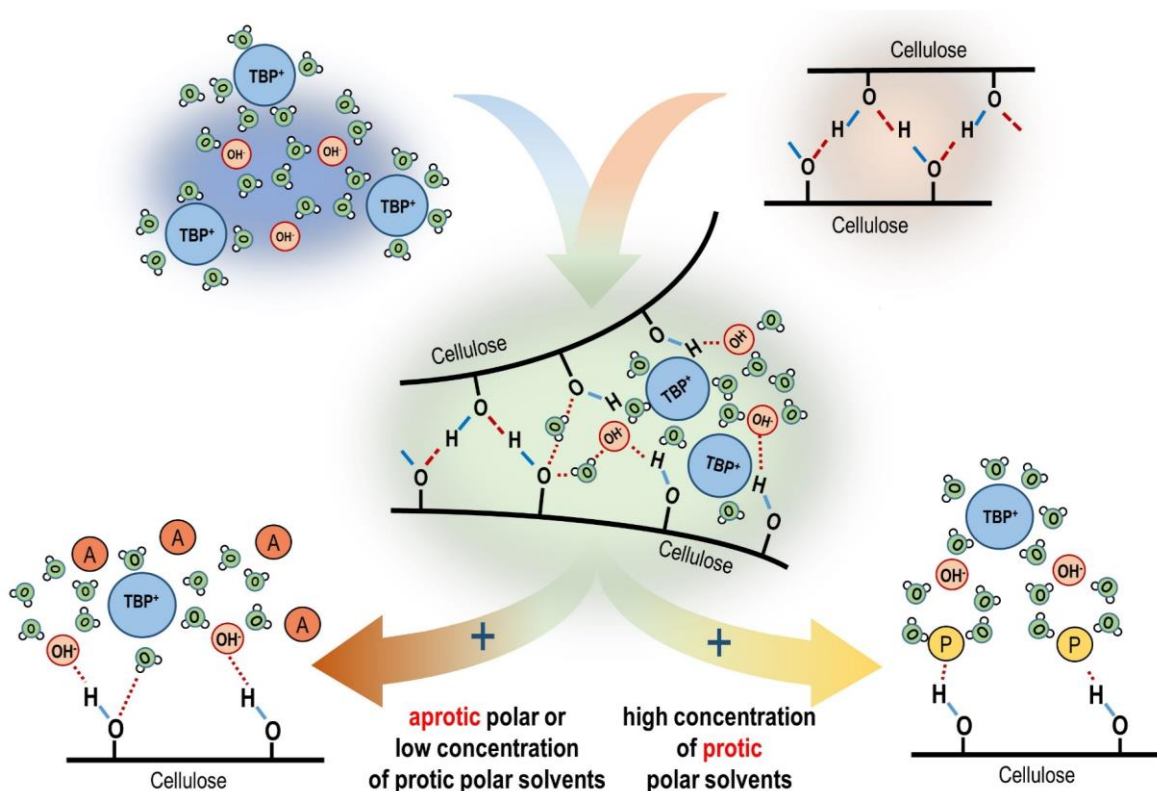


**Scheme 2.** Illustration of dissolving cellulose in traditional TBAF/DMSO/water and TBPH/water solutions: a) The fluoride anion forms strong H-bonds with the OH groups of the cellulose. b) In TBPH the situation is similar: They have a strongly interacting hydroxide anion and a large, innocent cation. c) In the TBAF/DMSO/water solutions the fluoride anion is fully hydrated by water molecules and can no longer attack the cellulose H-bond network. d) In the TBPH/water solution the hydroxide anion is hydrated in favourable way without losing its disruptive power. However, in the presence of water a completely different behavior can be expected. The fluoride anions interact strongly with both cellulose and water.<sup>[98]</sup> It can be assumed that every ion is surrounded by several water molecules. For example, for imidazolium-based ILs around seven to nine water molecules are coordinated around anion and cation.<sup>[99]</sup> Small concentrations of water strongly solvate the important anions e.g.  $[\text{F}]^-$ , preventing their association with the cellulose chains (Scheme 2c).<sup>[93]</sup>

In aqueous TBPH solution, the  $[\text{OH}]^-$  anion is even stabilized by water molecules and still connected to the cellulose (Scheme 2d). On one side the hydroxide anion transfers charge into the OH of the neighbored water molecule, on the other side it gains substantial amount of charge via cooperative charge transfer within the water hydrogen-bond network, which is maximized in cyclic structures. Thus, the  $[\text{OH}]^-$  anion can still provide the full disruption power to dissolve the hydrogen bond network. Water even enhances the disruptive power of  $[\text{OH}]^-$  rather than reducing it as in the TBAF/water solution. At the same time, the water molecules are highly mobile in this hydrogen-bond network resulting in overall higher diffusivities and reduced viscosities.<sup>[100]</sup> The key point here is the highly flexible hydrogen-bond network of

water including the hydroxide anion without reducing its ability to attack the strong hydrogen-bonds within cellulose.

Based on these argumentations, a simplified mechanism for the addition of additives is proposed (Scheme 3).



**Scheme 3.** A proposed simplified dissolution mechanism of cellulose in TBPH and after addition of protic and aprotic solvents

Introducing the cellulose into TBPH aqueous solution results in a fast disruption of the hydrogen-bonding network in cellulose via incorporation of the anion [OH]<sup>-</sup> into the network. I assumed that the cation [TBP]<sup>+</sup> ion has an additionally stabilizing effect,<sup>[101]</sup> as well as strengthen, thus, preventing re-coordination of cellulose sheets<sup>[102]</sup> and maintains the disruption power of the anion [OH]<sup>-</sup>. Note, around 1 - 1.5 units [TBP]<sup>+</sup> per AGU were estimated. Water molecules may still be coordinated near the ions. Therefore, for the addition of solvents, it can be emphasized that the water concentration decreases, but only a partial exchange of water and/or ions takes place. Cellulose remains dissolved. Only ethanol, a strong hydrogen bond donor, can cause cellulose precipitation in TBPH solution. The excess of water-coordinated [OH]<sup>-</sup> and stabilizing phosphonium ions enables the additional dissolution of

cellulose in the present cellulose/TBPH/water/solvent mixture, maximizing the amount of dissolved cellulose.

Explaining the change of viscosity in this solution, the van-der-Waals forces between anions and cations as well as hydrogen bonding between counter ions has to be taken into account.<sup>[103]</sup> At high viscosity, strong van-der-Waals forces in combination with hydrogen-bond interactions can be considered. Especially, the small  $[\text{OH}]^-$  anions are strongly polarized, and therefore have a powerful hydrogen bonding capacity to water and the  $\text{HO-CH}_2$  of cellulose. Aprotic polar solvents with less polarity do not have the ability to break these strong hydrogen-bonds. With increased solvent concentration still an exchange with water molecules can be emphasized, but due to high mobility in water, this exchange can be neglected. The van-der-Waals forces are reduced which results in lower viscosity. As a result, the cellulose remains dissolved. In the case of protic solvents (solvents with high polarity and high hydrogen-bond capability), the high mobility of water allows a fast water exchange. The polarity of methanol is nearly the same as that of water, thus, resulting in the interruption of the  $[\text{OH}]^-$  interaction with the cellulose sheets. This leads to precipitation of the cellulose.

In summary, the dissolution of cellulose in TBPH leads to a strong increase of the viscosity. Therefore, it is essential to reduce the viscosity of cellulose solution without changing its properties. The utilization of solvents can enable adjustment of the viscosity, by using high viscose to low viscose cellulose solution (Figure 29). The introduction of aprotic polar solvents thus allows the continued use of these cellulose/TBPH solvent mixtures without precipitation of cellulose. Only the addition of ethanol and large concentrations of water forces the precipitation of cellulose. Interestingly the addition of co-solvents has no influence on the further dissolution of cellulose.

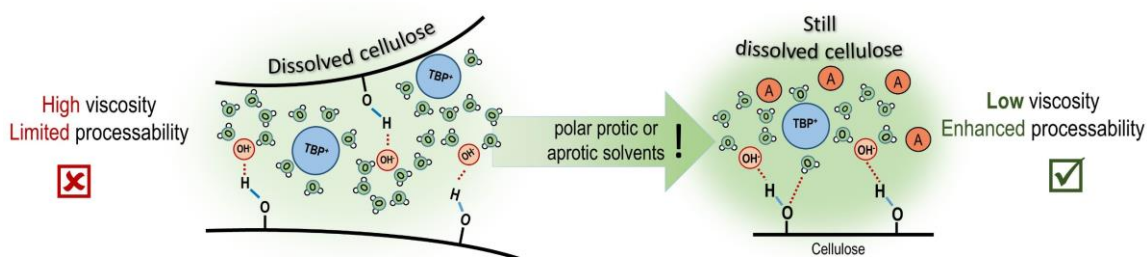


**Figure 29.** The effect of additives on the viscosity and dissolution of cellulose in TBPH

### 3.3 MDCell methodology for the preparation of the regenerated cellulose films <sup>2)</sup>

Searching for non-toxic and renewable co-solvents to decrease the viscosity of the cellulose solution and, thus, to increase the processability, organic carbonates have been investigated. Surprisingly, organic carbonates such as propylene carbonate (PC) were found with completely different behavior. Instead of dissolution, spontaneous solidification occurred within seconds. This enables a completely new methodology towards cellulose films. The development and the application of this method will be presented in this section.

#### 3.3.1 Introduction of MDCell methodology

A completely new methodology, so called MDCell process, was developed to obtain regenerated cellulose (RC) as powder or films (Figure 30). This methodology starts from the dissolution of cellulose (from microcrystalline cellulose or from biomass) with TBPH followed by coagulation with organic carbonates.

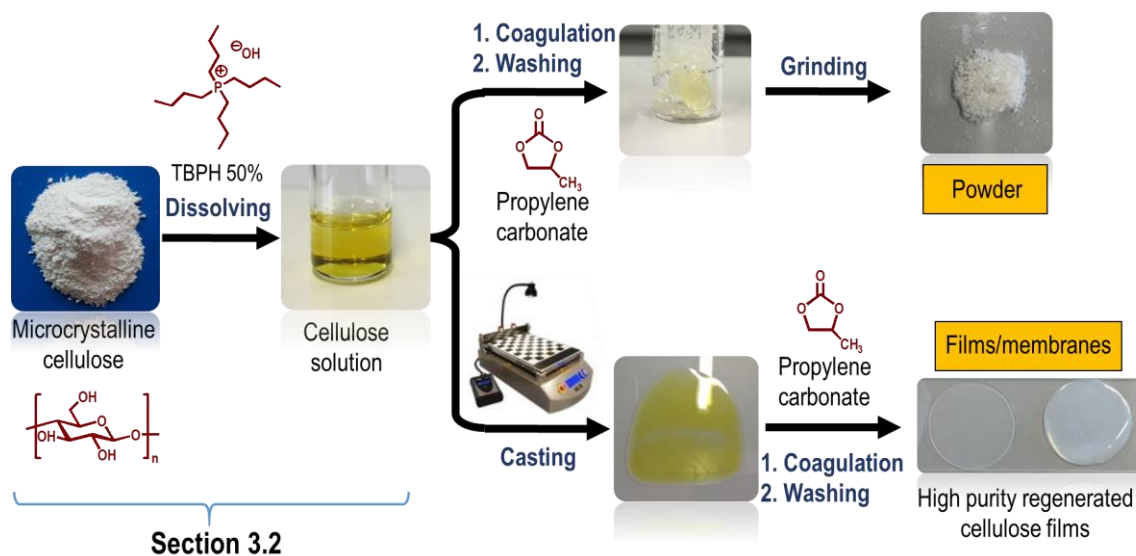


**Figure 30.** Preparation of regenerated cellulose by the MDCell process

A typical procedure involves the dissolution of 20 wt.% commercially available microcrystalline cellulose in TBPH 50 wt.% in 30 minutes at room temperature (23 °C) followed by simple addition of an organic carbonate such as PC - in principle formed by the reaction of CO<sub>2</sub> with diols or epoxides<sup>[69]</sup>. Solidification occurs in seconds. The solidified substances can be easily

<sup>2)</sup>Parts of these results have been published in *Communications Chemistry* **3**, 116 (2020).

washed with water, dried at 80 °C and then ground to obtain granulates or powder. In the following, this powder is referred to as RC powder.

To obtain the RC films, the cellulose solution is casted onto a glass plate to produce a cellulose casting layer of a defined thickness (e.g., 500 µm).<sup>[104]</sup> The casted liquid can be quickly immersed into a PC bath. Here, no change of the optical properties occurred. The RC films can be washed with distilled water to remove all water-soluble chemicals and impurities.

Distinct effects were observed with DMSO as co-solvent. DMSO is an excellent co-solvent promoting the dissolution process,<sup>[105]</sup> reducing the solvent amount for dissolution,<sup>[89a]</sup> and reducing the viscosity of cellulose solution without precipitation of cellulose as mentioned in section 3.2.1.<sup>[68]</sup> Indeed, the quality of the films is remarkably improved by DMSO. The films become more flexible, more homogeneous, and almost fully transparent.

With the MDCell process, RC powder and films can be fabricated at mild and green conditions. This process is the subject of a Patent application.<sup>[70]</sup> A movie of this manufacture can be found in this link:

[https://unibox.uni-rostock.de/getlink/fiNjMsW4FNLEg46yEjzo5jg/4003\\_MD\\_Cell\\_process\\_26\\_03\\_2020.mp4](https://unibox.uni-rostock.de/getlink/fiNjMsW4FNLEg46yEjzo5jg/4003_MD_Cell_process_26_03_2020.mp4)

Thus, in two simple, extremely fast steps, environmentally friendly, non-toxic and cost-effective, cellulose can be utilized to produce non-transparent and transparent RC films and high-quality RC powder. PC is employed as reagent for the coagulation step which occurs in seconds.

### 3.3.2 Investigation of the coagulation mechanism

The formation of the RC powder and RC films was quite surprising and interesting since organic carbonates are well known as green solvent.<sup>[106]</sup> Adding PC in the cellulose solution results in the solidification within seconds assuming a complete different precipitation mechanism compared to well-known anti-solvent mechanism. Thus, the coagulation mechanism was investigated in detail.

The TBPH-cellulose mixture after coagulation with PC was analyzed by liquid state <sup>13</sup>C NMR spectroscopy. For preparation the experiment, the *in-situ* reaction mixture was applied. First, the cellulose solution was transferred to the LS-NMR tube. Then PC was added inside the

cellulose solution from the bottom of the tube by a capillary syringe. No change of the tetrabutylphosphonium ion  $[TBP]^+$  was observed in  $^{31}P$  NMR. However, three new signals at 160.4, 68.4, and 67.8 ppm were obtained in  $^{13}C$  NMR (Figure 31). Note, the solidified cellulose cannot be detected by standard LS- $^{13}C$  NMR.

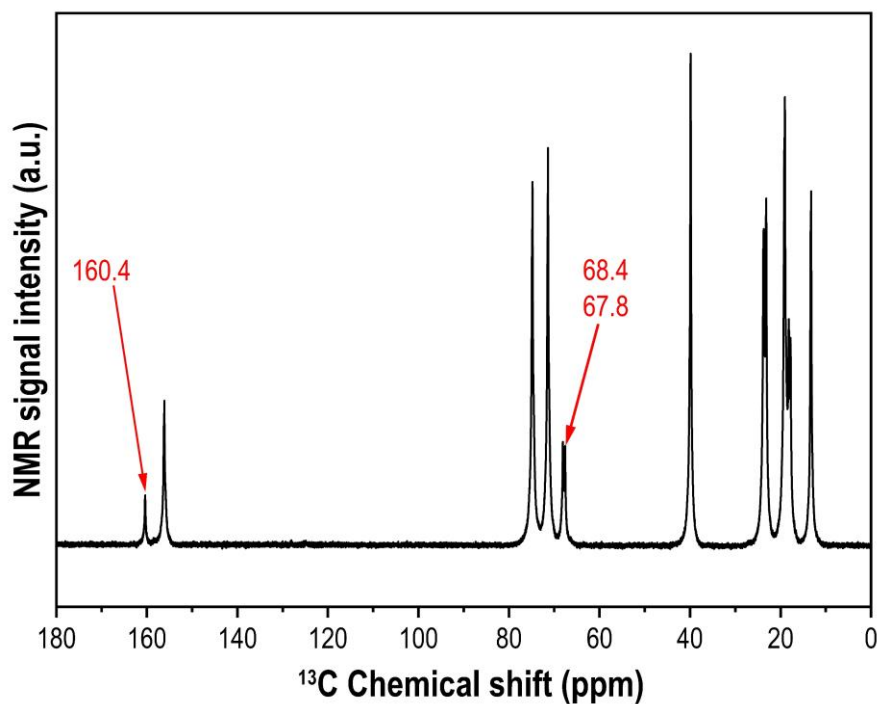


**Figure 31.** LS- $^{13}C$  NMR spectra of the *in-situ* reaction mixture after addition of PC to the TBPH/cellulose solution

To get further information, the single reaction between TBPH and PC was conducted and analyzed (Figure 32). Notably, the reaction between TBPH 50 wt.% and PC generated an amount of heat (the reaction temperature increased from 22.1 °C to 32.8 °C), which suggested a physical phenomenon (by the interaction when dissolve solution) or a chemical reaction (hydroxide group opens the cyclic carbonate). In Figure 32A and Figure 32B, new signals in  $^1H$  and  $^{13}C$  NMR (tagged as #) are detected, the same positions with the *in-situ* reaction (Figure 31). Since no deuterated solvent was used for the NMR measurements, 1,4-dioxane was added as internal standard (tagged as a \*). No shift in the  $^{31}P$  NMR spectra (Figure 32C) emphasizes again the inert character of the  $[TBP]^+$  cation.

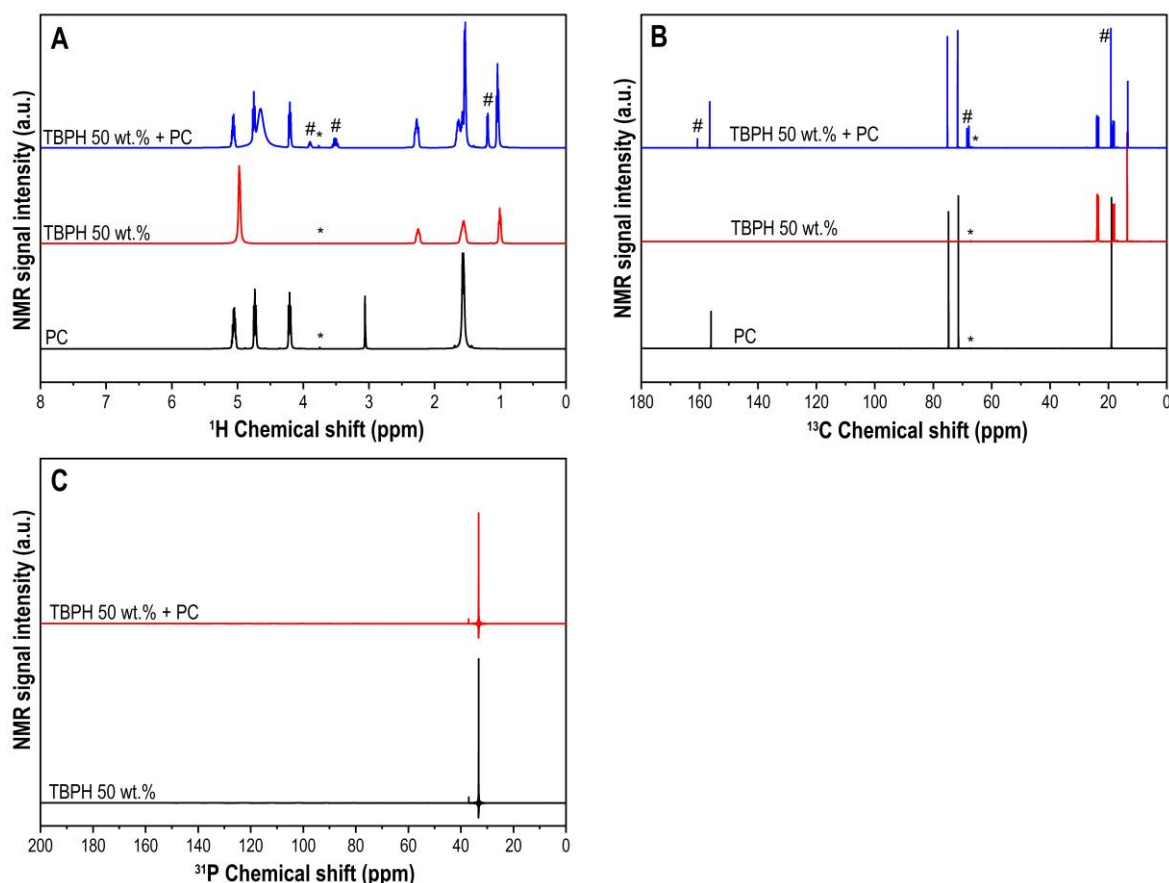


**Figure 32.**  $^1\text{H}$ ,  $^{13}\text{C}$ , and  $^{31}\text{P}$  NMR spectra of PC, TBPH and the reaction mixture of both

With two new signals at 67.8 and 68.4 ppm, many assumptions have been made. Two new signals may be from the coupling of phosphorous splitting or two single signals separated. To identify these new signals, the additional spectroscopic investigation in liquid state NMR such as  $^{13}\text{C}$  DEPT was used (Figure 33 - Figure 35) suggesting a reaction between PC and the hydroxide anion  $[\text{OH}]^-$ . Finally, the new signals were identified as 1,2- propanediol (labeled as PG - propylene glycol) and hydrogen carbonate (labeled as HC) which are explained in the next pages.

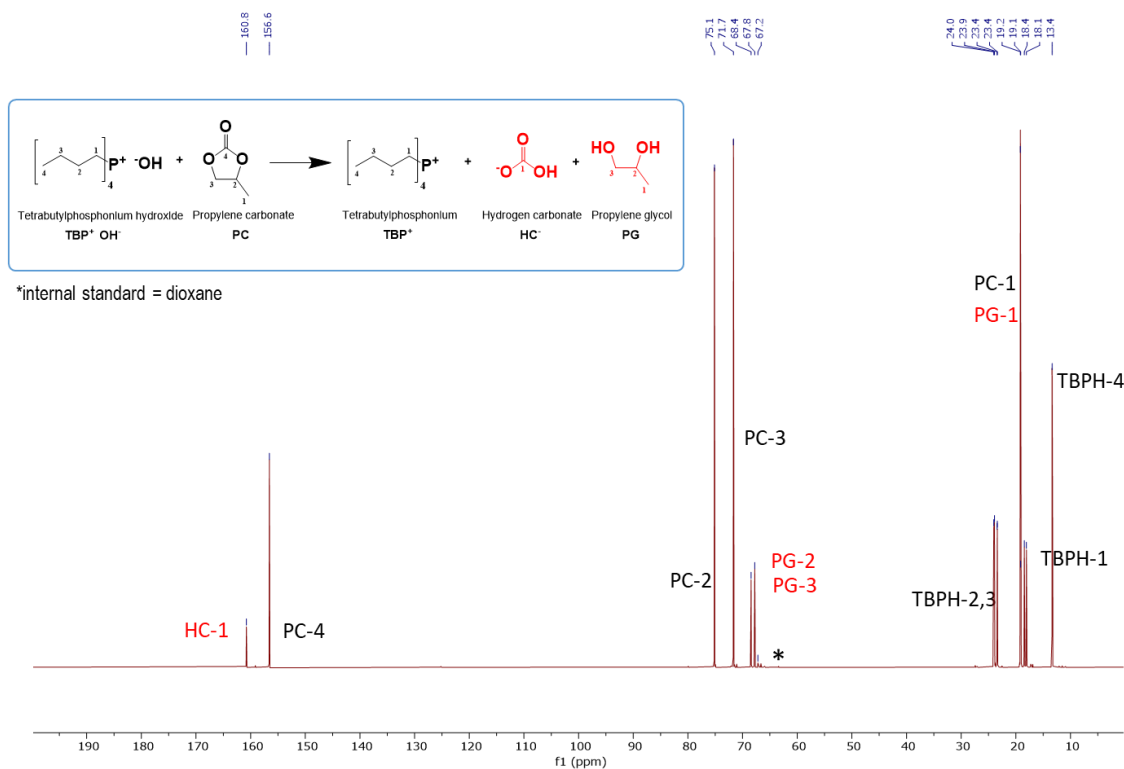


**Figure 33.** <sup>13</sup>C NMR spectra of the reaction mixture of PC and TBPH

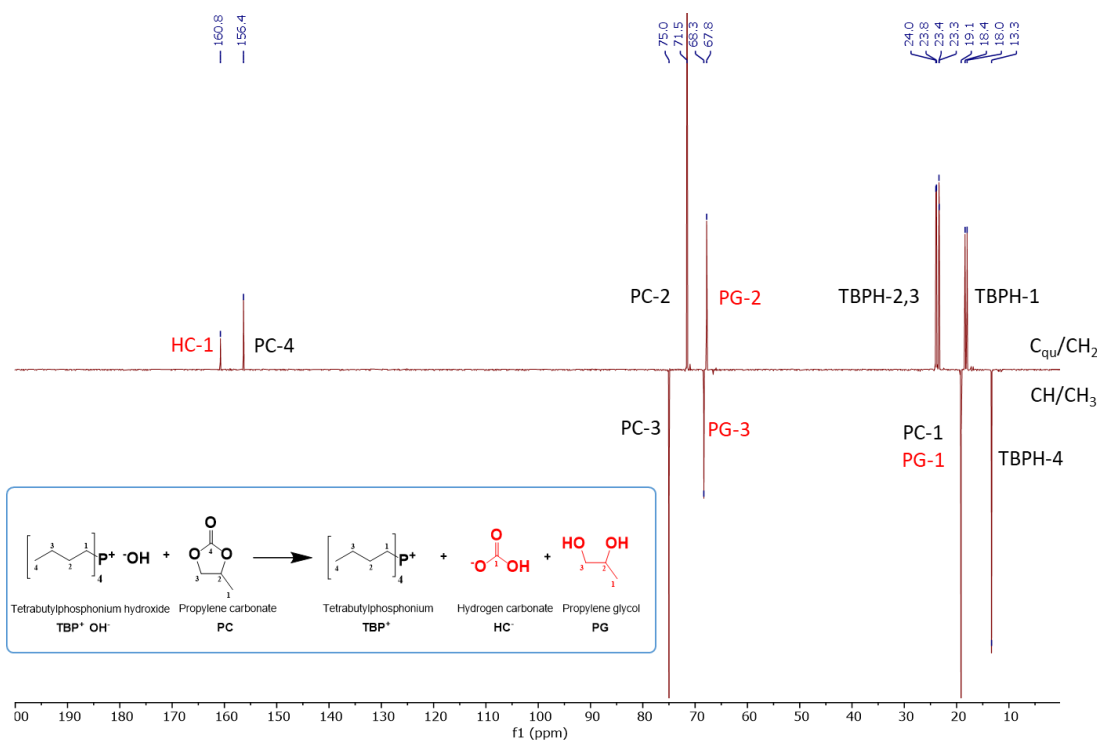


**Figure 34.** <sup>13</sup>C DEPT NMR spectra of the reaction mixture of PC and TBPH

The <sup>13</sup>C DEPT NMR spectra showed that two new signals (PG 2 and PG 3) were two separate CH<sub>2</sub> (at 67.8 ppm) and CH<sub>3</sub> (at 68.3 ppm) signals.

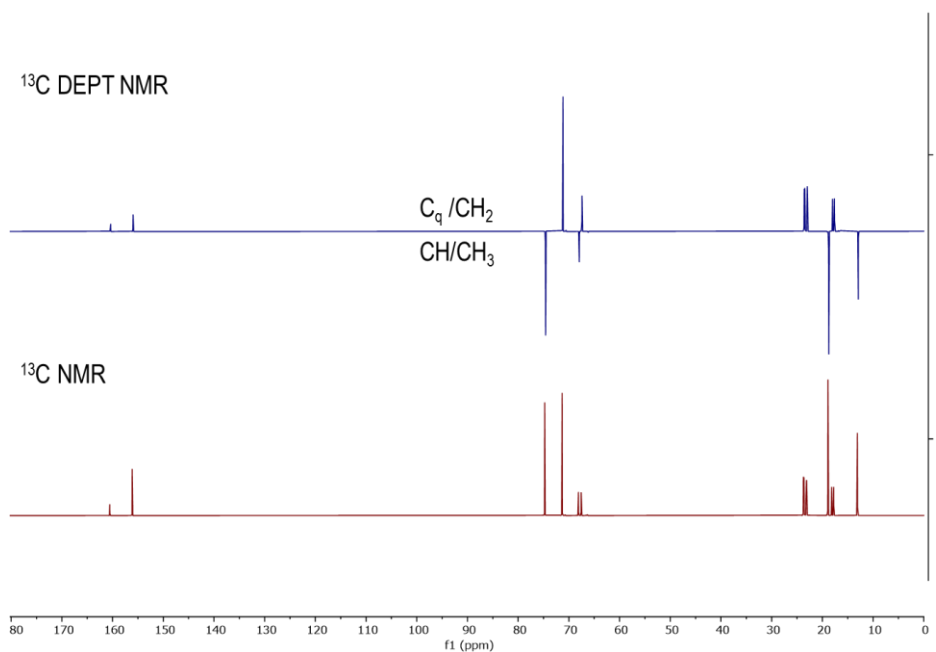


**Figure 35.** Comparison  $^{13}\text{C}$  and  $^{13}\text{C}$  DEPT NMR spectra of the reaction mixture of PC and TBPH

An detailed investigation by 2D NMR (HSQC, COSY and HMBC NMR) resulted in the identification of propylene glycol and hydrogen carbonate (Figure 36 - Figure 38)

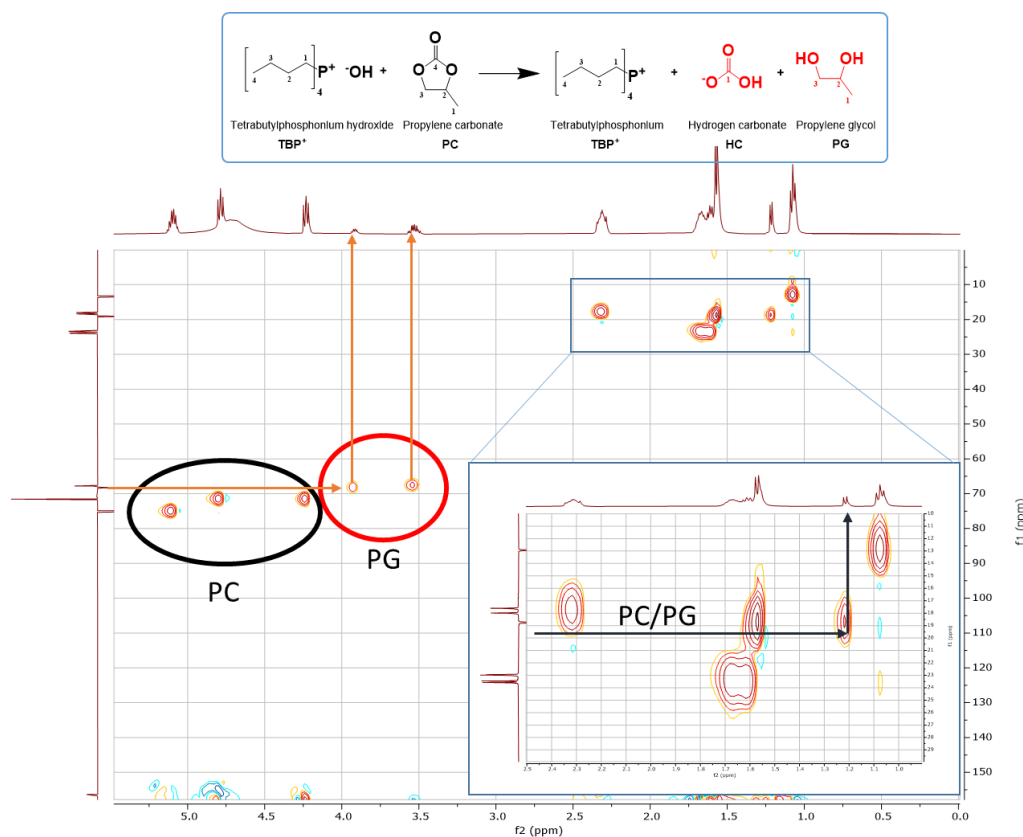


**Figure 36.**  $^1\text{H}$ - $^{13}\text{C}$  HSQC NMR spectra of the reaction mixture of PC and TBPH

The correlation of the PG-C2 and PG-C3 to PG-C2H and PG-C3H<sub>2</sub> are highlighted in red color. The carbon signal of PC-1 and PG-1 are overlapping in the <sup>13</sup>C NMR (Figure 33). However, since the hydrogen signals are separated, the inset shows the separated <sup>1</sup>H-<sup>13</sup>C coupling of the PC-1 and PG-1. No coupling of the signal at 160.4 ppm is detected suggesting a quaternary carbon.

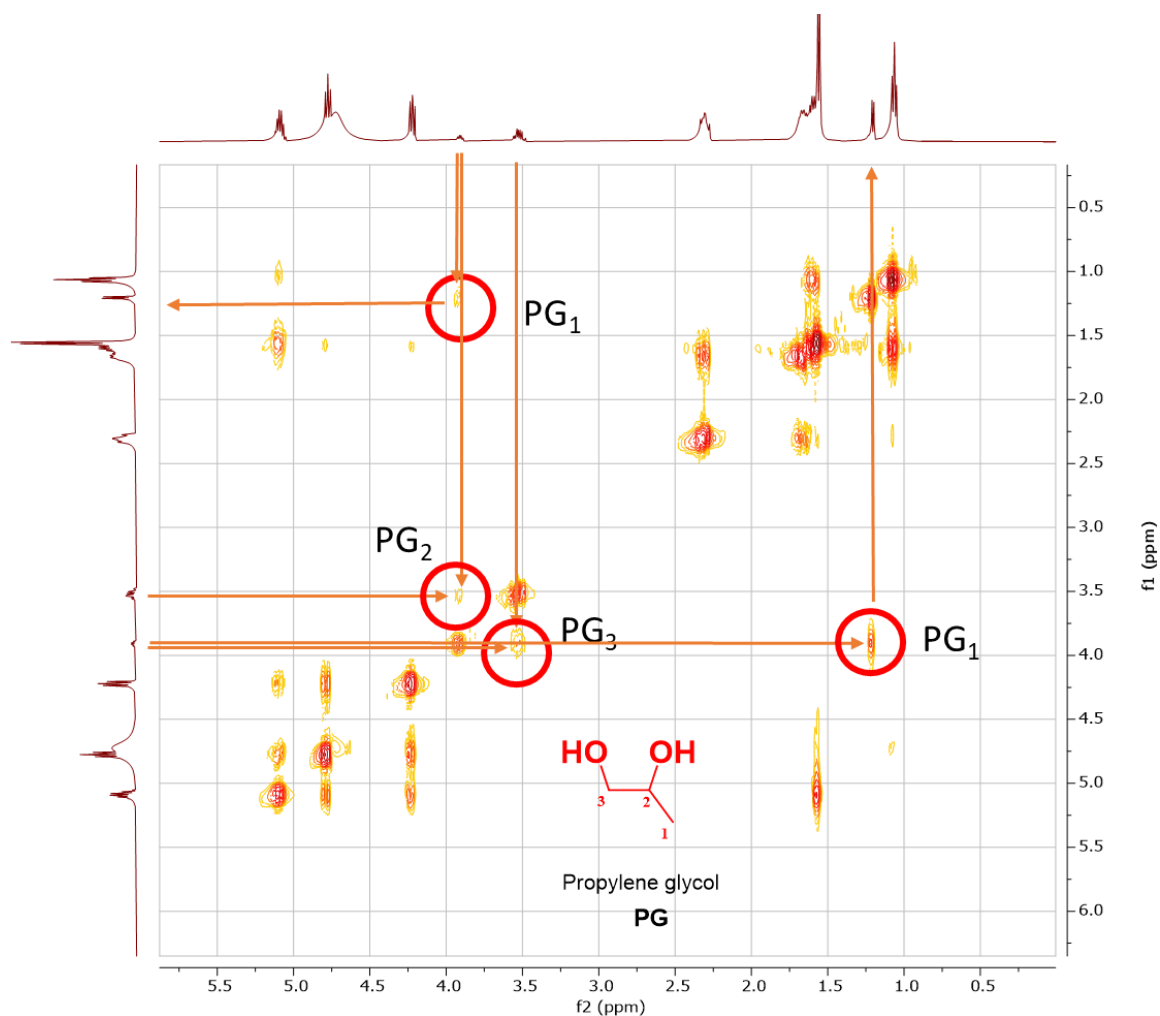


**Figure 37.** <sup>1</sup>H-<sup>1</sup>H COSY NMR spectra of the reaction mixture of PC and TBPH

Here the coupling between the hydrogen of PG-2/3 and PG-1 can be detected.

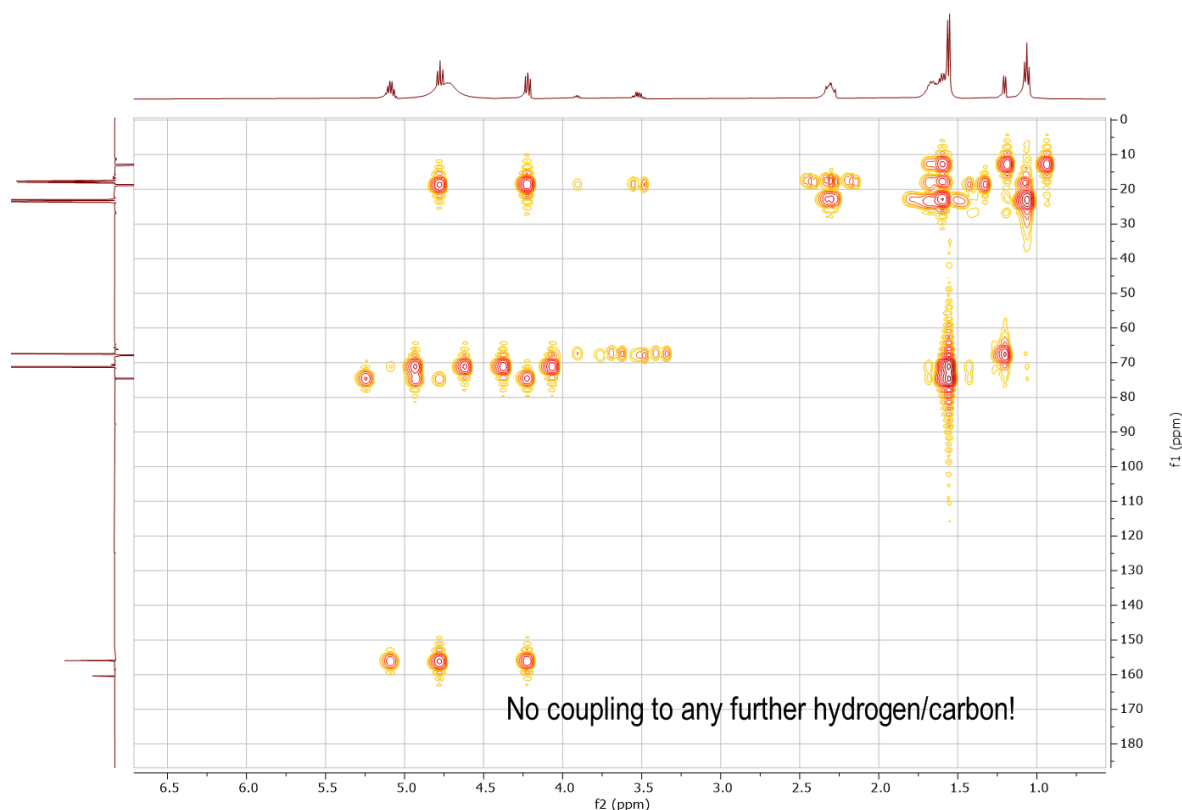
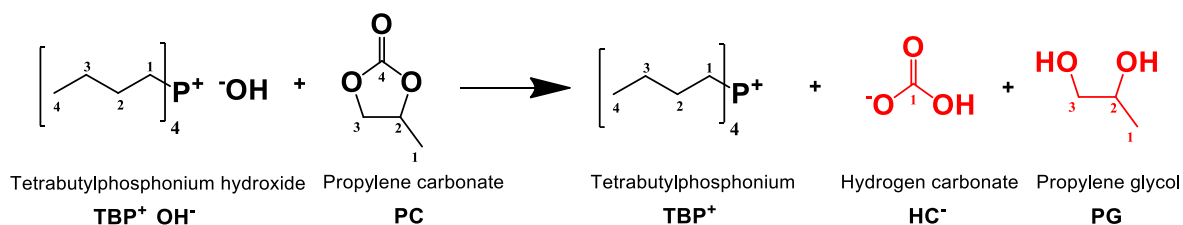


**Figure 38.**  $^1\text{H}$ - $^{13}\text{C}$  HMBC NMR spectra of the reaction mixture of PC and TBPH

In the HMBC, the coupling of carbon in one molecule can be detected. However, the signal at 160.4 ppm shows no coupling to any carbon indicating the formation of hydrogen carbonate. This assumption was proven by a measurement of dissolved  $\text{CO}_2$  in the pure aqueous TBPH solution.

The conclusion according to the LS-NMR investigation implies that the three new formed signals (from two substances HC and PG) result from the reaction between  $[\text{OH}]^-$  ions with organic carbonates (Scheme 4), which leads to the elimination of  $[\text{OH}]^-$  and thus to the immediate coagulation of cellulose.



**Scheme 4.** The reaction between TPBH and PC

The formation of the films can be summarized by the proposed mechanism for the reaction between cellulose solution and PC in Figure 39.

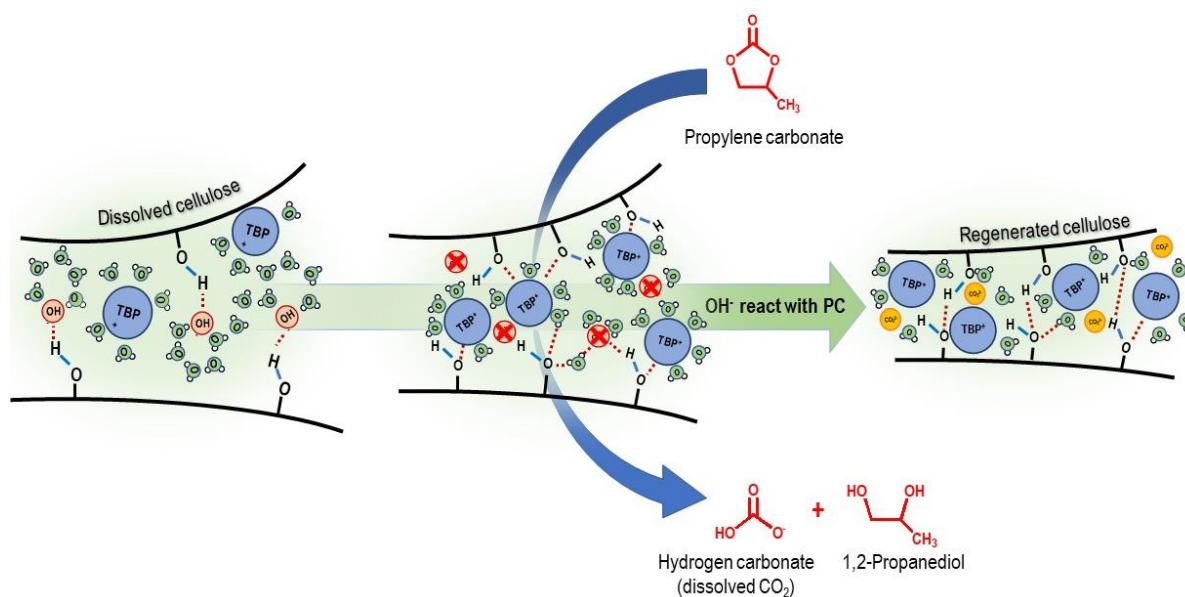


**Figure 39.** Proposed mechanism for the reaction between cellulose and PC

Indeed, the  $[\text{OH}]^-$  ion plays an essential role in the dissolution abilities of the TBPH solution [68]. The hydroxide ions  $[\text{OH}]^-$  of TBPH can break the strong hydrogen bonds between the cellulose chains, which leads to the dissolution of cellulose. However, when the cellulose solution contacts with the coagulant organic carbonates such as PC, a nucleophilic attack of the  $[\text{OH}]^-$  ions occurs. The reaction between anion  $[\text{OH}]^-$  and PC generated hydrogen carbonate and propylene glycol. Thus, no hydroxide ions are available to stabilize the dissolved cellulose. The hydrogen bonds are rearranged between the cellulose chains lead to the coagulation of cellulose occurs immediately.

Note that in principle the coagulation can proceed via solvent exchange mechanism as well e.g. with the formed propylene glycol (PG). Indeed, the coagulation with PG proceeds, but with a much slower rate. It took 21 minutes (RC film 1) and 17 minutes (RC film 2) compared to PC (6 minutes for RC film 1 and 3 minutes for RC film 2). The solidification on the surface happens immediately when the casting cellulose solution comes into contact with PC. It means the coagulation of cellulose occurs due to the reaction between PC and  $[\text{OH}]^-$  in TBPH. The PG generated from the reaction between the PC and the anion  $[\text{OH}]^-$  does not contribute to the coagulation process.

For the coagulation process, a large excess of PC was used to obtain a higher surface quality of the films (discussed in more detail in section 3.3.3). Of course, the solution after precipitation

of cellulose accumulated  $[\text{TBP}]^+[\text{HCO}_3]^-$ , PG and  $\text{H}_2\text{O}$  but the entire coagulation bath can be used several times. It does not result in the loss of coagulation ability of cellulose.

### 3.3.3 Production of RC powder and films

#### 3.3.3.1 Structural and chemical characterization of RC powder

First, the structural and chemical characterization of RC powder was analyzed. Due to the simple manufacturing process, the powder was used for these investigations instead of the film.

FT-IR was employed to examine the changes in chemical structure of cellulose during the dissolution in TBPH and regeneration in PC (Figure 40).

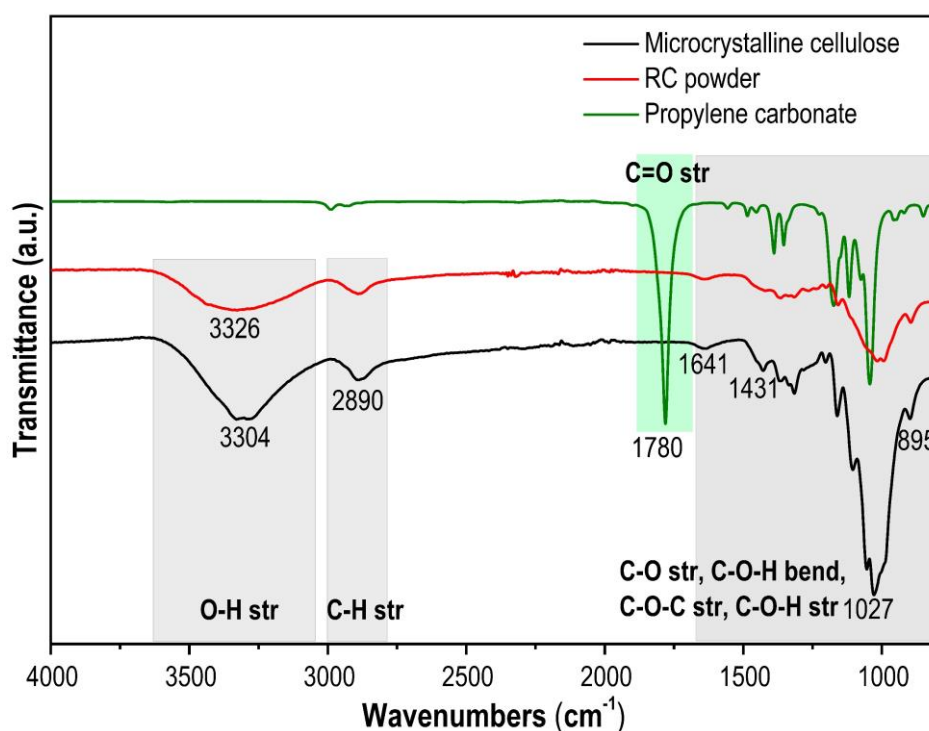


**Figure 40.** FT-IR spectra of the microcrystalline cellulose, RC powder, and PC

The main functional groups in microcrystalline cellulose are detected at  $3304\text{ cm}^{-1}$  (O-H hydroxyl group stretching vibration), the band at  $2890\text{ cm}^{-1}$  belong to the asymmetrically stretching vibration of C-H in a pyranoid ring,  $1431\text{ cm}^{-1}$  to the  $-\text{CH}_2-$  alkyl bending stretching, and  $1027\text{ cm}^{-1}$  can attributed to the C-O of cellulose and  $892\text{ cm}^{-1}$  to  $\beta$ -glucosidic linkages between the sugar units, respectively. The absorption at  $1641\text{ cm}^{-1}$  can be assigned to the absorbed water.

The regenerated cellulose powder exhibited similar bands compared to microcrystalline cellulose indicating no change of the cellulose structure during the dissolution and regeneration. However, the O-H stretching vibration shifted to a higher wavenumber of  $3326\text{ cm}^{-1}$ , which could be due to the decreased hydrogen bonding in cellulose after regeneration. Surprisingly, no PC was incorporated into the cellulose structure which can be visualized by the absence of the carbonyl bond at  $1781\text{ cm}^{-1}$ .

Furthermore, LS- $^{13}\text{C}$  NMR was used to investigate the chemical structure of RC powder (Figure 41). For this, the RC powder obtained were dissolved again in TBPH 50 wt.% and then measured without deuterated solvent.

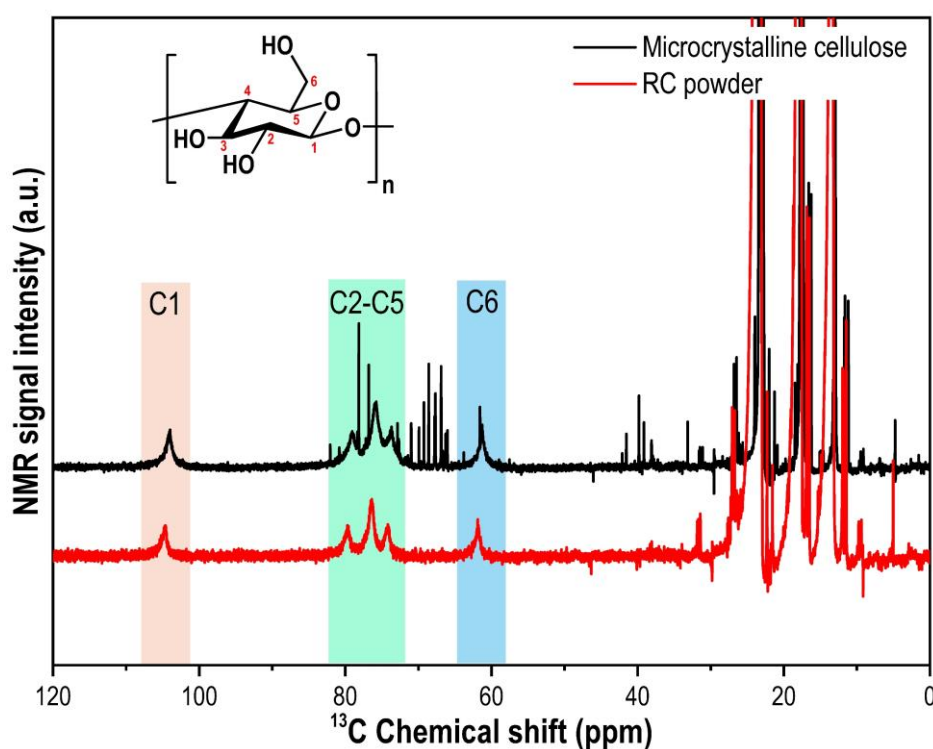


**Figure 41.** LS- $^{13}\text{C}$  NMR of cellulose and RC powder dissolved in TBPH 50 wt.%

Figure 41 shows the  $^{13}\text{C}$  NMR of cellulose from 104 ppm to 61.5 ppm.<sup>[86]</sup> The glycosidic C1 atom can be detected at 104 ppm. The signals for C2 - C5 appear in the range of 73 ppm - 80 ppm. The signal at 61.5 ppm is assigned to the  $\text{CH}_2$  group of the C6 atom. Interestingly, the spectra obtained by LS- $^{13}\text{C}$  NMR spectroscopy highlight the purification effect of the new MDCell process and the improved quality of the regenerated cellulose. The impurities found in commercial microcrystalline cellulose (sharp signals of glucose monomers and dimers of cellobiose at around 40 ppm and 70 ppm) are not presented in the re-dissolved RC powder.

XRD analysis was utilized to compare the crystallinity of cellulose before and after the regeneration (Figure 42).

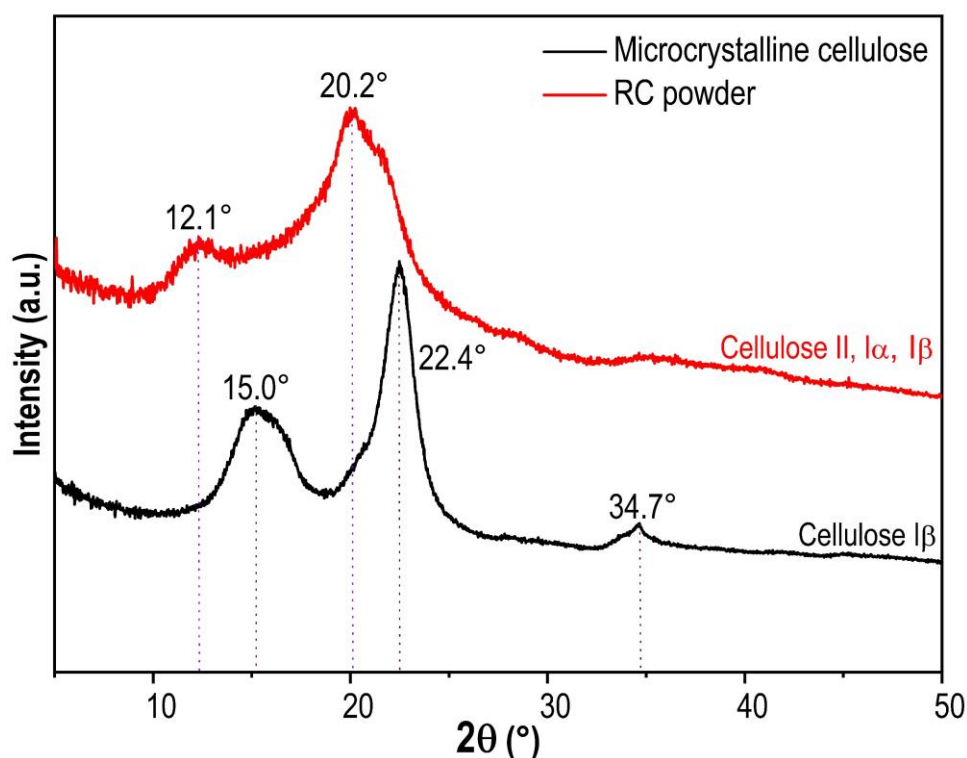


**Figure 42.** XRD patterns of commercially available microcrystalline cellulose (cellulose I) and RC powder (mainly cellulose II)

The commercially available microcrystalline cellulose exhibited the typical crystal lattice of cellulose I with main diffraction reflections at  $2\theta = 15^\circ$  and  $22.4^\circ$ . They correspond to the diffraction planes of a secondary overlapped (101) and  $(10\bar{1})$  and a primary (002) lattice plane reflection, respectively. The produced regenerated cellulose shows the different diffraction reflections at  $2\theta = 12.1^\circ$  (110);  $20.6^\circ$  (a primary  $10\bar{1}$  reflection overlapping with a reduced 002 reflection). They correspond mainly to cellulose II.<sup>[79d, 85]</sup> Thus, the XRD measurements indicated a transformation from cellulose I to cellulose II (regenerated cellulose) occurring during the process of dissolution combined with a coagulation with PC.

Note that the reflections of regenerated cellulose showed a decreased intensity as well as broad features. The broad reflection typically formed from amorphous fraction as the crystallinity index decreased from 78.7 % (commercially available MCC) to 68.7 % (RC powder) (calculated using Eq. 1, section 3.1.2). Indeed, TBPH rapidly broke intermolecular and intramolecular hydrogen bonds in the dissolution process and destroyed the original

crystalline structure of the crystalline cellulose. Regeneration with PC results in a spontaneous partially ordered rearrangement of the cellulose macromolecules.

Initially, a chemical modification of cellulose during the transformation with PC (e.g., via the reaction of PC with the OH groups of cellulose) to form PC-Cellulose materials was suggested.<sup>[107]</sup> However, the investigation of the chemical and structural properties using FT-IR, XRD and LS-NMR did not reveal any chemical transformation. Thus, the “regeneration” process of the MDCell process is characterized without changing the chemical structure.

As an alternative to the PC employed, other organic carbonates were tested for the coagulation (Figure 43). The regenerated cellulose powders were characterized by FT-IR and XRD. No difference was detected.

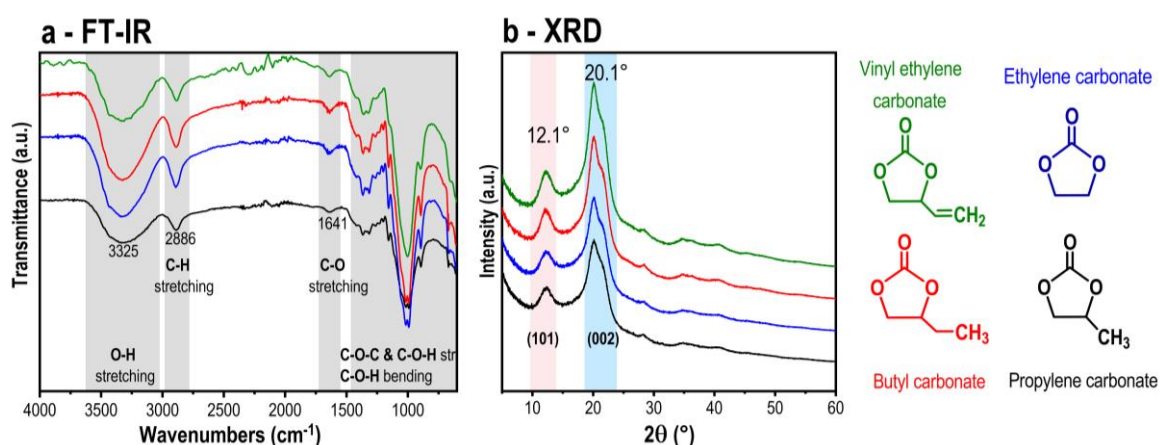


**Figure 43.** FT-IR spectra and XRD patterns of RC powder with different kind of organic carbonate. (A) FT-IR spectra; (B) XRD patterns

Thus, vinyl ethylene carbonate, butyl carbonate, and ethylene carbonate lead to the same regenerated cellulose. However, PC constitutes the best organic carbonate due to price, availability and liquid state at 25 °C. It is remarkable that the amount of cellulose (Figure 44A), the amount of PC (Figure 44B) and the origin of cellulose (Figure 44C) do not influence the structure of the regenerated cellulose.

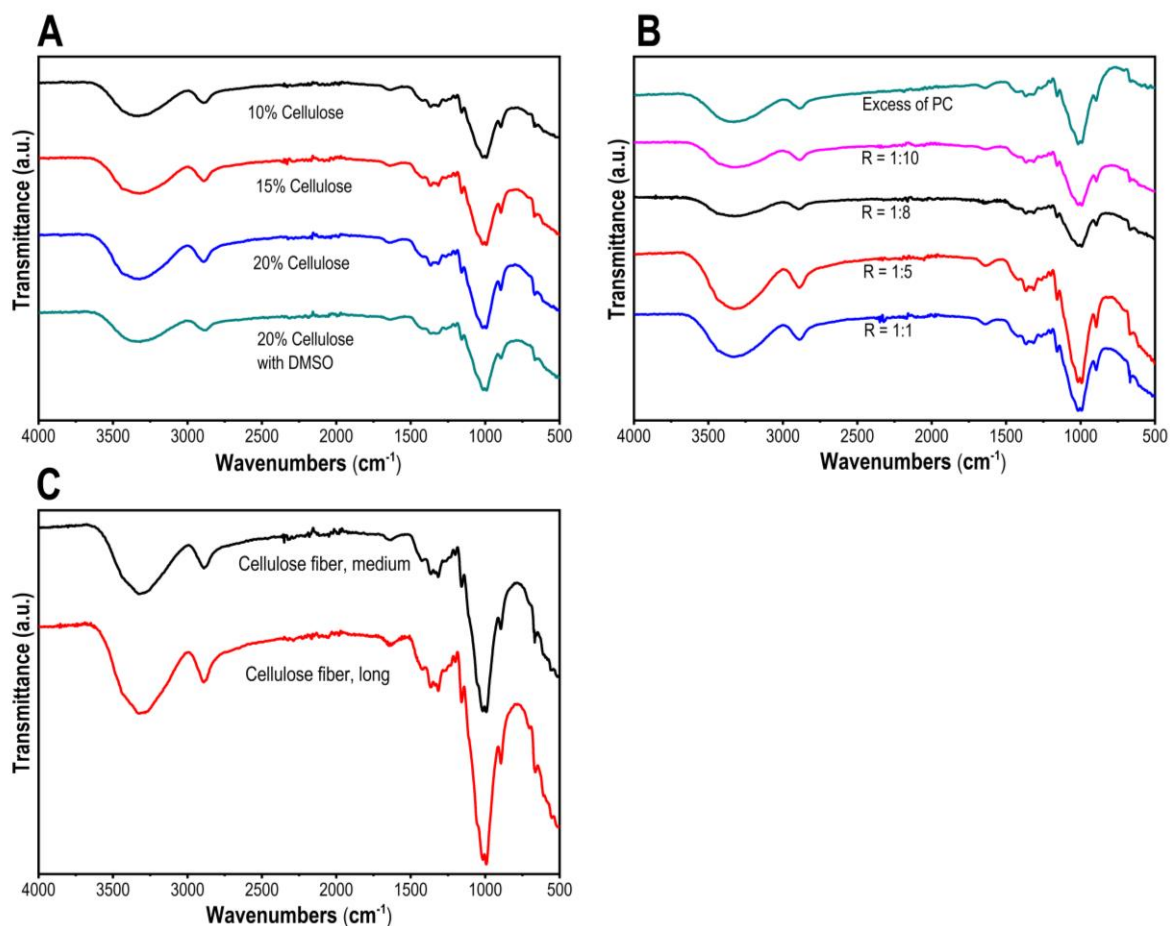


**Figure 44.** FT-IR spectra of RC powder with (A) different amount of cellulose; (B) different ratio of PC; (C) different kind of cellulose material

### 3.3.3.2 Production, characterization and properties of RC films from microcrystalline cellulose

The spontaneous solidification of RC powder is the base for the application of this new technique to prepare the film. Indeed, the RC films can be produced by casting cellulose solution on a glass plate via hand casting or casting machine. Best quality was achieved by using an automated casting machine with the speed of knife is 5 mm s<sup>-1</sup> (Figure 45).

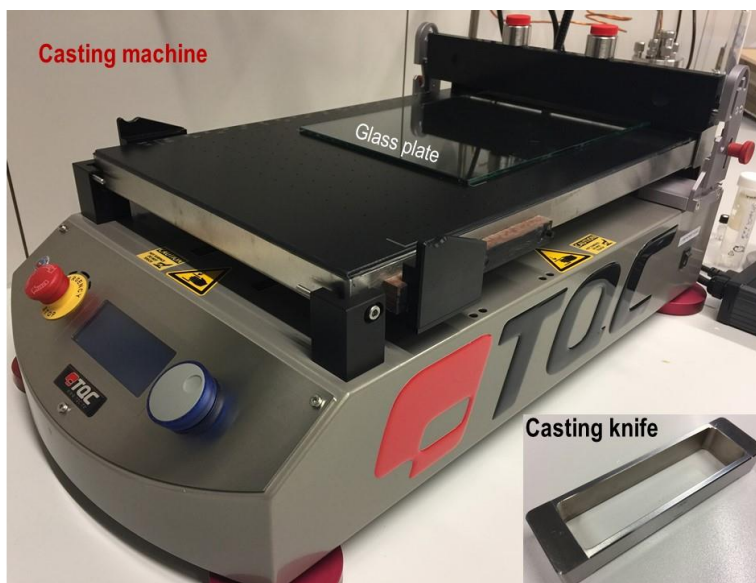


**Figure 45.** Casting machine with casting knife

Two important factors that influence the quality of the film are the amount of chemicals and the way to produce the film. The difference amount of cellulose and PC were tested together with the way the film is made (Table 6).

**Table 6.** The difference amount of cellulose and PC to produce the RC films

Sample	Cellulose (wt.%)	Molar ratio PC:TBPH 50 wt.%			
		1:1	5:1	10:1	Excess
1	5 wt.%	x	x	x	x
2	10 wt.%	x	x	x	x
3	15 wt.%	x	x	x	✓
4	20 wt.%	x	x	x	✓

✓ - Good surface; x - Not good surface

In fact, for the preparation of the RC films, the molar ratio between PC and  $[\text{OH}]^-$  is 1:1 based on the reaction between TBPH 50 wt.% and PC (Section 3.3.2 and Scheme 4). 1 ml of TBPH 50 wt.% ( $3.6 \text{ mol lit}^{-1}$ ) was used for dissolving cellulose. 0.152 ml PC with the concentration of  $11.8 \text{ mol lit}^{-1}$  had to be used for the occurrence of the coagulation process. However, it is impossible to immerse the casting cellulose solution in 0.152 ml PC to produce the RC films, even if the molar ratio of PC:TBPH increase to 10:1. Here, the casting solution was immersed in 250 ml of PC. The amount of PC is large enough to consume all amount of the  $[\text{OH}]^-$  added and to cover the entire surface of the casting solution.

With some advantages for the dissolution of cellulose, DMSO is added in cellulose solution as a co-solvent. Surprisingly, with the volume ratio 1:1 (TBPH:DMSO), the transparent film was obtained. Note that, the overall concentration of cellulose reduces from 20 wt.% to 10 wt.%. The RC film produced with DMSO containing 10 wt.% of cellulose is more stable than RC film containing the same amount of cellulose without DMSO.

For the preparation of the RC film, there are several possibilities to dip the casting cellulose solution into the PC bath (Figure 46). Because of the solidification within seconds, the surface of the RC film was not good with method 1, 2 and 3. The amount of PC was not high enough for the solidification. The best condition is to dip the glass plate with casting cellulose solution in upside down direction (Method 4). When the cellulose solution comes into contact with the PC bath, the surface will change to solid state.

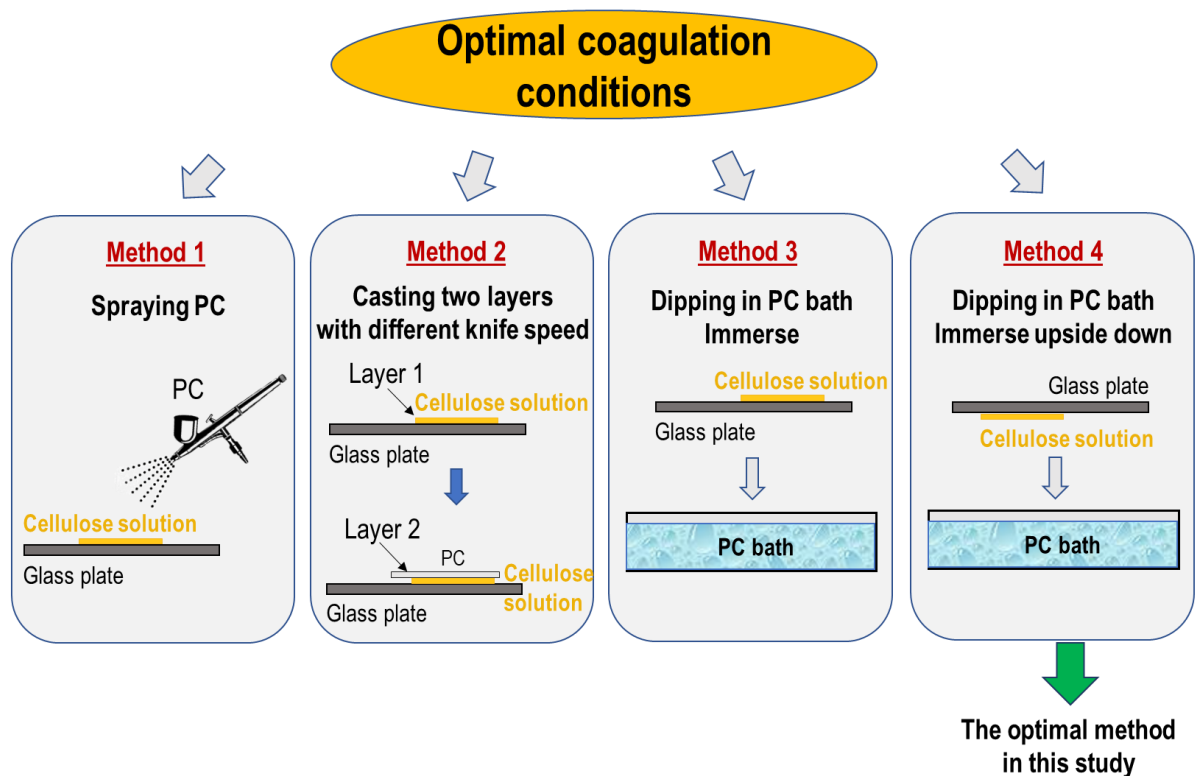


**Figure 46.** Optimal coagulation conditions to form the RC film

To obtain the film with high quality of shape by visual observation, the optimal condition was chosen: 20 wt.% cellulose is dissolved in TBPH 50 wt.%, and then is dipped upside down into the PC bath. Two different types of RC film were produced (Figure 47). RC film produced from 20 wt.% cellulose in TBPH 50 wt.% without DMSO (tagged RC film 1), and RC film produced

from 20 wt.% cellulose in TBPH 50 wt.% with DMSO (tagged with RC film 2) were investigated. For the latter, the volume ratio between DMSO and TBPH was 1:1. The repeatability of the preparation of the RC films is generally quite good. The RC films can be prepared many times without changing their properties.



**Figure 47.** RC film 1 (without DMSO), left and RC film 2 (with DMSO), right

The chemical structure as well as the macroscopic structure and mechanical properties of both RC films were investigated in more detail. From this information, an application of these films can be visualized.

#### 3.3.3.2.1 Characterization

The chemical composition (by IR spectroscopy) and the diffraction pattern (by XRD) of both RC films were not different from the RC powder mentioned before. Cellulose structure did not change during the dissolution and regeneration (Figure 48).

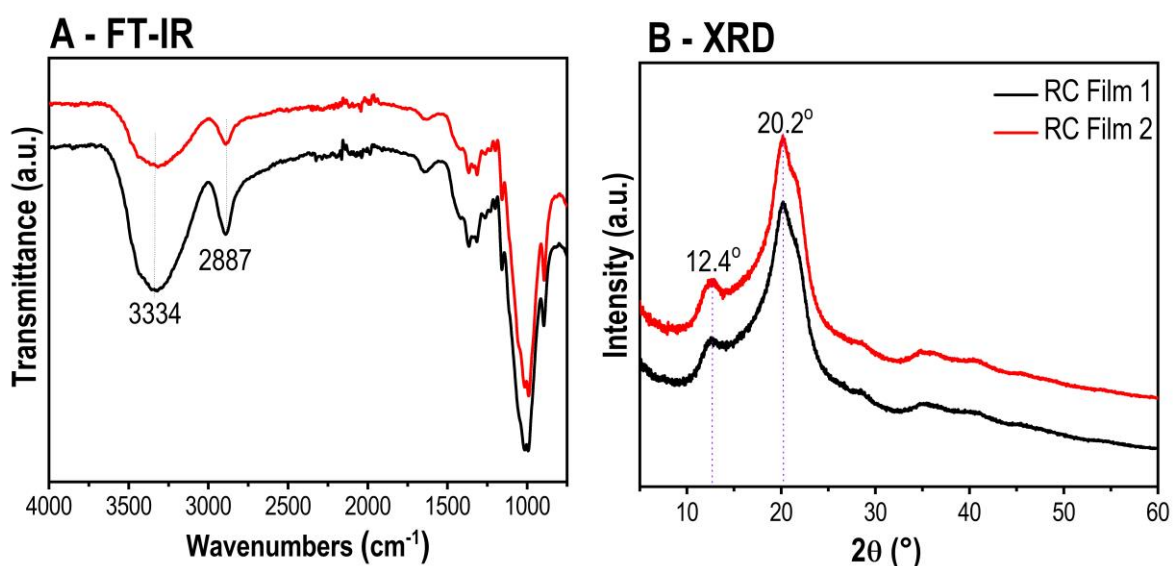


**Figure 48.** Characterization the films by IR spectroscopy and XRD

The same observation was proven by thermogravimetric analyzes (TGA) which verify the thermal stability before and after cellulose regeneration, as shown in Figure 49.

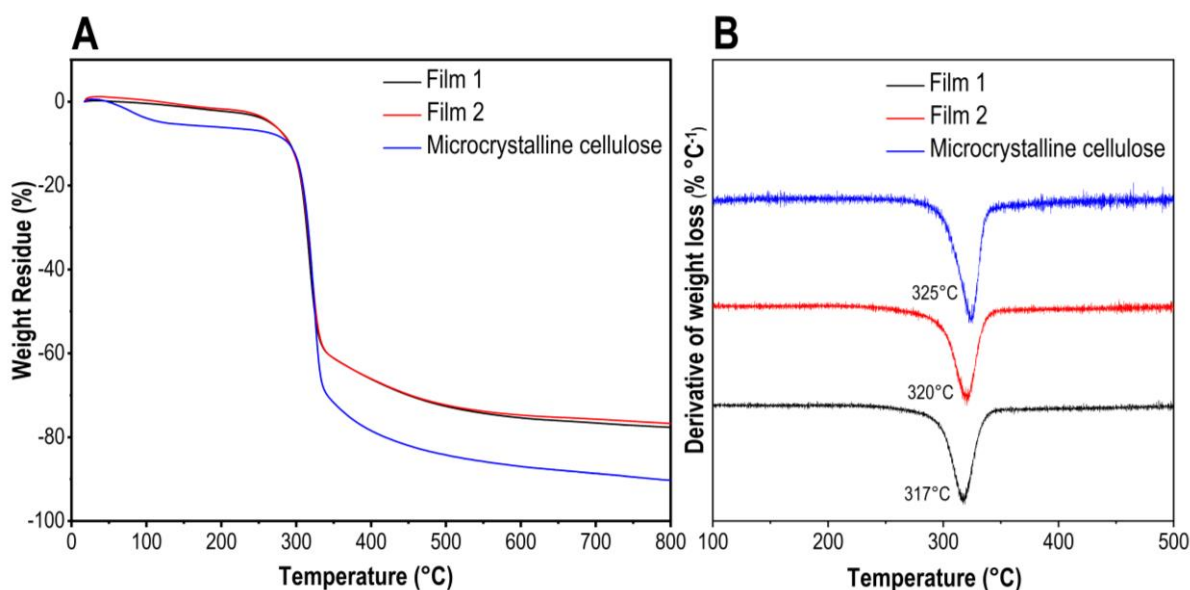


**Figure 49.** Thermal gravimetric analysis of RC films and microcrystalline cellulose

The thermal decomposition of the samples was investigated from 20 °C to 800 °C. It can be divided into two major weight loss stages, corresponding to the slow pyrolysis and fast pyrolysis stages.<sup>[108]</sup> At the early and slow pyrolysis stage of the curve (from 20 °C to 250 °C), weight loss is mainly due to the volatilization and vaporization of moisture from the cellulosic samples. The mass of regenerated cellulose changed continuously in that temperature range due to lower intermolecular forces and hydrogen bonding after the regeneration process. Fast

pyrolysis occurred at 250 °C to 350 °C. Further weight loss was relatively fast, which was associated due to continuous decomposition of the cellulose chain. From the thermograms, it can be seen that the microcrystalline cellulose and RC samples start to decompose at 271 °C and 294 °C, respectively. The temperature at the maximum degradation rate did not differ significantly between microcrystalline cellulose (325 °C) and the regenerated cellulose films (317 °C for film 1 and 320 °C for film 2).

To shed further light on structural differences between RC film 1 (non-transparent) and RC film 2 (transparent),  $^{13}\text{C}$ -NMR experiments in the solid-state under magic-angle spinning (MAS) and dynamic nuclear polarization (DNP) were performed on frozen and wet films (Figure 50 and Figure 51). An enhancement of 25 and 18 was achieved with DNP enhancement spectra of RC film 1 and RC film 2, respectively.

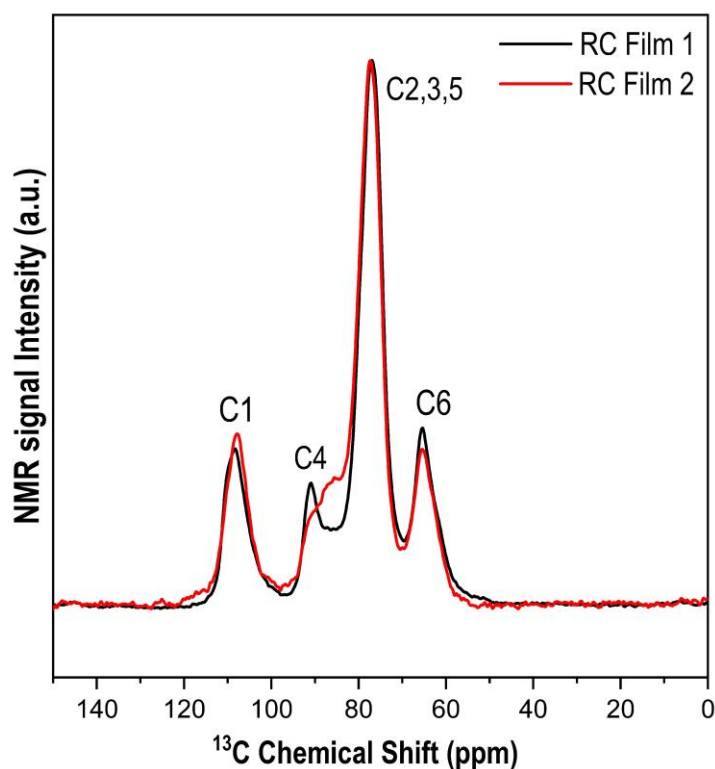


**Figure 50.**  $^1\text{H}$ - $^{13}\text{C}$  Cross Polarization (CP) MAS NMR spectra under DNP at 110 K. Spectra have been scaled to the same signal intensity

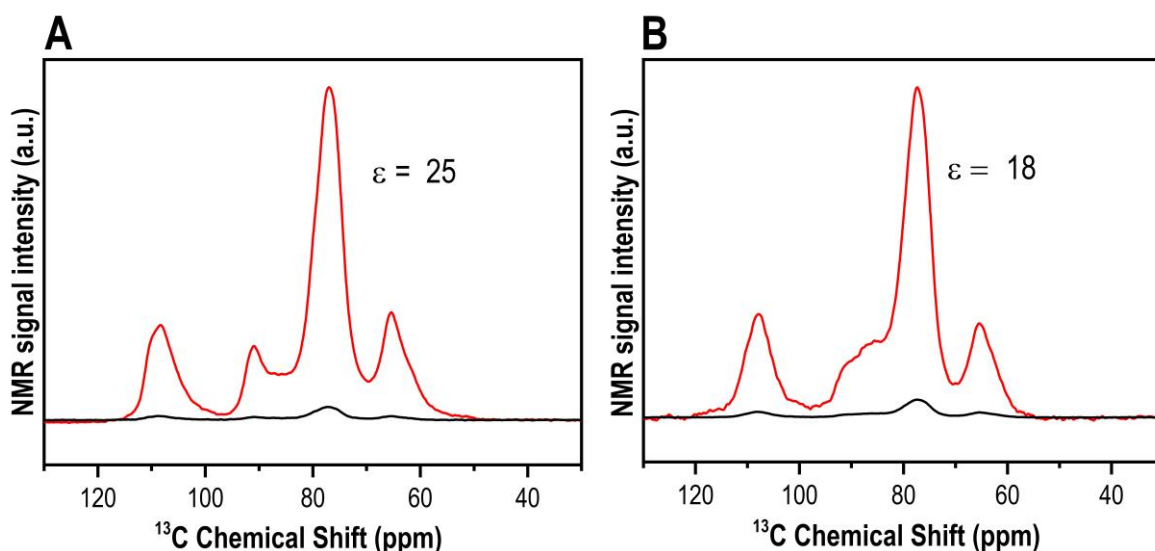


**Figure 51.** DNP enhancement spectra of RC film 1 (A) and RC film 2 (B). Black without microwave irradiation, red with microwave irradiation

The results show significant differences in the spectral distribution of the glucose-linking residues C1 and C4. A significant fraction of the residue C4 of RC film 2 is shifted up-field away from the resonance signal of bulk crystalline cellulose indicating a larger number of surface-accessible sites <sup>[109]</sup>. In contrast, RC film 1 shows a major contribution from crystalline cellulose. Solid-state NMR measurements of wet films as well as of dried samples under ambient conditions confirm this tendency (Figure 52). These variations in surface-to-bulk ratio are correlated with the transparency of RC film 2 and opacity of RC film 1.

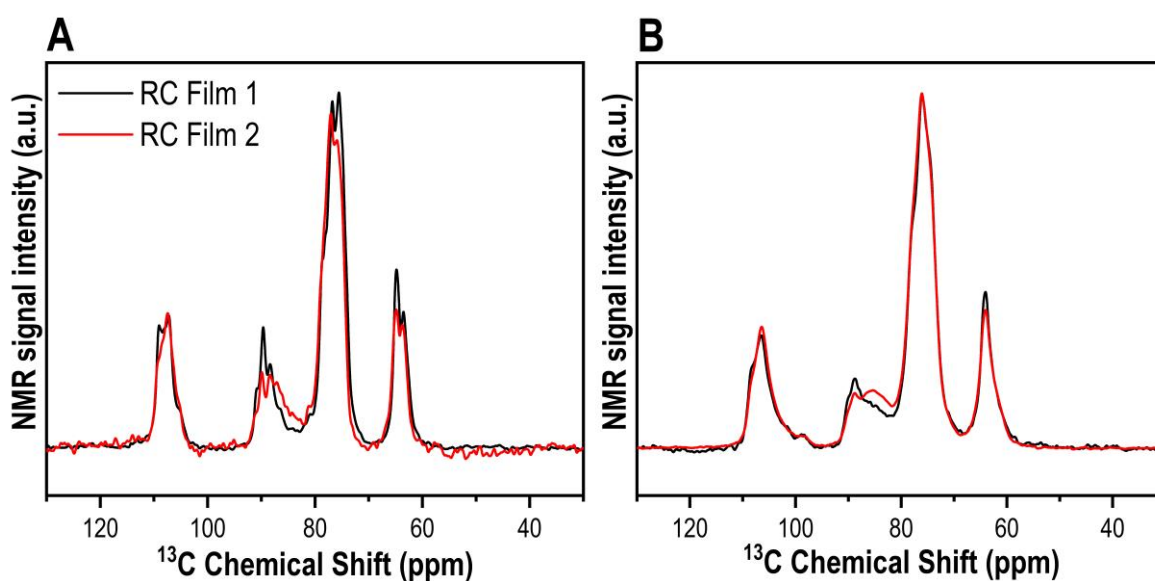


**Figure 52.** <sup>1</sup>H-<sup>13</sup>C Cross Polarization (CP) MAS NMR spectra of RC film 1 and RC film 2 in wet (A) and dried phase (B)

Next the quality of the RC films was investigated by LS-NMR. These RC films were dissolved in TBPH 50 wt.% (Figure 53). The internal standard (dioxane) is tagged with a \*.

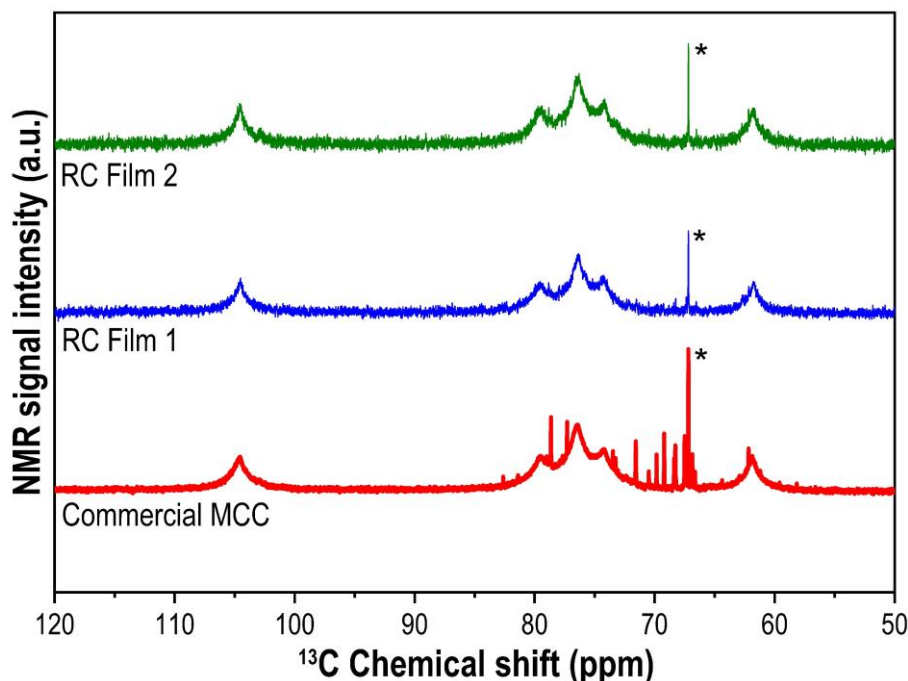


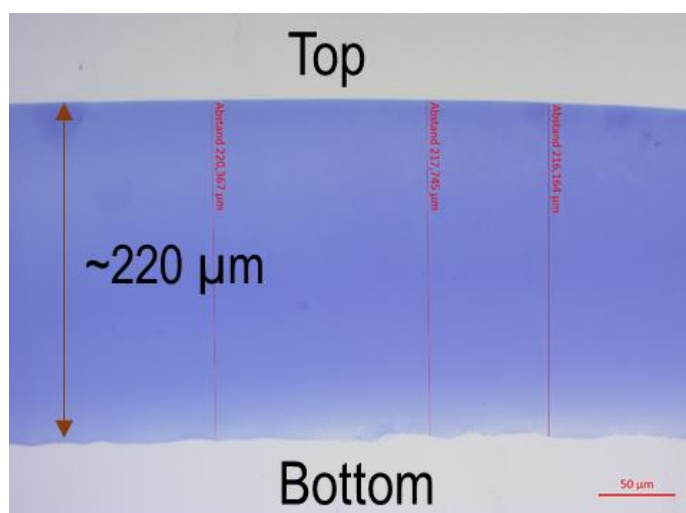
**Figure 53.** LS- $^{13}\text{C}$  NMR spectra of the produced RC films 1 and 2 and commercially microcrystalline cellulose

The sharp signals are observed in commercially microcrystalline cellulose spectra corresponding to small sugar impurities. However, dissolution in TBPH and coagulation with PC resulted in the production of high pure RC films. No signals of the impurities are detected. The obtained RC films has the same high purity as the RC powder discussed above (section 3.3.3.1). Thus, purification takes place by the MDCell method.

### 3.3.3.2.2 Properties

The detection of amorphous, surface-accessible sites was a strong motivation for the investigation of the surface morphology of the films. Applying Light microscopy, Transmission Electron Microscopy (TEM), Scanning Electron Microscopy (SEM), and Atomic Force Microscopy (AFM), the structure of the films was investigated regarding the macroscopic and microscopic structure and topography.

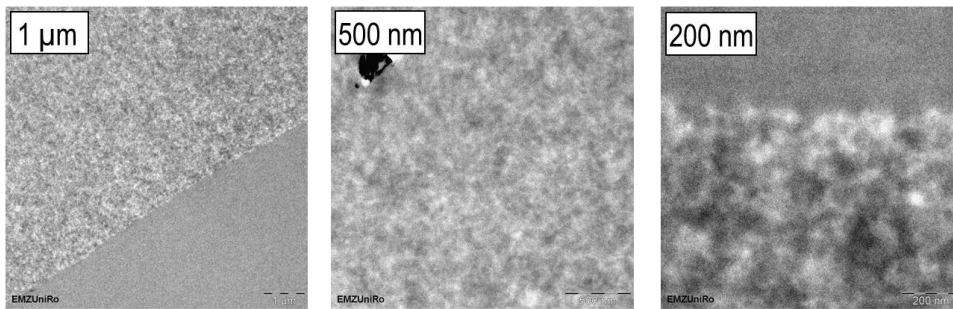
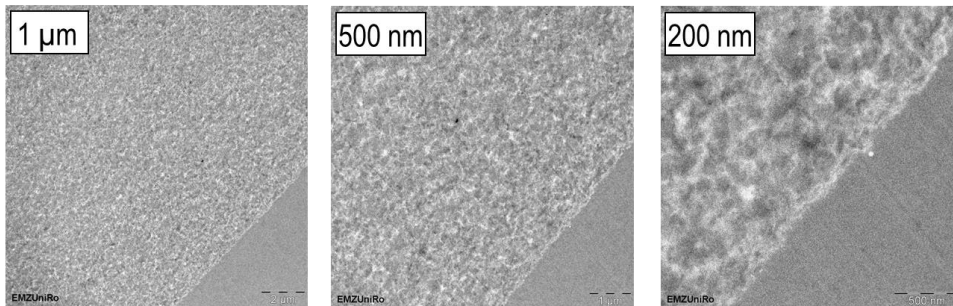
First, the wet film was inspected by light microscopy of a 500  $\mu\text{m}$  section of RC film 2 stained with Toluidine blue (Figure 54).



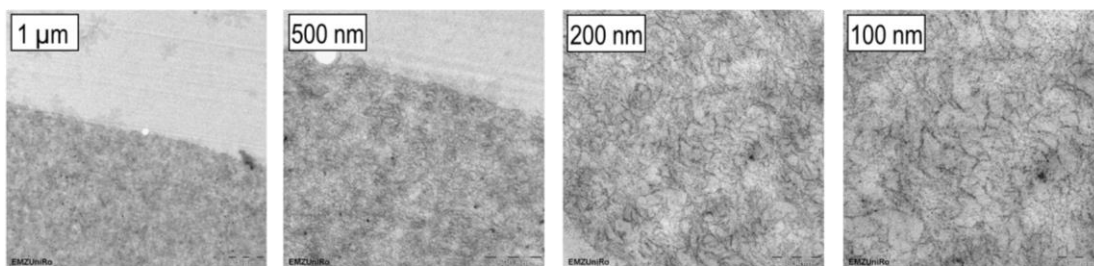
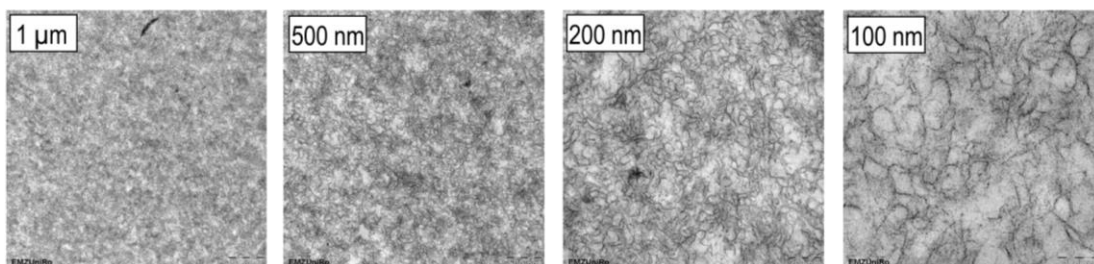
**Figure 54.** Light microscopic image of a semithin cross section

Here, a homogeneous distribution of the toluidine blue over the entire size of regenerated cellulose was detected. The thickness of the films decreased from 500  $\mu\text{m}$  (casing solution thickness) to around 200  $\mu\text{m}$ . It means a shrinkage process of the layer is 55 % due to the formation of regenerated cellulose. No capillary pores were visible. Only tiny differences in the density and roughness of the top and bottom side of the film can be observed which are probably from the casting solution on the glass surface.

To obtain more detailed information about the surface morphology, the standard TEM was applied by embedding the films without contrast (Figure 55). The films have a smooth surface, however, no difference in structure or any pore were observed.

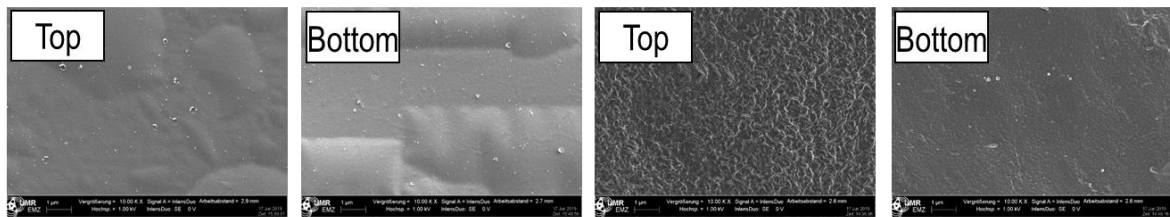
**RC film 1****RC film 2****Figure 55.** TEM analysis with uncontrasted films

Then, to visualize the cellulose microfibrils, iTEM camera control and imaging software were used with contrast reagents such as lead citrate and uranyl acetate in subsequent high resolution TEM imaging (Figure 56).<sup>[110]</sup> The lead sticks to the cellulose films and thus enable a very sensitive detection of the fibrils. Here an irregular, net-like structure of branched microfibrils was perceivable, with a size of the net meshes in the range of approx. 30-100 nm.

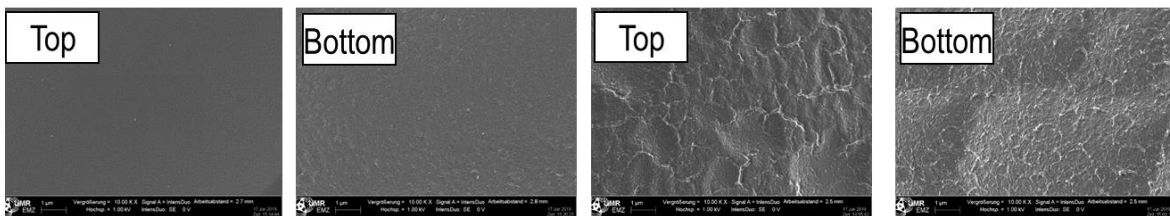
**RC film 1****RC film 2****Figure 56.** High resolution TEM of cellulose microfibrillary after contrasting of thin sections (approx. 50 nm) contrasted with uranyl acetate and lead citrate

Next, the surface and cross-sectional morphology were examined by using SEM. SEM analysis for surface measurement was carried out under air dried condition and freeze-dried conditions to measure the top and bottom surface of RC film 1 and RC film 2 (Figure 57). The advanced SEM measurement under freeze-dried condition were performed to gain more information about the pore size and structure under real conditions.

### RC film 1



### RC film 2



Air-dried films

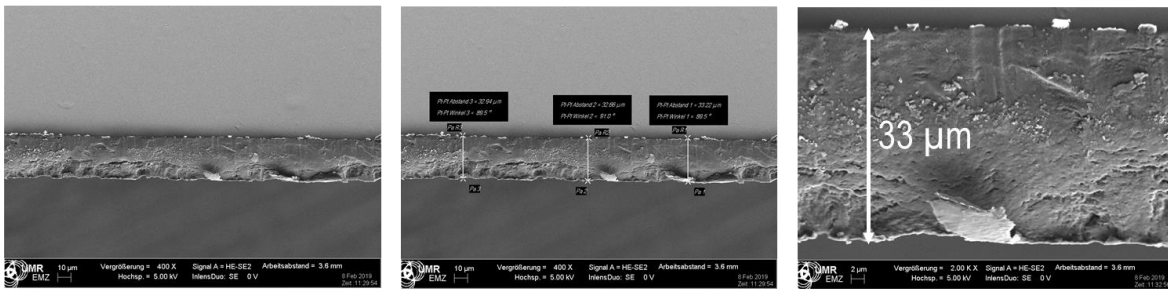
Freeze-dried films

**Figure 57.** SEM analysis of top and bottom surface of the air-dried and freeze-dried films

The top surface is the side directly in contact with the coagulant PC and the bottom surface is the side in contact with glass plate. Under air dried condition, these results reveal a very smooth surface and dense texture. However, the surface observations did not display an image of the pore because of the significant shrinkage of the membrane during air drying. Drying in air reduces size of the film by 25,11 % and 21,74 % area for the film 1 and 2, respectively, to compare with the film in wet condition.

For cross-sectional morphology, the air-dried film was cut through showing the thickness of the films. The SEM images of the cross-section RC films are depicted in Figure 58. The film thickness of RC film 1 (without DMSO) decreases from 500  $\mu\text{m}$  to 33  $\mu\text{m}$  and even to 20  $\mu\text{m}$  of RC film 2 (with DMSO) It means the shrinkage process of the film's thickness under air drying is almost 95 %.

## RC film 1



## RC film 2

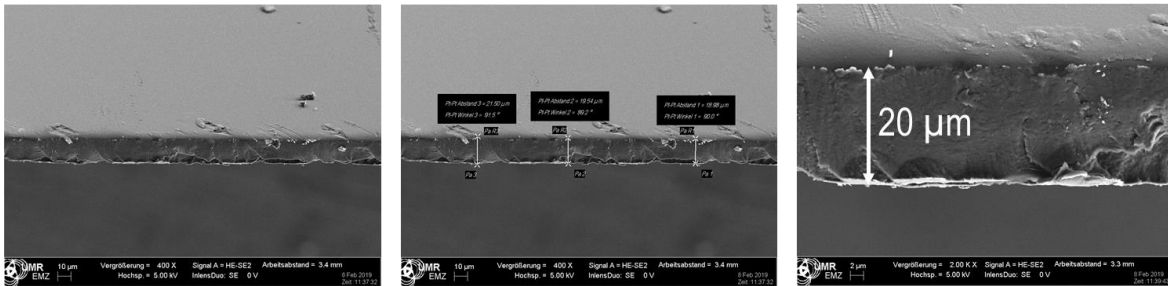


Figure 58. SEM cross section image of RC films

Interestingly, a film 2 was frozen in liquid nitrogen, then directly bend and broken. The RC film exhibited multiple uniform layers arranged in parallel under scale bar 200 nm by SEM analysis (Figure 59).

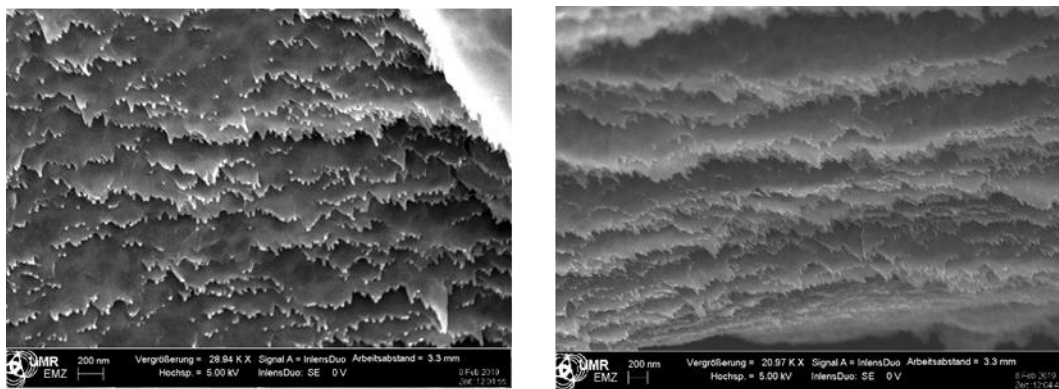
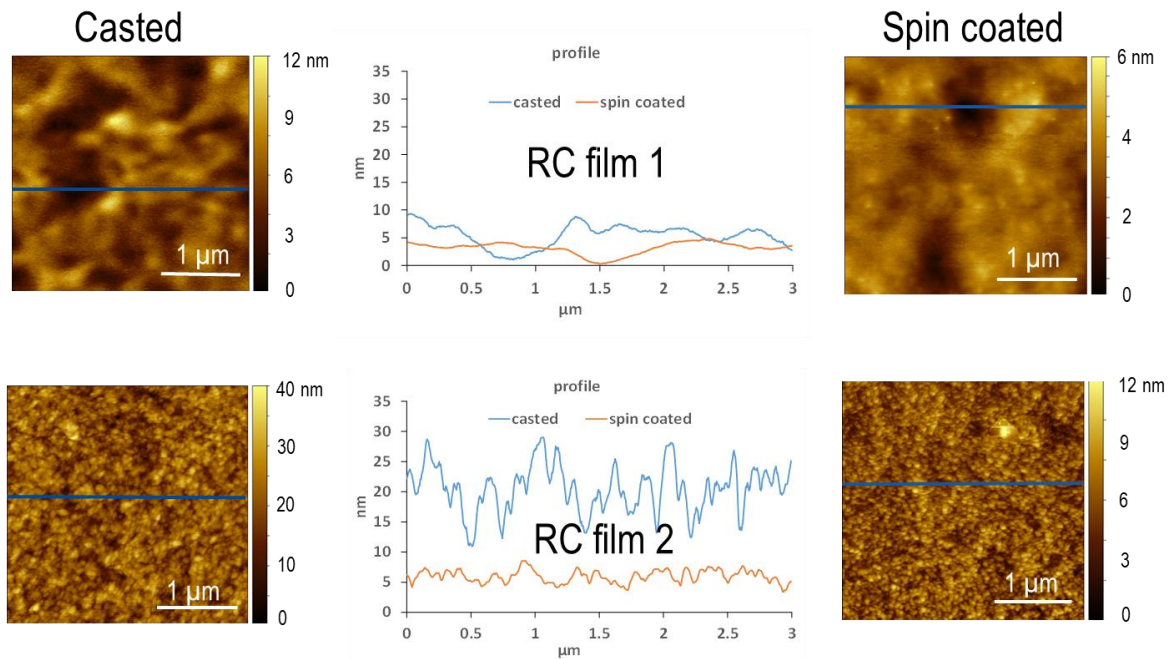


Figure 59. SEM analysis layer of freeze-dried film 2

In summary, the films produced consist of a compact, very uniform, dense but layered structure. Each layer has a microfibril structure with a size of the net meshes in the range of approx. 30-100 nm. No pore was detected.

To measure the surface roughness, the dry films were investigated by AFM (Figure 60). The films were prepared by the casting technique (TQC casting machine with film thickness

500  $\mu\text{m}$ ) as well as by spin coating (Polos spin coater with film thickness  $<1 \mu\text{m}$ ) and dried afterwards in air.



**Figure 60.** AFM of casted and spin coated RC film 1 and 2

These experiments revealed a very smooth surface with low average surface roughness of only  $R_a \approx 3 \text{ nm}$ . All results indicate a fast and homogeneous penetration and reaction with PC.

After investigating the structure, both films were utilized both as membranes. All the experiments were carried out by the home-made filtration system (Figure 61).

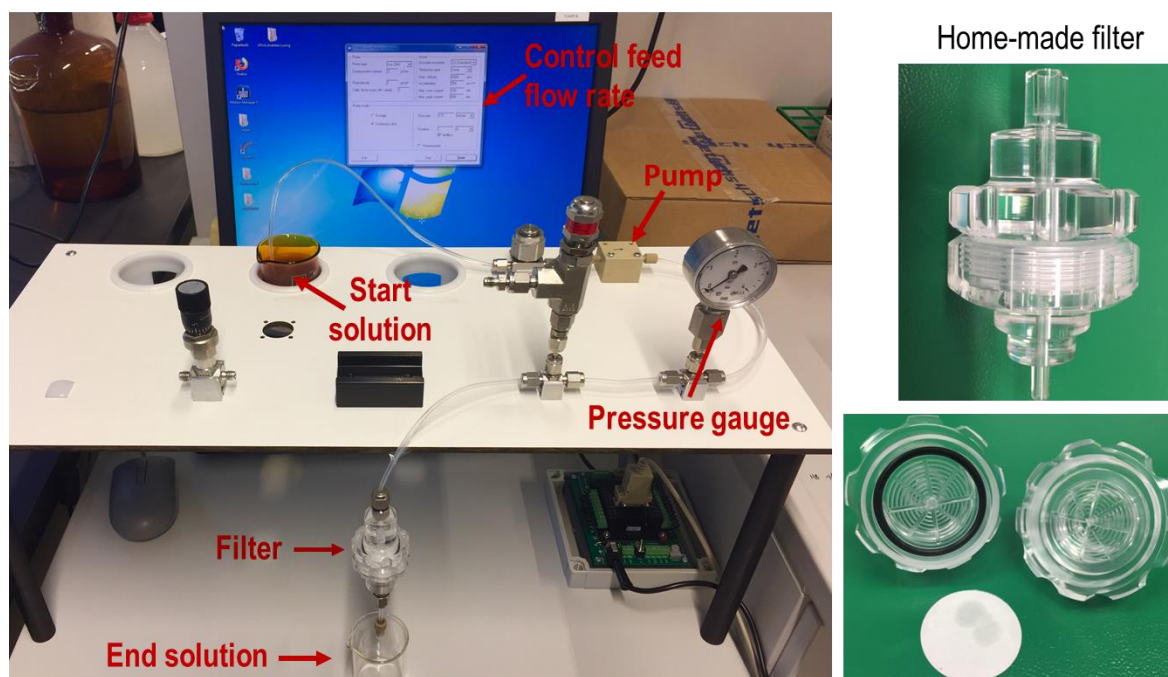


**Figure 61.** Home-made filtration system

First, the water flux of both synthesized films was investigated (Figure 62). In general, the water flux is affected by the porosity and amount of pores in the membranes.<sup>[111]</sup> Thus, the water flux at several differential pressures was measured showing an increased water flux between  $4.75 \pm 0.11$  (at 0.52 bar) to  $14.51 \pm 0.06$  L h<sup>-1</sup> m<sup>-2</sup> (at 2.2 bar) for RC film 1. Interestingly, a higher water flux for RC film 2 was detected. The resulting water flux raised from  $10.56 \pm 0.04$  L h<sup>-1</sup> m<sup>-2</sup> (at 0.48 bar) to  $17.63 \pm 0.1$  L h<sup>-1</sup> m<sup>-2</sup> at 1.08 bar over pressure. The resulting permeability was  $7.22 \pm 0.88$  L m<sup>-2</sup> h<sup>-1</sup> bar<sup>-1</sup> for RC film 1 and  $18.55 \pm 2.47$  L m<sup>-2</sup> h<sup>-1</sup> bar<sup>-1</sup> for RC film 2. The nearly three-fold higher permeability of RC film 2 compared to RC film 1 is due to the dilution of cellulose by DMSO.

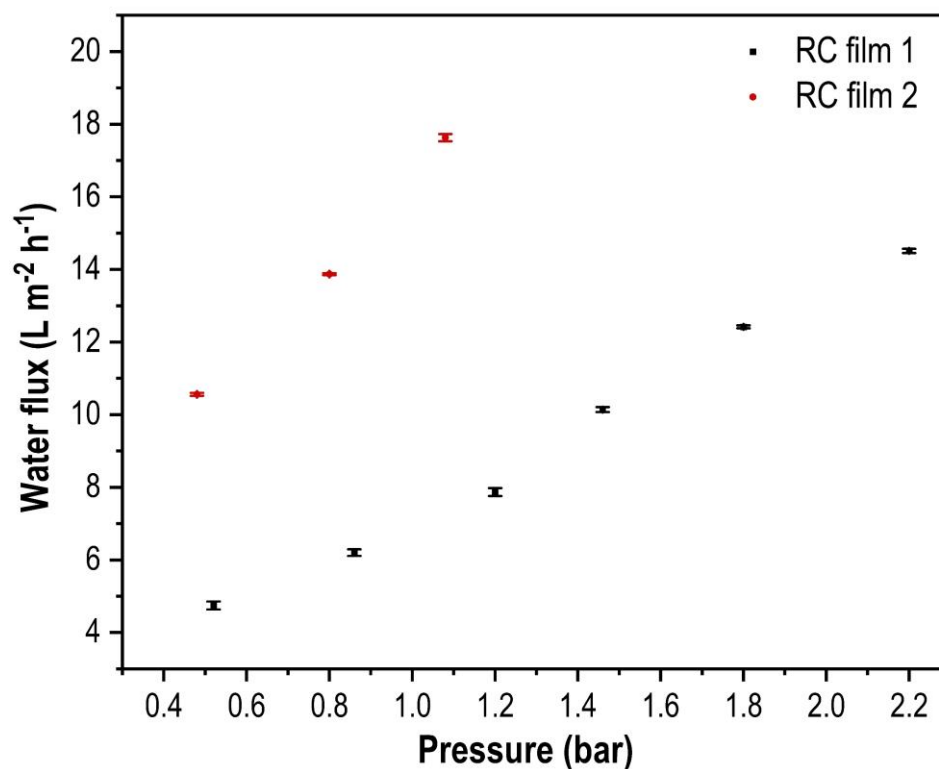


**Figure 62.** Water flux through RC films as a function of water pressure

Next, the identification of the pore size was carried out using polyethylene glycol (PEG) as molecular probes.<sup>[112]</sup> The molecular weight of PEG (from 1000 to 1000000 g mol<sup>-1</sup>) is correlated to its Stokes–Einstein diameter as shown in the Table 7.<sup>[113]</sup>

**Table 7.** Molecular weight and solutions diameter of the polyethylene glycol series

No.	Name	Molecular weight	Diameter average
		Mw (g/mol)	d (nm)
1	PEG 1000	950 - 1050	0.16
2	PEG 6000	5000 - 7000	0.43
3	PEG 8000	8000	0.50
4	PEG 35000	28000 - 38000	1.14
5	PEO 200000	200000	27.00
6	PEO 400000	400000	40.56
7	PEO 1000000	1000000	69.46

The initial concentration was 2000 ppm. PEG concentrations after going through the films are determined by injecting PEG samples into a HPLC system without column (Figure 63). The signal is detected by RI detector with retention time (10 min). The flow rate of eluent is 0.1 ml min<sup>-1</sup>. For each sample an average value of 4 injections is used to determine the average PEG concentration.

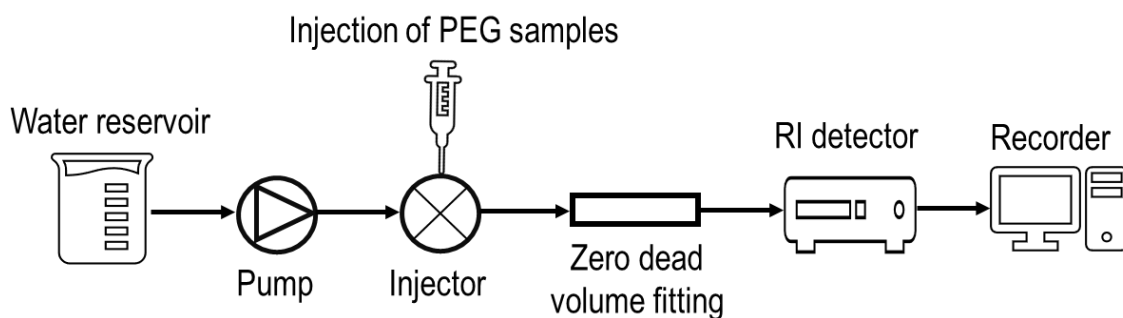


**Figure 63.** Apparatus used to measure PEG concentration after going through RC films

In fact, both films have nearly the same pore distribution of 10 - 70 nm. Since no capillary pores are presented, the filtration ability is restricted by the interlayer space of the microfibrils detected by TEM and SEM. The best retention was achieved with polyethylene oxide (PEO) 1000000 (molecular probe diameter of 69.46 nm). The rejection of 92 % (RC film 1) and 82 % (RC film 2), respectively, identify the molecular weight cut-off for both films. This opened up the application of these films as micro- and ultrafiltration membranes.

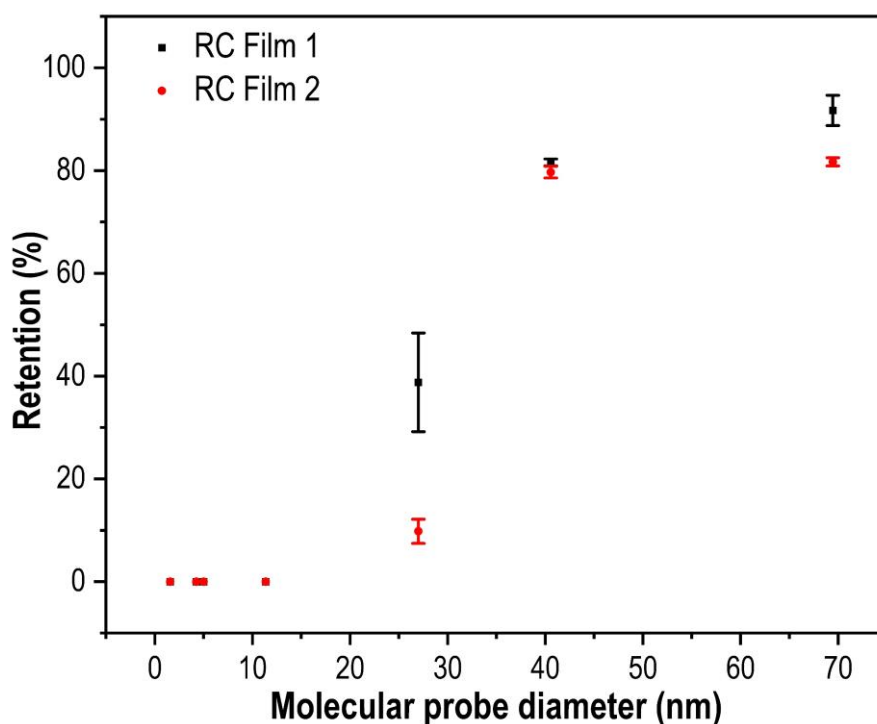


**Figure 64.** PEG retention of the films at a PEG concentration 2000 ppm (1.5 ml min<sup>-1</sup> of feed flow rate, 1 bar pressure, 5 ml of volume sample)

Next, the mechanical durability of the films was investigated based on the hydraulic pressure of the flow through the film (Figure 65). RC film 1 was destroyed at a pressure 2.5 bar corresponding to the flow rate 4.5 ml min<sup>-1</sup>. Meanwhile, RC film 2 was broken at a pressure

1.4 bar corresponding to the flow rate  $2.5 \text{ ml min}^{-1}$ . This result indicated that RC film 1 is more stable than film 2 due to the higher concentration of cellulose in RC film 1. Two RC films also were tested for stability under the influence of pH. They were immersed in acid media ( $\text{pH} = 3$ , the dash dot line) and basic media ( $\text{pH} = 10$ , the dot line) for 2 days. The hydraulic pressure was comparable with the fresh RC films, showing a high storage stability in these media. Due to structural changes in the films, the load-bearing capacity of the films reduces under changing conditions of pH. However, this change was not significant.

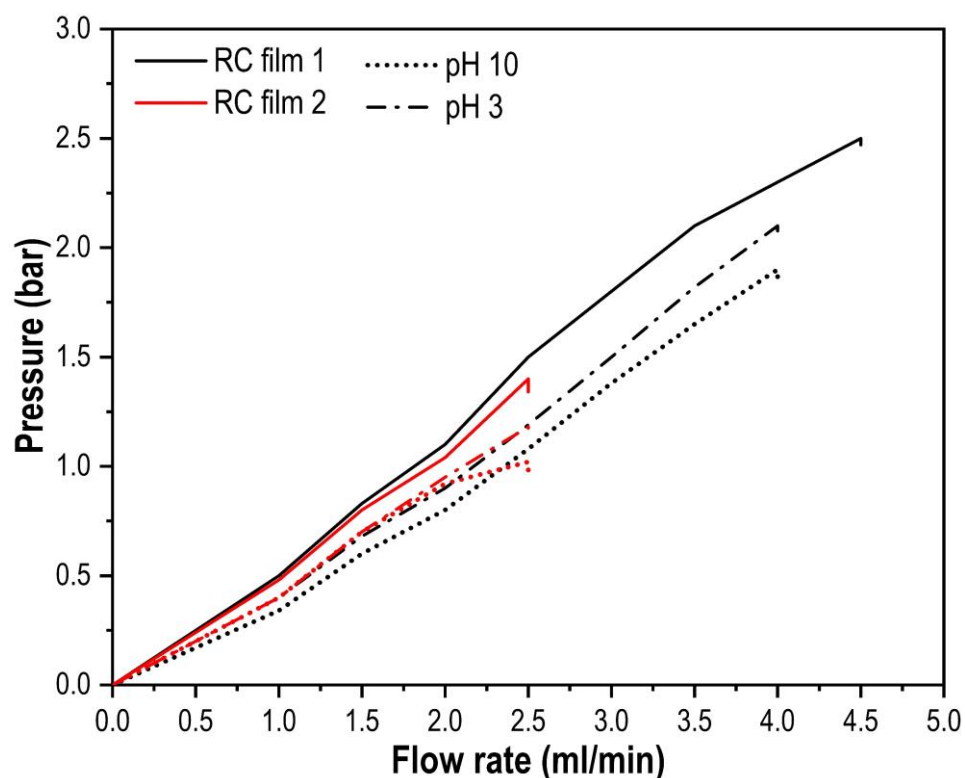


**Figure 65.** The stability test of the RC films

The materials properties show a high dependence on the presence of DMSO during the coagulation process. On the one hand, DMSO reduces the surface tension,<sup>[68]</sup> which allows a fast diffusion of PC and thus a quicker coagulation. This can lead to a bigger distance between the fibrillar structures in this material,<sup>[114]</sup> which is indicated by the triple higher permeability as well as a larger pore distribution compared to RC film 1. The weaker interaction and the higher porosity are responsible for the lower stability.

As a final assessment of their properties, the surface charge of the RC films was investigated. The surface charge at the solid/water interface determines the electrostatic interaction between the solid surface and dissolved components in the aqueous phase. It changes upon

dissociation of surface functional groups or adsorption of ions. The surface charge and its changes are described by the zeta potential. The zeta potential is an important parameter to describe solid surface and their interaction with the surrounding liquid. Here, for the RC film 2, a negative zeta potential  $\zeta = -21$  mV (between pH 5-9) was detected (Figure 66). Indeed, the induced polarization at the membrane surface may correspond to a sorption of negative hydroxyl ions or to partially ionization via the positive charged [TBP]<sup>+</sup> cation. As a consequence, the RC films have a possibility to adsorb the positively charged ones.

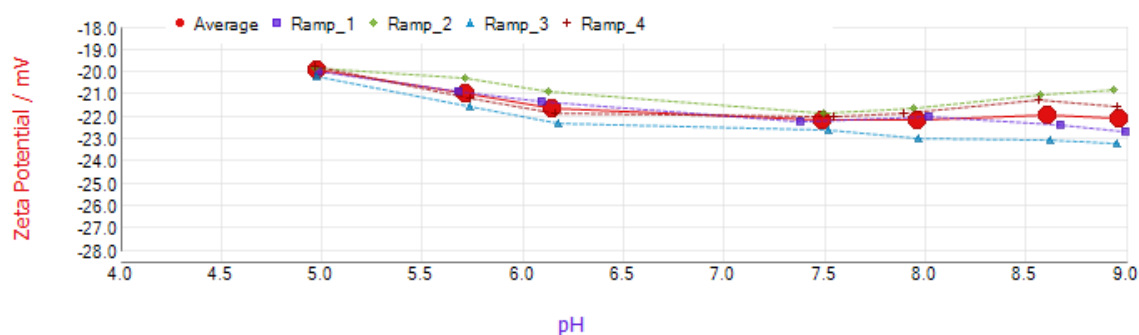
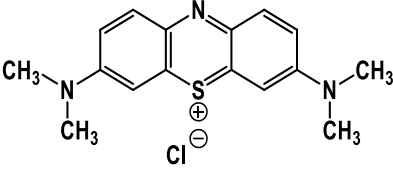
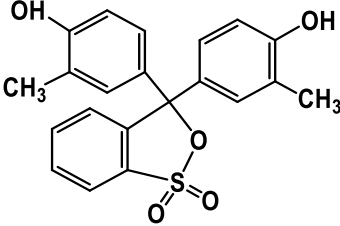
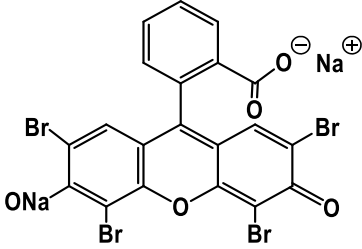
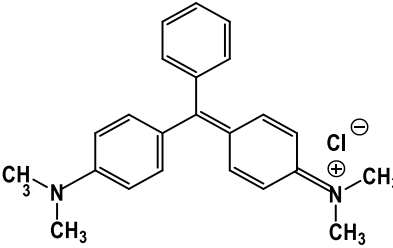
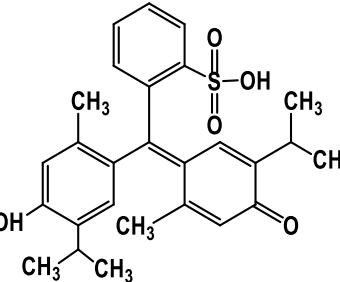
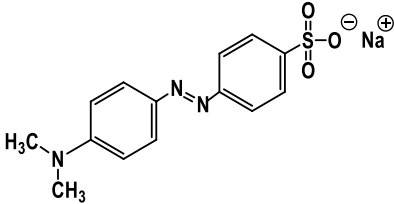


Figure 66. Zeta potential of regenerated cellulose film 2

### 3.3.3.3 Application of the RS films as separation media

Due to a negatively charged surface, the RC films have a high selectivity towards retention of positive charges. This property was applied for the removal or separation of dyes. This could be relevant for the purification of wastewater from textile industry. Six organic dyes with different charges were selected, which are classified with negative charges (Eosin Y disodium salt - EY, Methylene orange - MO), neutral charges (Cresol red - CR, Thymol blue - TB) and positive charges (Methylene blue - MB, Malachite green - MG) (Table 8).

**Table 8.** Schematic structural illustration of the six organic dyes with different charges

Positive charges	Neutral charges	Negative charges
		
Methylene blue	Cresol red	Eosin Y disodium salt
		
Malachite green	Thymol blue	Methylene orange

The pH of organic dye solutions in this range of pH is shown in Table 9.

**Table 9.** pH of organic dye solutions

Positive charge	Neutral charge	Negative charge
Methylene blue pH = 6.76	Cresol red pH = 5.42	Eosin Y disodium salt pH = 7.57
Malachite green pH = 5.01	Thymol blue pH = 5.45	Methylene orange pH = 5.38
pH of ultra-pure water = 6.40		

Using continuous flow online UV-Vis spectroscopy, online detection of the dyes was performed using homemade filtration equipment connected to a micro-flow cell (Avantes) (Figure 67). The concentration of start solution is 10 ppm. This solution goes through the membrane and is detected continuously by UV-Vis spectroscopy.

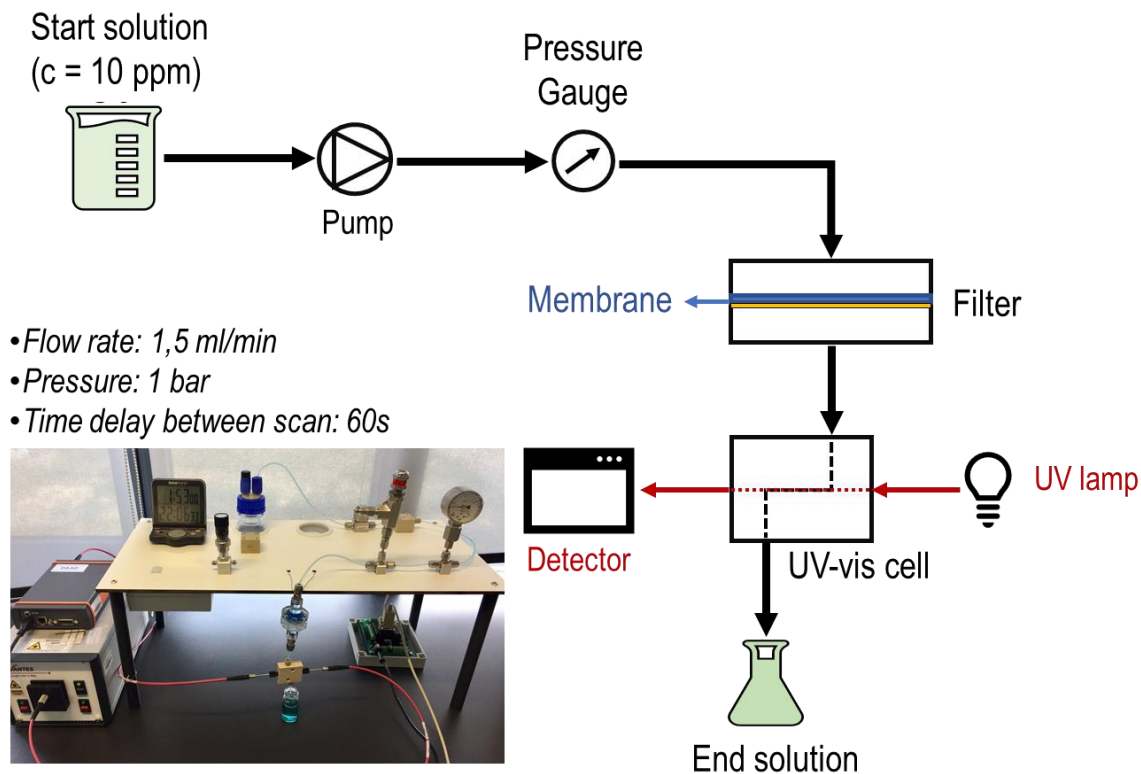


**Figure 67.** Online UV-Vis measurement system with continues flow

In principle the process of penetration and filtration depends on the diffusion of the molecules to the boundary of the membrane, then diffusion into the membrane surface and finally, they diffuse into the porous structure. These processes always depend on the pore size, pore structure and the chemical structure of the surface and membrane, adsorption and desorption capability of the membrane and finally on the surface charge.

Negatively charged and neutral dyes (Figure 68A - Figure 68D) can penetrate without barriers through the cellulose microfibrils, the change in adsorption occurred immediately. The equilibrium was reached after 20 to 40 minutes. The fast adsorption rate at the initial stage may be explained by an increased availability in the number of active binding sites on the adsorbent surface. The sorption rapidly occurs and is normally controlled by the diffusion process from the bulk to the surface. In the later stage, the sorption is likely an attachment-controlled process due to less available sorption sites. Positively charged dyes are retained and delayed by both RC films (Figure 68E and Figure 68F). Equilibrium concentration of RC film 1 and 2 was reached after more than 16 hours and 10 hours, respectively.

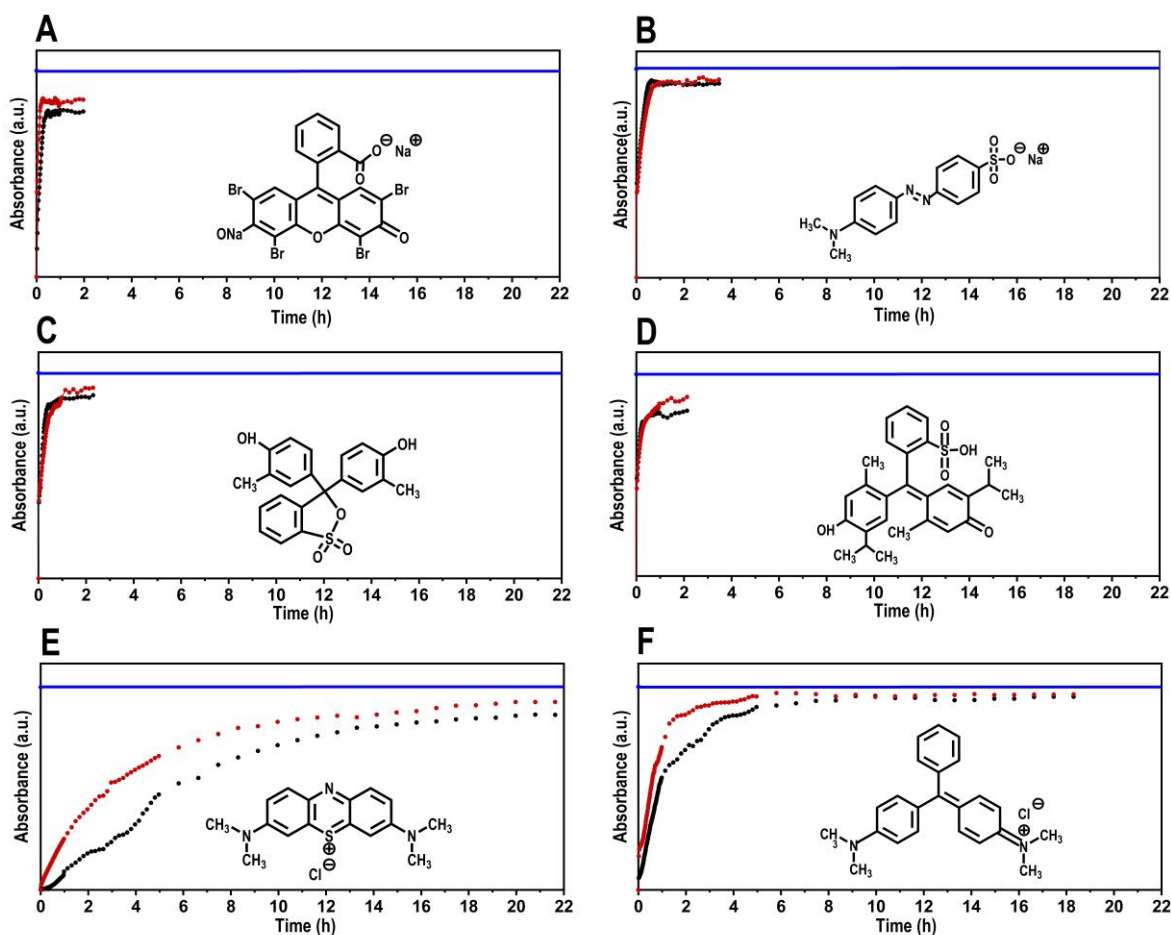


**Figure 68.** Online continuous flow UV-Vis spectroscopy for charged dyes. (A) Eosin Y disodium salt, (B) Methylene orange, (C) Cresol red, (D) Thymol blue, (E) Methylene blue, (F) Malachite Green. Blue line: Start solution ( $c = 10$  ppm). Black dots: absorbance after going through RC film 1. Red dots: absorbance after going through RC film 2

Taking into account the molecular size of the organic dyes, the interlayer distance of the detected microfibrils is much larger than the molecular size. For example, the length of a methylene blue molecule is  $13.82 \text{ \AA}$ ,<sup>[115]</sup> and the width is approximately  $9.5 \text{ \AA}$ . So, there is absolutely no retention by filtration.

The adsorption efficiency of RC films with increasing adsorption time and adsorption volume for the adsorbing MB dye (positive charge), CR dye (neutral charge) and EY dye (negative charge) are shown in Figure 69. It can be seen that both RC films allowed for high removal efficiencies with positive charges. These results indicate a strong adsorption effect and thus lead to a retention of the positively charged. Neutral and negative dyes were not adsorbed. Using 10 ml of MB solution, over 76.6 % and over 63.43 % of the MB was removed by RC film

1 and RC film 2 after 60 minutes, respectively. With 20 ml of organic dye solution, over 65.68 % and over 49.86 % of the MB was removed by RC film 1 and RC film 2 after 60 minutes, respectively. Note that, methylene blue removal after the adsorption process with the 10 ml volume of MB was 74.37 % for RC film 1 and 69.12 % for RC film 2 (Figure 68).

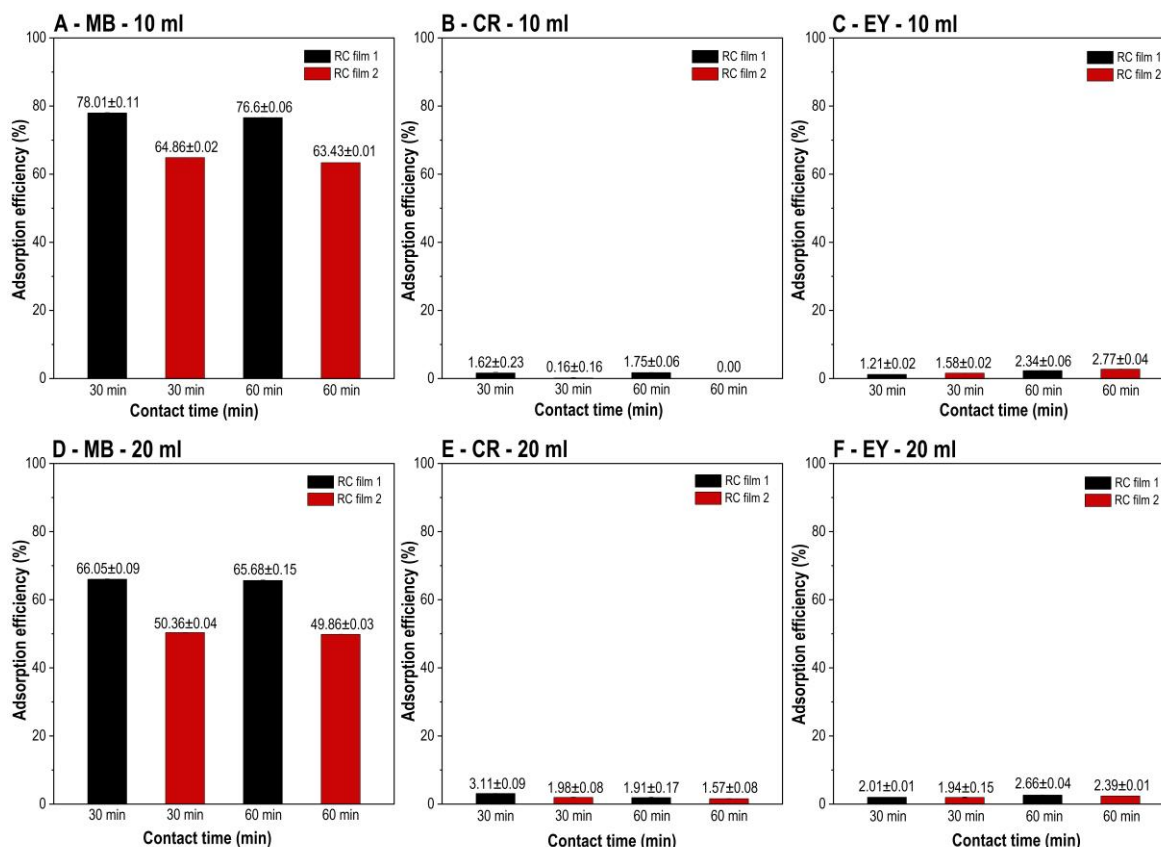


**Figure 69.** Adsorption efficiency of RC film 1 and 2. Initial organic dye concentration: 10 ppm; Amount of wet RC film 1:  $0.158 \pm 0.003$  g; Amount of wet RC film 2:  $0.136 \pm 0.006$  g; Volume of organic dye solutions: 10 ml and 20 ml

At the contact time of 30 minutes and 60 minutes with volume of 10 ml and 20 ml, the removal percentages of MB of RC film 1 and 2 is the same. This result indicates the full adsorption of MB. After 30 min, the adsorption processes the equilibrium of RC film 1 and 2 were achieved with  $78.01 \% \pm 0.11 \%$  and  $64.86 \% \pm 0.02 \%$ , respectively.

In principle, the positively charged dye is adsorbed on the membrane. When all positions are occupied, then the dye will pass completely through the membrane and reach the adsorption of the starting solution. In this case, the solution cannot reach the concentration of the starting solution after equilibrium adsorption. These phenomena could be due to the fact that at slow

permeate flow rates ( $0.054 \text{ ml min}^{-1}$  for RC film 1 and  $0.123 \text{ ml min}^{-1}$  for RC film 2) organic dye solutions were degraded by the UV-Vis light (Figure 70).

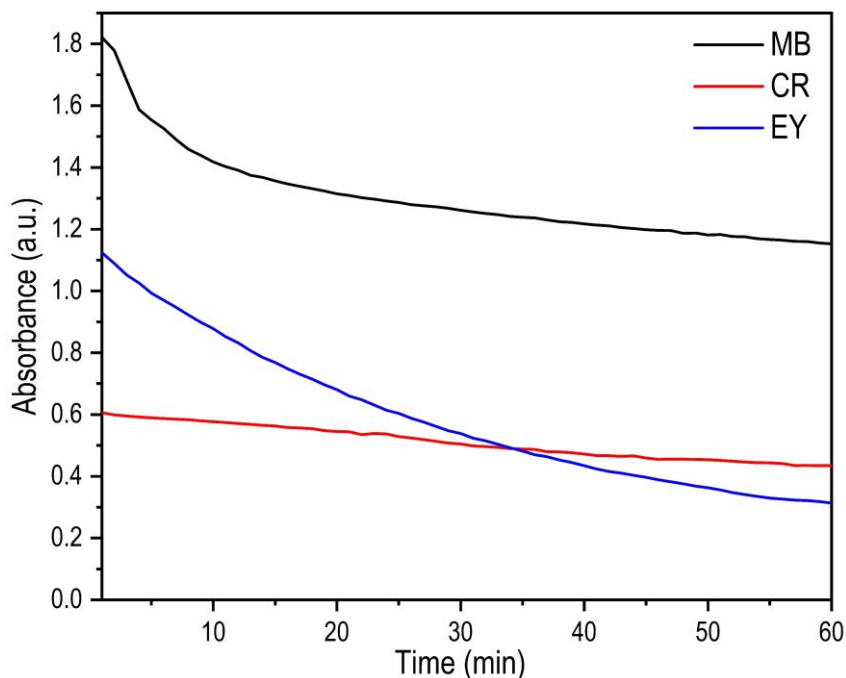


**Figure 70.** The degradation of organic dyes under UV-Vis light

#### 3.3.3.4 Production and characterization of RC films from extracted cellulose

Our method MDCell for fabricating regenerated cellulose films was not limited to commercial microcrystalline cellulose (section 3.3.3.2). This method can be applied to the extracted cellulose isolated from rice straw (or for recycling of used cellulose). Again, two types of RC films were synthesized (Figure 71). The film 1 consists of 10 wt.% extracted cellulose in TBPH 50 wt.% without DMSO, and film 2 consists of 10 wt.% extracted cellulose in TBPH 50 wt.% with DMSO (Ratio between DMSO and TBPH is 1:1). A typical process for preparing regenerated cellulose films was described in section 3.3.1.<sup>[70]</sup>

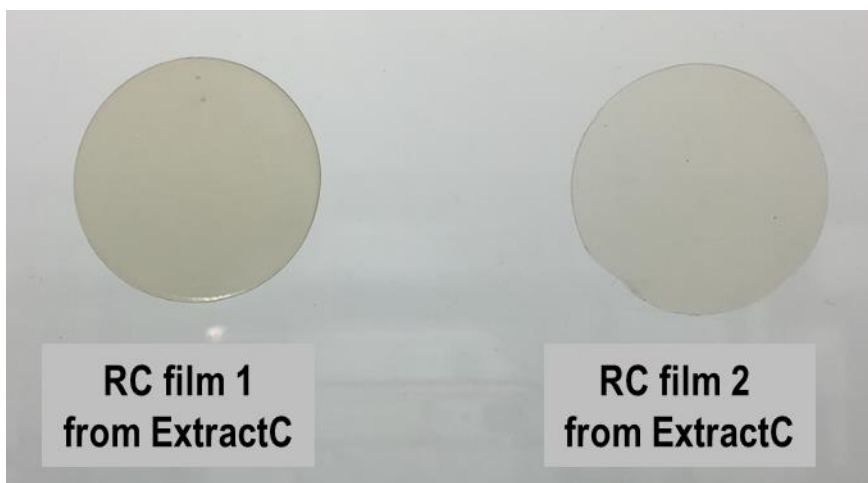


**Figure 71.** The regenerated cellulose films from extracted cellulose

The films have the smooth and homogenous surface suggesting that good regeneration of the extracted cellulose in the TBPH solvent through the hydrogen-bonding rearrangement to the cellulose macromolecules and fast penetration of the coagulant PC occurred. Noticeable, the films have pale yellow color (Figure 71).

With the results obtained in the previous section, the characterization of films was studied. There is no difference in chemical composition (by IR spectroscopy) and the crystallinity (by XRD) (Figure 72) between RC films from extracted cellulose and from the microcrystalline cellulose as mentioned before (paragraph 3.3.3.2.1).

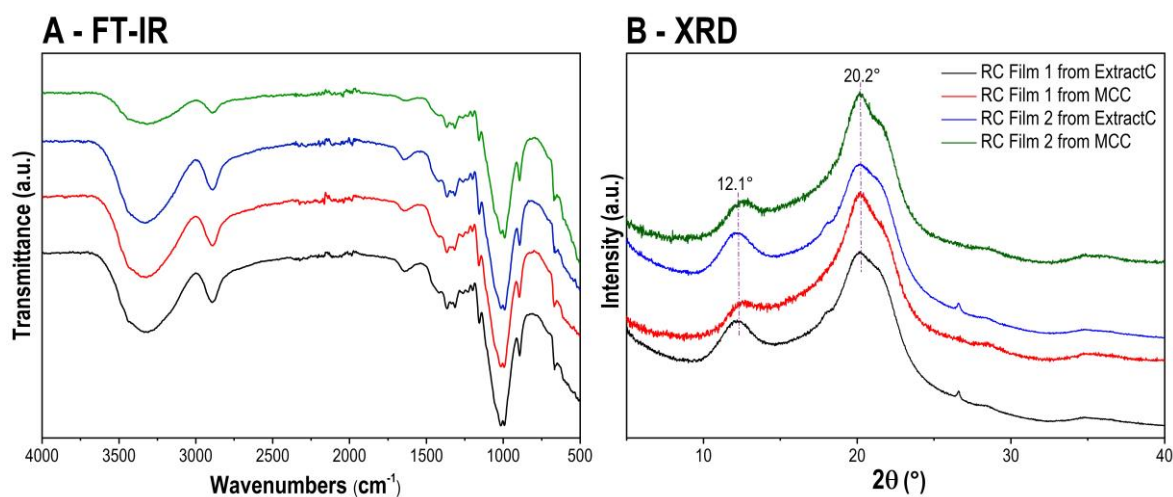


**Figure 72.** Characterization of the RC films from extracted cellulose and microcrystalline cellulose (A) FT-IR spectra, (B) XRD patterns

However, with SS-NMR (Figure 73), a small amount of lignin can be confirmed in the extracted cellulose responsible for the pale yellow color of the films.

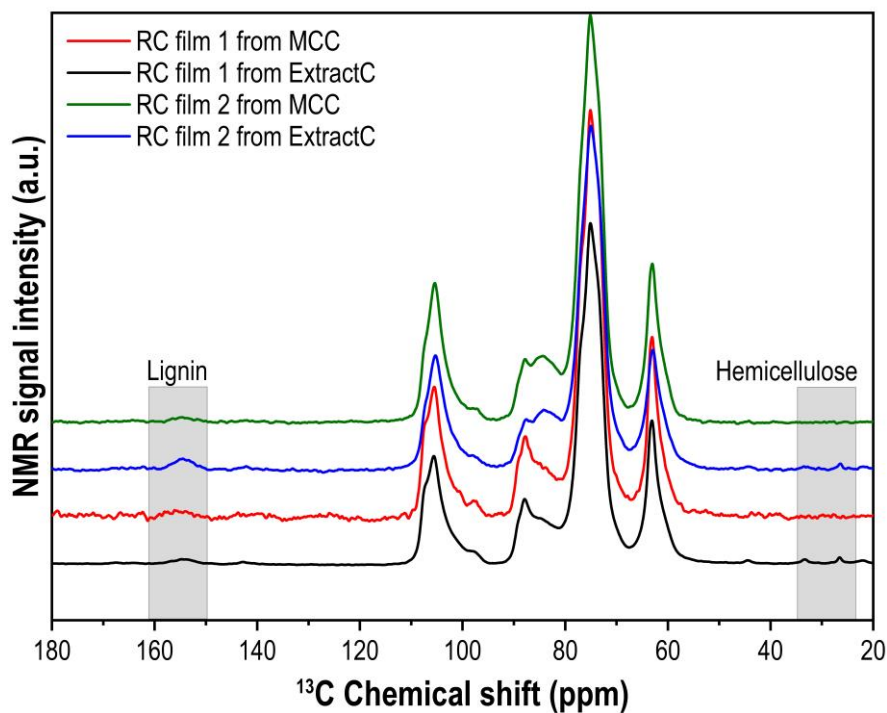


**Figure 73.** SS -<sup>13</sup>C NMR of the RC film from extracted cellulose and MCC

To eliminate this, the extracted cellulose was purified by dissolving the extracted cellulose again in TBPH 50 wt.% and precipitating it according to the diagram in Figure 74 .

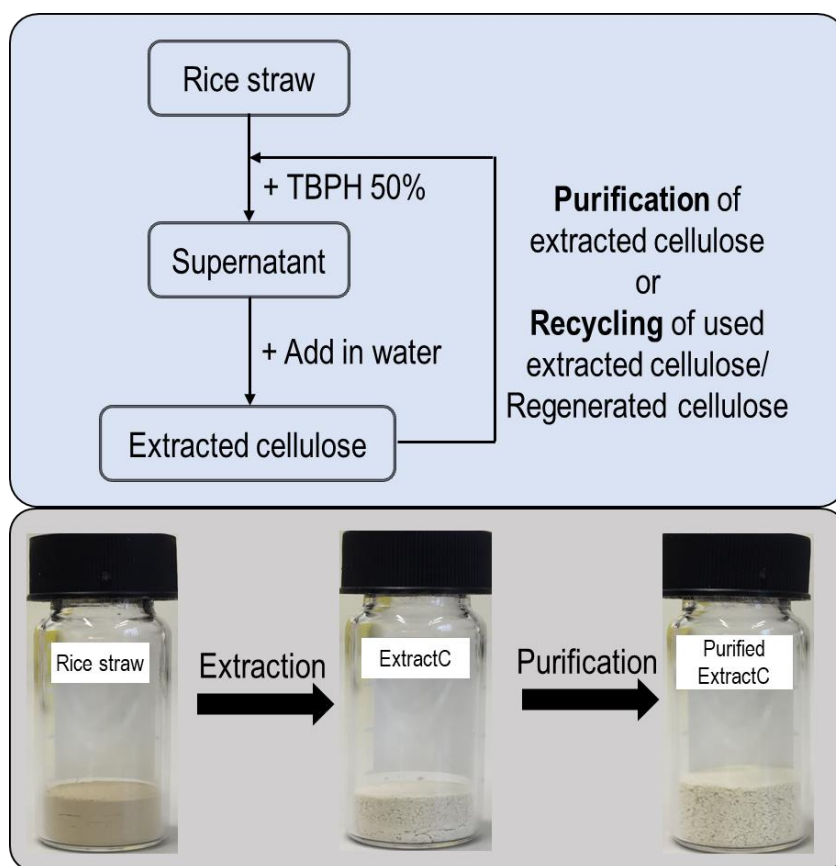


**Figure 74.** Purification of the extracted cellulose

However, the quality of the two extracted cellulose observed by SS-NMR was the same (Figure 75).

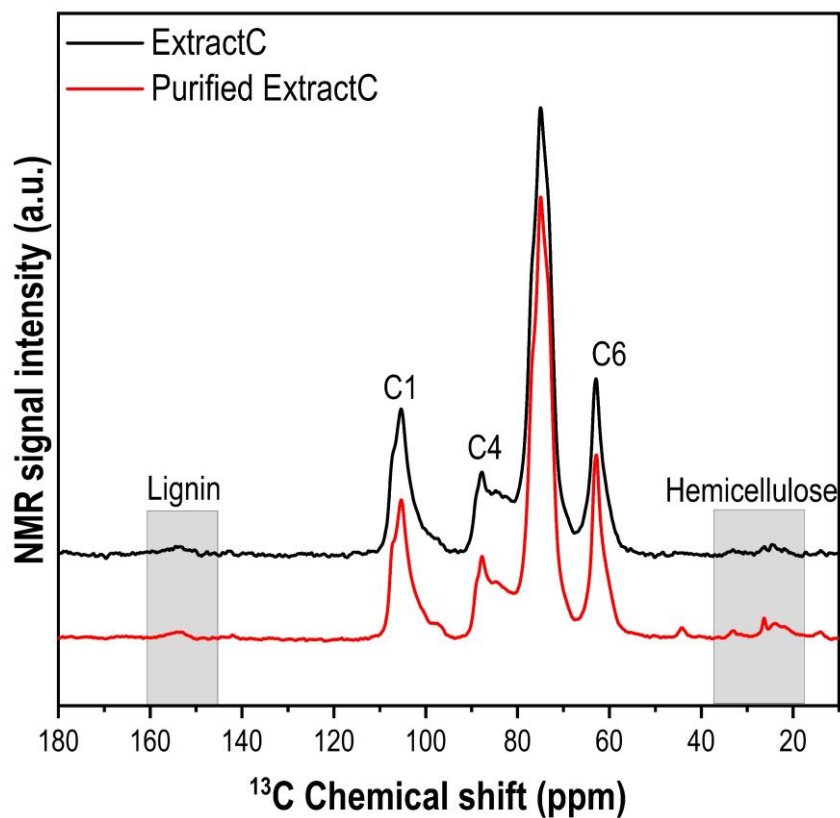


**Figure 75.** SS-<sup>13</sup>C NMR of extracted cellulose and purified extracted cellulose

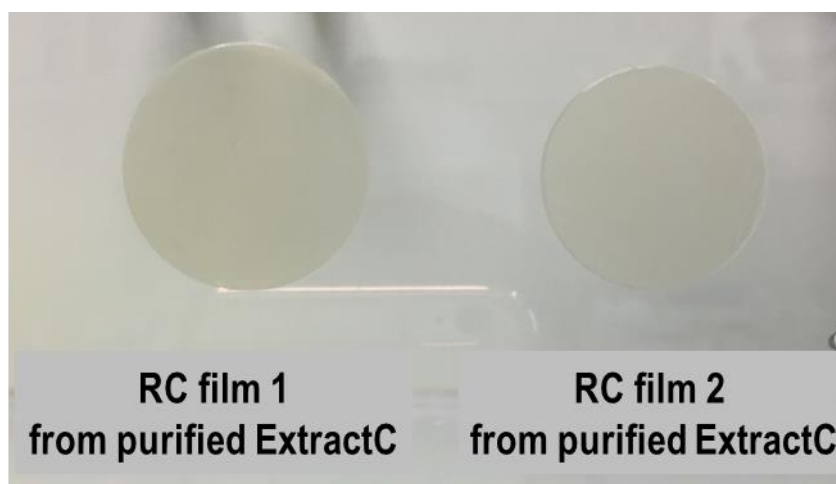


**Figure 76.** The RC films from purified extracted cellulose

There is not much difference between the RC films from extracted cellulose and purified extracted cellulose (Figure 77).

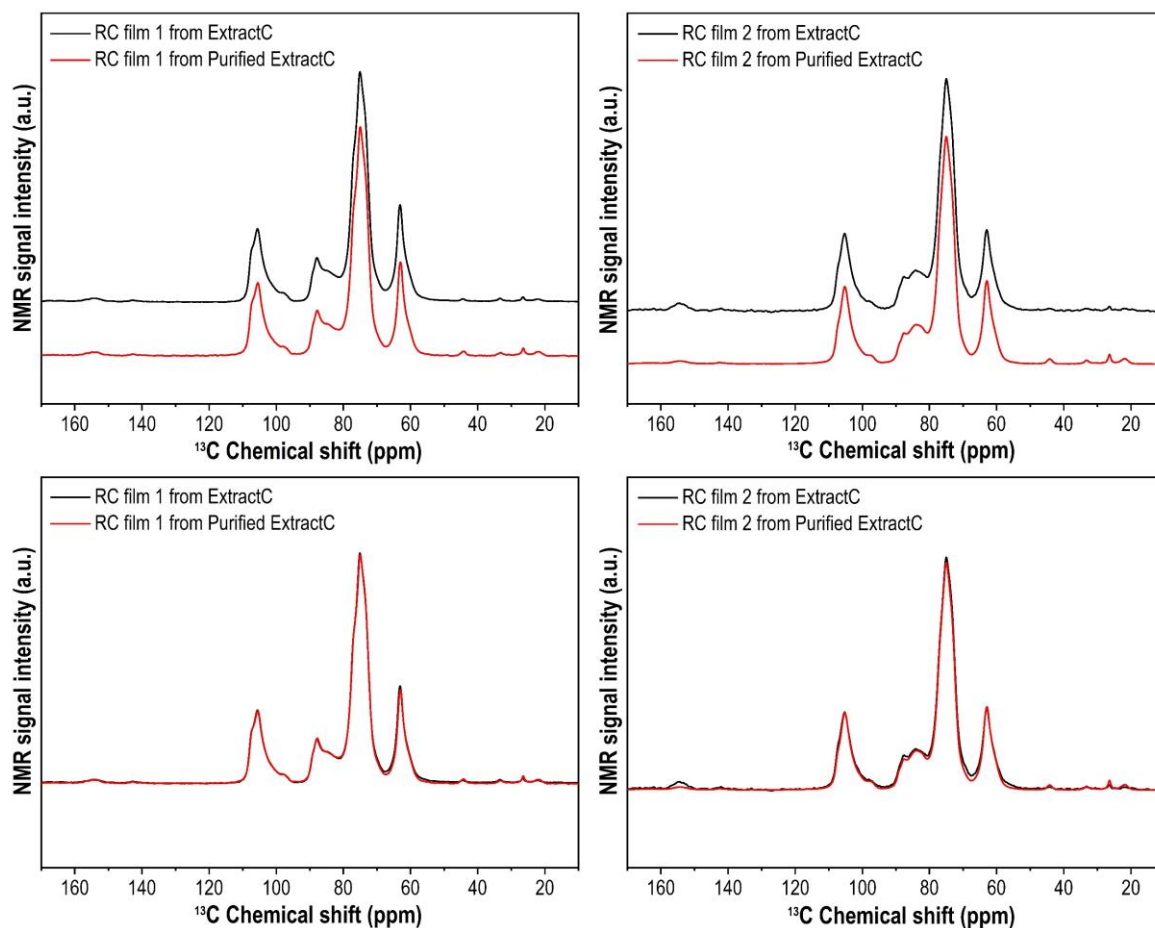


**Figure 77.** SS- $^{13}\text{C}$  NMR of RC films from extracted cellulose and purified extracted cellulose

RC film synthesized from extracted cellulose will be studied in more detail in terms of properties in the future. This film can be applied as a filter in wastewater treatment which is of great importance due to its biodegradability and environmental friendliness.

### 3.3.4 Recycling of TBPH and PC

The most important substance using in this research was TBPH. Due to the high cost of the phosphonium salt, recycling of phosphonium salt should be performed to make the process economical. In principle, TBPH can be recycled via ion exchange. The phosphonium salt is used in fractionation and recovered by anion metathesis as a carbonate salt. The carbonate salt is converted back to the hydroxide by means of ion exchange.<sup>[116]</sup> The full process cycle was reported by Kilpeläinen.<sup>[65]</sup>

The PC coagulation bath can be used many times before recycling, even impurities of water or TBPH do not result in the loss of the coagulation ability. The mixtures of PC, PG and  $[\text{TBP}]^+[\text{HCO}_3]^-$  could be separated via solvent extraction (Figure 78).

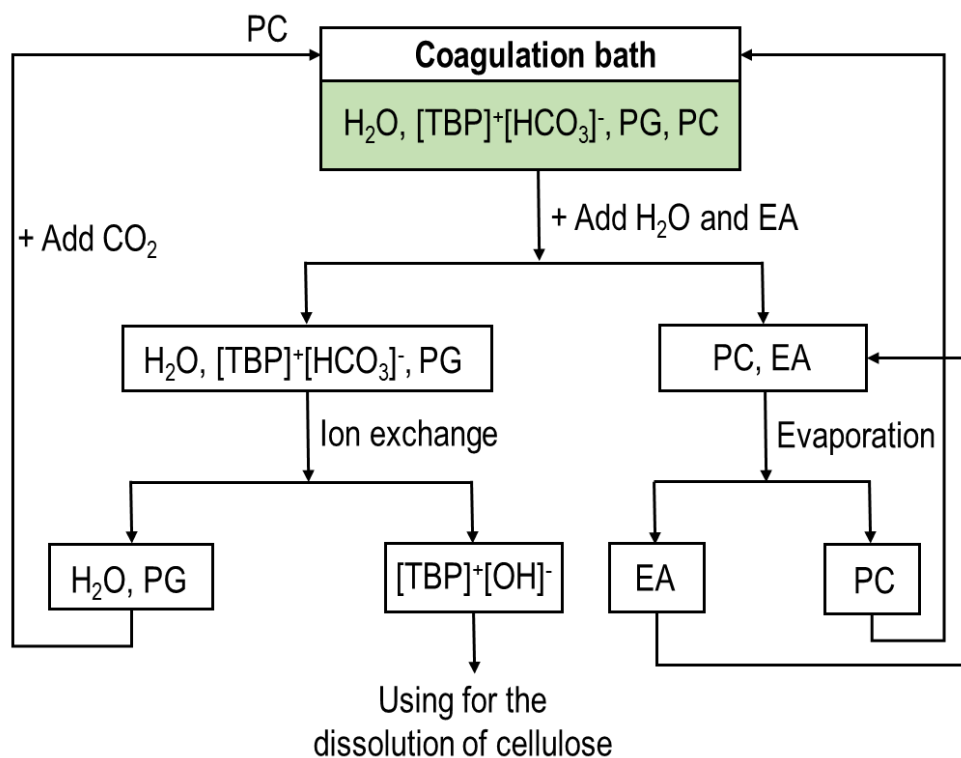


**Figure 78.** A proposed process scheme for solvent extraction to separate mixture of PC, PG and  $[TBP]^+[HCO_3]^-$

PC is a polar aprotic organic solvent while TBPH/ $H_2O$  is an electrolyte solution which is miscible in water. Adding a water insoluble solvent such as ethyl acetate (EA) resulted in the separation of mixture to two layers. The two layers were easily separated by using a separatory funnel. The top layer included PC and EA was separated by rotary evaporation due to the lower boiling point of EA. The bottom layer included  $H_2O$ ,  $[TBP]^+[HCO_3]^-$  and PG can be separated by ion exchange.  $[TBP]^+[HCO_3]^-$  will be converted to  $[TBP]^+[OH]^-$  in different process. PG can be converted back to PC by the reaction of PG and  $CO_2$ .<sup>[17]</sup> This PC will be used again in the coagulation bath. Due to time restrictions, a part of recycling process was done (recycling of PC). However, a complete process recycling and detailed experiments should definitely be investigated in future.

Recycling of the membrane can be done easily via another dissolution step in TBPH (Figure 74). These results indicate great potential of this new methodology for the sustainable preparation and recycling of the cellulose powders, films, and membranes for ultra- or microfiltration.



## 4. SUMMARY AND OUTLOOK

### 4.1 Summary

Within this PhD study, the research can be summarized as followed:

- TBPH is useful solvents for the dissolution of lignocellulosic materials (rice straw), in particular, cellulose. The combination of the TBPH with a polar aprotic molecular solvent (DMSO) is found to be necessary to accelerate the dissolution.
- The dissolution of commercial microcrystalline cellulose resulted in a strong increase of the viscosity. However, introduction of solvents such as dimethyl sulfoxide, acetonitrile, acetone, tetrahydrofuran reduced the viscosity without precipitation of cellulose which enables the further processability of these cellulose/TBPH solvent mixtures. Only the addition of ethanol and large concentrations of water forced the precipitation of cellulose.
- Cellulose was extracted from rice straw by simple two steps. Rice straw was dissolved in TBPH 50 wt.% followed by addition of an excess of water resulting in the selective precipitation of cellulose. Quantitative amounts of extracted cellulose with high quality and purity were obtained.
- Applying a new methodology (MDCell process), regenerated cellulose powder and films of high quality can be synthesized. This methodology is easy to handle, fast, without need for inert gas, feasible at room temperature, and environmentally friendly. The RC films are stable in water and can be stored for several months. This technique can be used as recycling process of used cellulose membrane as well.
- The full mechanism was evaluated and clarified by using NMR spectroscopy. Selective reaction of PC with  $[\text{OH}]^-$  occurs resulting in the formation of propylene glycol as well as hydrogen carbonate.
- The RC films have a high selectivity towards retention of positive charges due to a negatively charged surface. It is applied as an adsorbent for the separation of organic dyes.

## 4.2 Outlook

The films produced by the MDCell method have a good quality. They are very smooth, highly pure, and dense films. However, the mechanical durability based on the hydraulic pressure of the flow is maximum of 2.5 bar to pressure during filtration experiments. Therefore, the development of modified RC films to achieve better stability under wet and dry conditions is necessary. One of promising methods for this purpose is the incorporation of polymer into the regenerated cellulose films. Preliminary experiments showed that the RC films became completely stable through the incorporation of polypropylene carbonate. Interestingly, polypropylene carbonate dissolved in DMSO, and then this solution was mixed with cellulose solution, the coagulation occurs without using propylene carbonate. The mechanical properties (tensile strength, ultimate elongation...) should definitely be investigated in future to open a new perspective for the future applications of the regenerated cellulose films.

Another application and modification of MDCell methodology is cellulose-photocatalysts composite films. The films based on cellulose and photocatalysts can be produced and applied in advanced photocatalytic membrane reactor. The cellulose composite film with photocatalysts incorporated has a great opportunity for application in water treatment due to their sustainability, biodegradability and biocompatibility of the RC film and photostability, strong oxidation capacity of photocatalyst. This study is the subject of the Master work of Duong Thi Luong 2020 (Master student for 6 months exchange study under the framework of ROHAN - Rostock - Hanoi DAAD SDG Graduate School on "Catalysis as key towards sustainable resource management").

The MDCell process was modified by dispersing the nanoparticles photocatalyst inside the cellulose solution. Afterwards the film can be obtained via casting this solution followed by coagulation with PC (Figure 79). This enables an immobilization and "trapping" of the photocatalysts in the film.

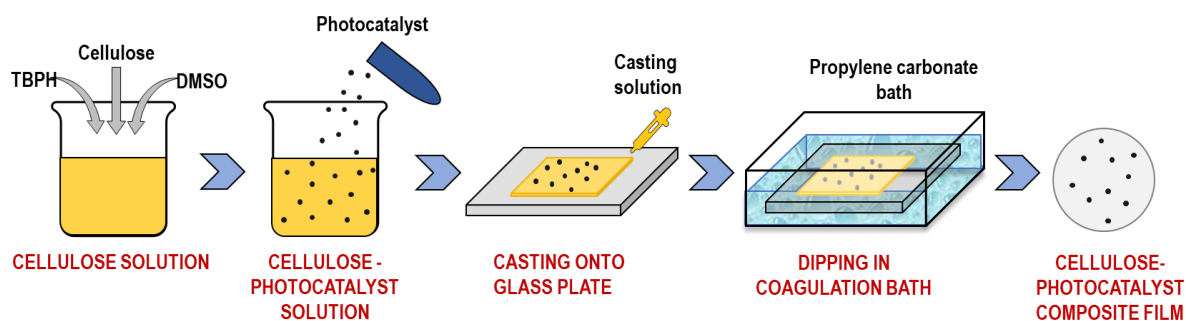


**Figure 79.** Synthesize cellulose-photocatalyst composite films

The immobilization of photocatalyst on the cellulose substrate aims to increase the separation ability of photocatalyst after degradation. Two different photocatalysts were applied including Au-TiO<sub>2</sub> as inorganic photocatalyst and Au-C<sub>3</sub>N<sub>4</sub> as organic photocatalyst (Figure 80). These photocatalysts were synthesized by deposition-precipitation method.<sup>[118]</sup>

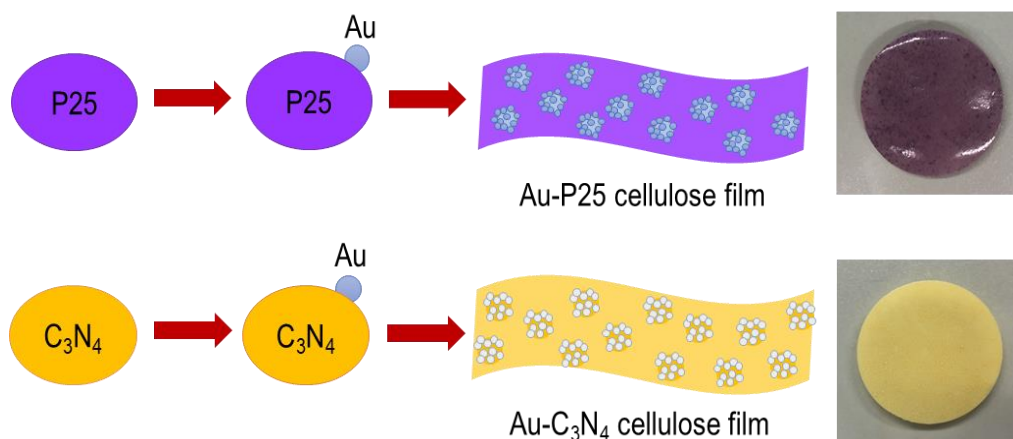


**Figure 80.** Cellulose-photocatalyst films

Another focus will be the prevention of the shrinking process during drying as well as the introduction of higher flexibility in order to enable the application as a transparent film.

Due to the high cost of the phosphonium salt, recycling of phosphonium salt and soluble biomass (lignin and hemicellulose) should be performed to make the process economical. Besides that, extracted cellulose from rice straw still contains a small amount of lignin. Extracted cellulose should be treated by addition method to achieve higher purity. This will be implemented in the future.

The application of the RC film as a membrane for filtration is also interesting. The RC films have a dense layer structure of microfibrils with a mesh of about 10-70 nm indicating the great potential of these films as membranes for ultra- or microfiltration in wastewater treatment.



## 5. MATERIALS AND METHODS

### 5.1 Materials

Tetrabutylphosphonium hydroxide (TBPH) containing 40 wt.% in water was purchased from Acros. Microcrystalline cellulose (MCC) with the size 20  $\mu\text{m}$ , xylan, lignin (alkali) used in this study were purchased from Sigma Aldrich. Rice straw was harvested from a local farm in Thai Binh province, Vietnam and was cut into small pieces of about 0.5 cm by a crusher. Propylene carbonate (PC, 99.7 % purity), vinyl ethylene carbonate (VEC, 99 % purity), ethylene carbonate (EC, 98 % purity) and butylene carbonate (BC, 98 % purity) were obtained from Sigma Aldrich. Polyethylene glycol (PEG) with molecular weight in the range as follows: PEG 950-1050, PEG 35000, PEO 200000, PEO 400000, PEO 1000000 were provided from Sigma Aldrich. Methylene blue (MB), Malachite green (MG), Cresol red (CR), Thymol blue (TB), Eosin Y disodium salt (EY) and Methylene orange (MO) were obtained from Sigma Aldrich. Acetone (Ace), acetonitrile (MeCN), dimethyl sulfoxide (DMSO), ethanol (EtOH), tetrahydrofuran (THF) were obtained from Sigma Aldrich. Ethyl acetate (EA) was purchased from Fisher Scientific.

### 5.2 Preparation methods

#### 5.2.1 Grinding rice straw to powder

Simple grinding process was carried out in the planetary ball mill Retsch PM 200, which can be done only by loading 1 gram dried rice straw 0.5 cm lengths with 15 balls into a rotated milling vial with speed 400 rpm in 180 minutes. The material of the ball and the vial is agate.



**Figure 81.** Grinding rice straw by the planetary ball mill with different time

#### 5.2.2 Cellulose isolation from rice straw

1 gram rice straw powder was mixed in 80 ml hot water at 60 °C for 2 hours to remove all the water-soluble extractable compounds. The insoluble residue was collected by centrifugation

(Eppendorf Centrifuge 5810R) at room temperature with speed 4000 rpm in 20 minutes, washed 3-4 times with distilled water, followed by drying at 60 °C overnight, and named as rice straw 1. After removing the water-soluble extractable compounds, rice straw 1 was dissolved in 10 ml TBPH 50 wt.% at room temperature for about 3 hours under stirring at 400 rpm to ensure all carbohydrates in rice straw soluble totally. The solution was separated by centrifugation (Hettich Mikro 22R) with high speed 14000 rpm in 1 hour. The pellet was washed 2-3 times with TBPH 50 wt.%. The resulting liquid after centrifugation has brown color is called supernatant. This supernatant was dropped into excess of distilled water resulting the precipitate of cellulose. The precipitated cellulose can be isolated by centrifugation (Eppendorf Centrifuge 5810R) at 4000 rpm in 30 minutes and washing with water (4 times with 50 ml water) followed by freeze drying for 1 day.

### 5.2.3 Dissolution of cellulose in TBPH 50 wt.%

TBPH 40 wt.% was condensed to higher concentration by using rotary evaporation at 60 mbar below 40 °C. The concentration of TBPH was confirmed by Karl Fischer Titration.

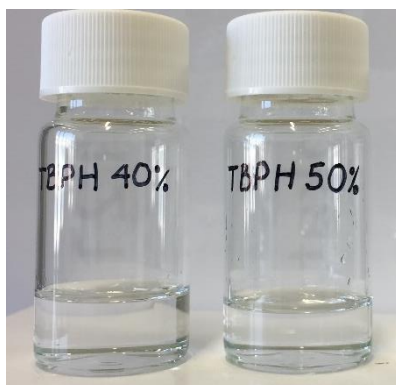


**Figure 82.** Tetrabutylphosphonium hydroxide 40 wt.% and 50 wt.%

20 wt.% cellulose (1.978 g) was dissolved in TBPH 50 wt.% (1 ml) under stirring at 300 rpm within 30 min at 23 °C.

### 5.2.4 The viscosity of cellulose solution

Viscosity is a material property which depends on different parameters such as mechanical stress and strain, time as well as temperature and other ambient conditions. The viscosity measurement was carried out on the Rheo Stress 1 Thermo Scientific Haake. It was fitted with cone-plate geometry 1° with a 35mm diameter cone. All measurements were performed at 25 °C with the shear rate was set from 1 to 100 (1/s). Using a rotational viscometer, the

viscosity was calculated from the measured torque and rotational speed as well as the dimensions of the measuring geometry. All tests were run using the Rheowin Job Manager software.



**Figure 83.** Viscosity equipment Rheo Stress 1 Thermo Scientific Haake

The dynamic viscosity  $\eta$  gives:

$$\eta = \frac{\tau}{\dot{\gamma}} \quad (2)$$

$\eta$  - viscosity (Pa s)

$\tau$  - shear stress (N/m<sup>2</sup>)

$\dot{\gamma}$  - shear rate (1/s)

The measured viscosity shows the results at three times shear rate of 6, 10, 50 (1/s).

After cellulose was completely dissolved in TBPH 50 wt.%, the additives were added at different molar ratio.

$$R = \frac{n_{\text{Additives}}}{n_{\text{TBPH}}} \quad (3)$$

R - Molar ratio

$n_{\text{Additives}}$  - Molar concentration of additives (mol)

$n_{\text{TBPH}}$  - Molar concentration of TBPH (mol)

### 5.2.5 Producing regenerated cellulose films from microcrystalline cellulose and extracted cellulose

A typical process to produce regenerated cellulose films involved dissolving 20 wt.% cellulose or 10 wt.% extracted cellulose in TBPH 50 wt.% at room temperature (23 °C) under stirring at 300 rpm for 30 minutes to ensure the complete solubility of cellulose/extracted cellulose. The cellulose solution was casted onto a glass plate to produce a cellulose casting layer of a defined thickness (e.g., 500 µm).<sup>[119]</sup> The casted liquid was quickly immersed into a PC bath for coagulation and then washed with deionized water. The way to dip the glass plate into the coagulation bath was described in section 3.3.3.2.

### 5.2.6 Water flux

The water flux is the flow rate through a membrane expressed in gallons of flow per square foot or membrane filter surface area per day. It was calculated by following equation:

$$WF = \frac{V}{S \cdot t} (\text{L m}^{-2} \text{h}^{-1}) \quad (4)$$

V - The volume of water goes through a membrane (L)

S - Surface area of the membrane (m<sup>2</sup>)

t - Time to take the volume of water (h)

The measurement was conducted under 23 °C. The RC films with the same diameter (d = 26 mm) were inserted in the filter. The feed flow rate was controlled by the pump at different rates such as 1 ml min<sup>-1</sup>; 1.5 ml min<sup>-1</sup>; 2 ml min<sup>-1</sup>; 2.5 ml min<sup>-1</sup>; 3 ml min<sup>-1</sup>; 3.5 ml min<sup>-1</sup>.

### 5.2.7 Determination of pore size distribution

A series of polyethylene glycol polymers were used as molecular probes (Table 7). For preparation of start solution 2000 ppm, 0.2 g of polyethylene glycol was taken in a 100 ml volumetric flask and diluted up to the mark by addition of deionized water. Using the home-made filtration (Figure 61), 5 ml of the filtrate were then collected with the feed flow rate of 1.5 ml min<sup>-1</sup>. The concentration was determined by automatic injecting samples into HPLC system using the apparatus shown in Figure 63. In this apparatus, a pump provided a flow rate (0.1 ml min<sup>-1</sup>) of distilled water with a 20 µl sample loop was used to load the PEG solution after going through RC films. The signal is detected by RI detector with retention time (10 min). For

each sample an average value of 4 injections was used to determine the average PEG concentration.

PEG retention was calculated by following equation:

$$\text{PEG retention} = \frac{C_o - C_s}{C_o} \times 100 (\%) \quad (5)$$

$C_o$  - The initial concentration (2000 ppm)

$C_s$  - The concentration of PEG solution after filtration (ppm)

### 5.2.8 Preparation of dyes solution

For preparation of dyes solution 10 ppm, 10 mg of organic dye was taken in a 1000 ml volumetric flask and diluted up to the mark by addition of deionized water.

### 5.2.9 Online UV-Vis measurement with continues flow

Online detection of the dyes was performed using homemade filter equipment connected to a micro-flow cell (Avantes). The solution is measured absorbance by the Spectrometers – Avantes under the UV-Vis light with this condition (Integration: 3.00, Time delay for each scan: 60 seconds).

First, the starting solution (concentration 10 ppm) is pumped through the system at a flow rate of 5 ml min<sup>-1</sup>. Note that, the RC film is not inserted. The absorbance of start solution is given by the blue line (in Figure 68). After that, the whole system is washed three times with ethanol to clean all contaminate and dried with compressed air. Then, the RC film is inserted in the dead-end filter. The flow rate of organic dye solution is adjusted to 1.5 ml min<sup>-1</sup> by the pumped. That means the permeate flow rate is 0.054 ml min<sup>-1</sup> for RC film 1 and 0.123 ml min<sup>-1</sup> for RC film 2. The absorbance of solution after going through the RC films is given by the red and black dots (in Figure 68).

### 5.2.10 Adsorption experiment

The adsorption capacity of MB, CR and EY on RC films carried out in the batch adsorption experiment by investigating the effect of experimental variable such as contact time and organic dye volume. The concentration of the starting solution is 10 ppm. The RC film 1 and 2 was added in 10 ml and 20 ml of organic dye solutions for 30 minutes and 60 minutes under stirring at 400 rpm. The amount of absorbance dose (one RC wet film) for RC film 1 and RC

film 2 is  $0.158 \pm 0.003$  g and  $0.136 \pm 0.006$  g, respectively. After the adsorption time, the absorbance of organic dye solutions was measured by UV-Vis spectrophotometer (Analytik Jena Specord 200).

The adsorption efficiency was calculated:

$$\text{Adsorption efficiency} = \frac{C_o - C_s}{C_o} \times 100 (\%) \quad (6)$$

$C_o$  - The initial concentration (10 ppm)

$C_s$  - The concentration of dye solution after adsorption time (ppm)

### 5.3 Characterization methods

#### *Fourier Transform Infrared Spectroscopy (FT-IR)*

Infrared spectra of samples were recorded with a Bruker FT-IR Alpha II spectrometer in ATR mode. The specimens were measured directly with a scan range from  $400 \text{ cm}^{-1}$  to  $4000 \text{ cm}^{-1}$ .

#### *Liquid State Nuclear Magnetic Resonance (NMR)*

The samples were measured without using deuterated solvents with a Bruker spectrometer AVANCE Neo 500 at 125.8 MHz (10000 accumulations, 2 s pulse delay, at  $25 \text{ }^\circ\text{C}$ ). The NMR spectra were calibrated to an internal standard/reference namely 1,4-Dioxane.

#### *Solid State Nuclear Magnetic Resonance*

Solid State NMR experiments were performed under magic angle spinning (MAS) using a Bruker AVANCE III HD spectrometer operating at 400.2 MHz proton frequency with a Bruker ASCEND DNP 9.4 T widebore (89 mm) magnet and a MASWVT400W1 BL4 X/Y/H triple channel probe operating in double-resonance mode. Samples were spun in 4 mm  $\text{ZrO}_2$  rotors (Bruker) at room temperature and 8 kHz MAS frequency. Radio frequency (rf) pulse powers were set to 83 kHz and 50 kHz for  $^1\text{H}$  and  $^{13}\text{C}$ , respectively.  $^1\text{H}$  power was matched to  $^{13}\text{C}$  during Hartmann-Hahn cross polarization (CP) with 1.5 ms contact time, SPINAL64 at 83 kHz was used for broadband decoupling of  $^1\text{H}$  during the detection windows of 20 ms with a recycle delay of 1 s. 3072 and 6144 scans were accumulated for dried film 1 and 2, respectively. 69632 and 147456 scans were accumulated for the wet film 1 and 2 samples, respectively. Spectra were processed in TopSpin 4.0.6 (Bruker) by exponential window multiplication (EM) with

50 Hz broadening parameter (LB) before Fourier transform and phase adjustment. The chemical shift was referenced to TMS (0 ppm) by using an external adamantane standard.

#### *Nuclear Magnetic Resonance under Dynamic Nuclear Polarization*

DNP NMR experiments were performed under MAS using a commercially available Bruker AVANCE II DNP spectrometer operating at 400.2 MHz proton frequency with a Bruker Ultrashield 9.4 T widebore (89 mm) magnet. 263.4 GHz microwaves were produced by a Bruker gyrotron with 60 mA beam current. Experiments were performed at 111 K with microwave irradiation and at 106 K without microwave irradiation; temperature was detected with a thermocouple inside the MAS stator. rf pulse powers were set to 100 kHz and 50 kHz for  $^1\text{H}$  and  $^{13}\text{C}$ , respectively.  $^1\text{H}$  power was matched to  $^{13}\text{C}$  during Hartmann-Hahn CP with 1.5 ms contact time, SPINAL64 at 100 kHz was used for broadband decoupling of  $^1\text{H}$  during the detection windows of 17 ms. MAS with a spinning frequency of 8 kHz was used. Polarization was allowed to build up for 3 s before each scan. Spectra were processed in TopSpin 4.0.6 (Bruker) by exponential window multiplication (EM) with 50 Hz broadening parameter (LB) before Fourier transform and phase adjustment. For the enhancement measurements, spectra with and without microwave irradiation were normalized to the equal number of scans (64 scans for spectra with and 768 (film 1) and 17408 (film 2) scans without microwave irradiation. The intensity ratio of the signal with and without microwave irradiation is then given as the enhancement factor  $\epsilon$ . The chemical shift was referenced to TMS (0 ppm) by using an external glycine standard.

#### *X-Ray Diffraction (XRD)*

XRD powder pattern were recorded on a Panalytical X'Pert diffractometer equipped with a Xcelerator detector using automatic divergence slits and Cu  $\text{K}\alpha_1/\alpha_2$  radiation (40 kV, 40 mA;  $\lambda = 0.15406$  nm, 0.154443 nm). Cu beta-radiation was excluded using a nickel filter foil. The measurements were performed in  $0.0167^\circ$  steps and 100 s of data collecting time per step. The samples were mounted on silicon zero background holders. The obtained intensities were converted from automatic to fixed divergence slits ( $0.25^\circ$ ) for further analysis. Peak positions and profile were fitted with Pseudo-Voigt function using the HighScore Plus software package (Panalytical). Phase identification was done by using the PDF-2 database of the International Center of Diffraction Data (ICDD).

### *Thermal Analysis (TGA)*

The thermogravimetric analysis (TGA) were carried out by using a Setram Labsys thermal analyzer. Amounts of about 5–15 mg of the carefully dried samples was sealed in aluminum crucibles and studied in the temperature range of 20 to 800 °C with heating rates of 10 °C min<sup>-1</sup> under inert atmosphere (50 ml min<sup>-1</sup> nitrogen).

### *Atomic Force Microscopy (AFM)*

AFM Topographies of dried cast and spin-coated samples have been obtained with a commercial device (Park Systems XE100) in dynamic mode using metal coated Si cantilevers (type ACTA, AppNano, Al-coating, 300 kHz and HA-HR, SpectrumInstruments, Au coating, 380 kHz). In order to avoid excessive sample contact, the device was operated in the so-called non-contact mode with small cantilever oscillation amplitudes of a few nm and moderate setpoint (~70 % of free amplitude) while the dither frequency was kept constant (amplitude modulation). Multiple sample locations were probed to ensure validity of obtained morphology.

Spin coating (spin coater SPIN150i, SPS-Europe) was used to obtain a very smooth homogenous film especially for AFM measurements. 200 µl of the cellulose solution without/with DMSO, resp., were dispensed on a glass cover slip that was rotating at 10000 rpm. After 5 min the rotation speed was decreased to 1000 rpm and PC was added for 1 min.

### *Scanning Electron Microscopy (SEM)*

Specimens were air-dried or freeze dried. For freeze drying specimens were rapidly frozen on a liquid nitrogen precooled polished copper block, immediately transferred to a liquid nitrogen precooled exsiccator and freeze dried under vacuum ( $5 \times 10^{-2}$  mbar) with subsequent warming to room temperature. Membrane fracturing was performed on rapidly frozen samples under liquid nitrogen with a pair of precooled forceps. Specimens were mounted on SEM stubs with adhesive carbon tape (Plano, Wetzlar, Germany) and coated with a carbon layer of approximately 15-20 nm (Leica SCD500, Leica Microsystems, Wetzlar Germany). Specimens were viewed in a field-emission SEM (Zeiss Merlin VP compact, Carl Zeiss Microscopy, Oberkochen, Germany) equipped with HE-SE and in-lens-Duo detectors. Images with a size of 1024x768 pixels were recorded at different steps of magnification. Measurements of distances were performed using the SmartSEM measurement tools (Carl Zeiss Microscopy).

### *Transmission electron microscopy (TEM)*

Specimens were cut off wet membranes with razor blades to a size of approx. 1x2 mm for subsequent processing for transmission electron microscopy (TEM). After fixation with an aqueous solution of 1 % osmium tetroxide for 1 hr and washes in distilled H<sub>2</sub>O, dehydration through an ascending acetone series to 100 % acetone was followed by infiltration with epoxy resin (Epon 812, Serva, Heidelberg, Germany) starting in a 1:1 mixture of acetone and resin o/n, followed by pure resin for 4 hrs. Specimens were transferred to rubber molds and the resin was allowed to cure at 60 °C for 2 days. The membranes were exposed from the resin blocks with a trimming tool (Leica EM Trim 2, Leica Microsystems, Wetzlar, Germany). Semithin sections (approx. 0.5 µm) and thin sections (approx. 50-70 nm) were cut on an ultramicrotome (Ultracut S, Reichert, Wien, Austria) with a diamond knife (Diatome, Biel, Switzerland). Semithin sections were stained with an aqueous solution of toluidine blue to visualize specimens for further trimming prior to thin sectioning and ultrastructural inspection. Thin sections were transferred to copper grids and were either examined directly without further contrasting agents or were alternatively contrasted with uranyl acetate and lead citrate. The sections were examined on a Zeiss EM902 electron microscope operated at 80 kV (Carl Zeiss, Oberkochen, Germany). Digital images were acquired with a side-mounted 1x2k FT-CCD Camera (Proscan, Scheuring, Germany) using iTEM camera control and imaging software (Olympus Soft Imaging Solutions, Münster, Germany).

### *Light Microscopy (LM)*

Semithin sections stained with toluidine blue were examined with a light microscope (Zeiss Axioskop 40, Carl Zeiss, Göttingen, Germany) and digital images were recorded with a camera (Zeiss AxioCam ERc5s) using acquisition software with integrated measurement tools (Zeiss ZEN blue edition).

### *Ultraviolet-visible spectra (UV-Vis)*

UV–Vis transmission spectra were recorded by a fiber system consisting of an AvaLight-DH-S-BAL Balanced Power Light Source and an AvaSpec-ULS2048 StarLine Versatile Fiber-optic Spectrometer (Avantes). Online detection of the dyes was performed using homemade filter equipment connected to a micro-flow cell (Avantes).

### *Zeta Potential*

Zeta potential measurements were performed on RC film 2 (2 × 1 cm) using the SurPASS system (Anton Paar, Ostfildern, Germany) to gain information on the surface charge. The measurements were performed in a 0.001 mol L<sup>-1</sup> KCl solution ranging from pH 5.0 to 9.0 with a gap height of 100 µm. The streaming current was determined depending on the pressure (max. 400 mbar). Finally, the zeta potential was calculated according to the method of Helmholtz-Smoluchowski.

## 6. REFERENCES

- [1] B. Bereiter, S. Eggleston, J. Schmitt, C. Nehrbass-Ahles, T. F. Stocker, H. Fischer, S. Kipfstuhl, J. Chappellaz, *Geophys. Res. Lett.* **2015**, *42*, 542-549.
- [2] P. Marion, B. Bernela, A. Piccirilli, B. Estrine, N. Patouillard, J. Guilbot, F. Jérôme, *Green Chem.* **2017**, *19*, 4973-4989.
- [3] a) P. T. Anastas, J. B. Zimmerman, *Green Chem.* **2019**, *21*, 6545-6566; b) H. C. Erythropel, J. B. Zimmerman, T. M. de Winter, L. Petitjean, F. Melnikov, C. H. Lam, A. W. Lounsbury, K. E. Mellor, N. Z. Janković, Q. Tu, L. N. Pincus, M. M. Falinski, W. Shi, P. Coish, D. L. Plata, P. T. Anastas, *Green Chem.* **2018**, *20*, 1929-1961.
- [4] H. E.-D. Saleh, M. Koller, in *Introductory Chapter: Principles of Green Chemistry*, Intech open, **2018**.
- [5] W. D. Jong, J. R. V. Ommen, in *Biomass as a Sustainable Energy Source for the Future*, John Wiley & Sons, Inc., Hoboken, New Jersey, United States of America, **2014**, pp. 36-68.
- [6] a) H. Zhu, L. Wei, C. P. N., Fang Zhiqiang, Zhu J. Y., Henriksson Gunnar, Himmel Michael E., Hu Liangbing, *Chem. Rev.* **2016**, *116*, 9305-9374; b) J. C. Courtenay, R. I. Sharma, J. L. Scott, *Molecules* **2018**, *23*, 654.
- [7] A. D. Ram B. Gupta, *Gasoline, Diesel, and Ethanol Biofuels from Grasses and Plants*, Cambridge University Press, **2010**.
- [8] V. B. Agbor, N. Cicek, R. Sparling, A. Berlin, D. B. Levin, *Biotechnol. Adv.* **2011**, *29*, 675-685.
- [9] D. Ussiri, R. Lal, *Biofuels* **2015**, *5*, 1-30.
- [10] Y. Sun, J. Cheng, *Bioresource Technol.* **2002**, *83*, 1-11.
- [11] L. Cadoche, G. D. López, *Biol. Waste* **1989**, *30*, 153-157.
- [12] T. Keskin, H. Nalakath Abubackar, K. Arslan, N. Azbar, in *Biohydrogen (Second Edition)* (Eds.: A. Pandey, S. V. Mohan, J.-S. Chang, P. C. Hallenbeck, C. Larroche), Elsevier, **2019**, pp. 321-346.
- [13] V. S. Chang, M. T. Holtzapple, *Appl. Biochem. Biotechnol.* **2000**, *84*, 5-37.
- [14] W. E. Karr, M. T. Holtzapple, *Biotechnol. Bioeng.* **1998**, *59*, 419-427.
- [15] S. J. B. Duff, W. D. Murray, *Bioresource Technol.* **1996**, *55*, 1-33.
- [16] T. H. Kim, J. S. Kim, C. Sunwoo, Y. Y. Lee, *Bioresource Technol.* **2003**, *90*, 39-47.
- [17] F. Teymouri, L. Laureano-Perez, H. Alizadeh, B. E. Dale, *Bioresource Technol.* **2005**, *96*, 2014-2018.
- [18] N. Jacquet, G. Maniet, C. Vanderghem, F. Delvigne, A. Richel, *Ind. Eng. Chem. Res.* **2015**, *54*, 150204081342000.
- [19] A. Hatakka, *FEMS Microbiol. Rev.* **1994**, *13*, 125-135.

- [20] U. S. D. o. A. (USDA), World Rice Production 2019/2020, **2020**.  
<https://apps.fas.usda.gov/psdonline/circulars/grain-rice.pdf>
- [21] a) N. M.D, *Sci. Develop.* **2012**; b) N. T. Q. N. Tran S.N, Nguyen H.C, Nguyen V.C.N, Le H.V and Ingvorsen K., *Can Tho University Science Journal* **2014**.
- [22] R. Gupta, *SANDEE Working Papers* **2012**, 66.
- [23] S. Z. M. Ngo T.T.T, Palis F.G, Wassman R., *Int. J. Environ. Rural Dev.* **2013**, 3.
- [24] N. Trach, *Livest. Res. Rural. Dev.* **1998**, 10, 80-94.
- [25] N. T. Nghi, R. R. Romasanta, N. Van Hieu, L. Q. Vinh, N. X. Du, N. V. C. Ngan, P. Chivenge, N. Van Hung, in *Sustainable Rice Straw Management* (Eds.: M. Gummert, N. V. Hung, P. Chivenge, B. Douthwaite), Springer International Publishing, Cham, **2020**, pp. 33-41.
- [26] N. Diep, K. Sakanishi, N. Nakagoshi, S. Fujimoto, T. Minowa, *Renew. Energy* **2015**, 74, 456-463.
- [27] K. H. Gardner, J. Blackwell, *Biopolymers* **1974**, 13, 1975-2001.
- [28] I. Spiridon, V. Popa, in *Hemicelluloses: Major Sources, Properties and Applications*, **2008**, pp. 289-304.
- [29] Y. Zeng, S. Zhao, S. Yang, S.-Y. Ding, *Curr. Opin. Biotech.* **2014**, 27, 38-45.
- [30] E. W. Qian, in *Research Approaches to Sustainable Biomass Systems* (Eds.: S. Tojo, T. Hirasawa), Academic Press, Boston, **2014**, pp. 181-204.
- [31] a) P. Lu, Y.-L. Hsieh, *Powder Technol.* **2012**, 225, 149-155; b) A. Abraham, A. K. Mathew, R. Sindhu, A. Pandey, P. Binod, *Bioresource Technol.* **2016**, 215, 29-36.
- [32] D. Klemm, H.-P. Schmauder, T. Heinze, *Cellulose*, Vol. 6, Wiley Online Library, **2005**.
- [33] R. H. Atalla, D. L. Vanderhart, *Science* **1984**, 223, 283.
- [34] P. K. Gupta, V. Uniyal, S. Naithani, *Carbohydr. Polym.* **2013**, 94, 843-849.
- [35] P. K. Chidambareswaran, S. Sreenivasan, N. B. Patil, H. T. Lokhande, *J. Appl. Polym. Sci.* **1982**, 27, 709-730.
- [36] S. Pérez, D. Samain, in *Advances in Carbohydrate Chemistry and Biochemistry*, Vol. 64 (Ed.: D. Horton), Academic Press, **2010**, pp. 25-116.
- [37] a) J. Credou, T. Berthelot, *J. Mater. Chem. B* **2014**, 2, 4767-4788; b) D. Klemm, B. Heublein, H.-P. Fink, A. Bohn, *Angew. Chem. Int. Ed.* **2005**, 44, 3358-3393.
- [38] M. Alger, *Polymer Science Dictionary*, Springer Netherlands, **1996**.
- [39] H. K. Benson, *Sci. Mon.* **1932**, 34, 454-457.
- [40] C. Woodings, in *Regenerated Cellulose Fibres* (Ed.: C. Woodings), Woodhead Publishing, **2001**, pp. 235-272.
- [41] H. C. Arca, L. I. Mosquera-Giraldo, V. Bi, D. Xu, L. S. Taylor, K. J. Edgar, *Biomacromolecules* **2018**, 19, 2351-2376.
- [42] C.-M. Lehr, *J. Control Release* **2000**, 65, 19-29.

- [43] C. F. Poole, *Thin Layer Chromatography in Chiral Separation and Analysis*, Vol. 98, American Chemical Society, **2007**.
- [44] T. Huber, J. Müssig, O. Curnow, S. Pang, S. Bickerton, M. Staiger, *J. Mater. Sci.* **2012**, 47.
- [45] T. Heinze, A. Koschella, *Polímeros* **2005**, 15, 84-90.
- [46] B. B. Y. Lau, E. T. Luis, M. M. Hossain, W. E. S. Hart, B. Cencia-Lay, J. J. Black, T. Q. To, L. Aldous, *Bioresource Technol.* **2015**, 197, 252-259.
- [47] M. Voges, M. Brück, H.-P. Fink, J. Gensrich, *Proceedings of the Akzo-Nobel Cellulosic Man-made Fibre Seminar*, Stenungsund, **2000**.
- [48] K. Kamide, K. Nishiyama, in *Regenerated Cellulose Fibres* (Ed.: C. Woodings), Woodhead Publishing, **2001**, pp. 88-155.
- [49] N. A. Hoenich, C. Woffindin, S. Stamp, S. J. Roberts, J. Turnbull, *Biomaterials* **1997**, 18, 1299-1303.
- [50] G. F. Davidson, *J. Text. I.* **1934**, 25, T174-T196.
- [51] a) C. Zhang, R. Liu, J. Xiang, H. Kang, Z. Liu, Y. Huang, *J. Phys. Chem. B* **2014**, 118, 9507-9514; b) A. Potthast, T. Rosenau, R. Buchner, T. Röder, G. Ebner, H. Bruglachner, H. Sixta, P. Kosma, *Cellulose* **2002**, 9, 41-53; c) A. M. Striegel, *Carbohydr. Polym.* **1997**, 34, 267-274.
- [52] a) T. Rosenau, A. Potthast, I. Adorjan, A. Hofinger, H. Sixta, H. Firgo, P. Kosma, *Cellulose* **2002**, 9, 283-291; b) T. Rosenau, A. Potthast, H. Sixta, P. Kosma, *Prog. Polym. Sci.* **2001**, 26, 1763-1837; c) K. E. Perepelkin, *Fibre Chem.* **2007**, 39, 163-172.
- [53] a) J. Zhang, J. Wu, J. Yu, X. Zhang, J. He, J. Zhang, *Mater. Chem. Front.* **2017**, 1, 1273-1290; b) M. Isik, H. Sardon, D. Mecerreyes, *Int. J. Mol. Sci.* **2014**, 15, 11922-11940; c) M. Gericke, P. Fardim, T. Heinze, *Molecules* **2012**, 17, 7458-7502.
- [54] A. Brandt, J. Gräsvik, J. P. Hallett, T. Welton, *Green Chem.* **2013**, 15, 550-583.
- [55] R. P. Swatloski, S. K. Spear, J. D. Holbrey, R. D. Rogers, *J. Am. Chem. Soc.* **2002**, 124, 4974-4975.
- [56] M. Kostag, K. Jedvert, C. Achtel, T. Heinze, O. A. El Seoud, *Molecules* **2018**, 23, 511.
- [57] M. Abe, K. Kuroda, H. Ohno, *ACS Sustain. Chem. Eng.* **2015**, 3, 1771-1776.
- [58] M. Abe, Y. Fukaya, H. Ohno, *ChemComm.* **2012**, 48, 1808-1810.
- [59] a) L. Lilienfeld, Vol. 1771462, U.S. Patent **1930**; b) L. Bock, *Ind. Eng. Chem.* **1937**, 29.
- [60] E. S. V. H. Krässig, *Chemie* **1954**, 14, 1-14.
- [61] A. A. Strepikheev, I. L. Knunyants, N. S. Nikolaeva, E. M. Mogilevsky, *Bull. Acad. Sci. USSR, Div. Chem. Sci.* **1957**, 6, 769-771.
- [62] T. Ema, T. Komiyama, S. Sunami, T. Sakai, *RSC Adv.* **2014**, 4, 2523-2525.
- [63] W. Wei, X. Wei, G. Gou, M. Jiang, X. Xu, Y. Wang, D. Hui, Z. Zhou, *RSC Adv.* **2015**, 5, 39080-39083.
- [64] M. Abe, T. Yamada, H. Ohno, *RSC Adv.* **2014**, 4, 17136-17140.

- [65] U. Hyväkkö, A. W. T. King, I. Kilpeläinen, *Bioresources* **2014**, 9, 13.
- [66] a) S. Khazalpour, M. Yarie, E. Kianpour, A. Amani, S. Asadabadi, J. Y. Seyf, M. Rezaeivala, S. Azizian, M. A. Zolfigol, *J. Iran. Chem. Soc.* **2020**; b) C. Maton, N. De Vos, C. V. Stevens, *Chem. Soc. Rev.* **2013**, 42, 5963-5977.
- [67] M. Sivapragasam, J. R. Jaganathan, J.-M. Levêque, M. Moniruzzaman, M. I. Abdul Mutalib, *J. Mol. Liq.* **2019**, 273, 107-115.
- [68] M. N. Nguyen, U. Kragl, D. Michalik, R. Ludwig, D. Hollmann, *ChemSusChem* **2019**, 12, 3458-3462.
- [69] B. Schöffner, F. Schöffner, S. P. Verevkin, A. Börner, *Chem. Rev.* **2010**, 110, 4554-4581.
- [70] N. N. Mai, D. Hollmann, U. Kragl, *Vol. DE 10 2020 103 195.5* (Ed.: U. o. Rostock), **2020**.
- [71] a) C. C. Piras, S. Fernández-Prieto, W. M. De Borggraeve, *Nanoscale Advances* **2019**, 1, 937-947; b) D. J. Schell, C. Harwood, *Appl. Biochem. Biotechnol.* **1994**, 45, 159-168.
- [72] H. Yamada, H. Miyafuji, H. Ohno, T. Yamada, *Bioresources* **2016**, 11, 839-849.
- [73] L. Ludueña, D. Fasce, V. A. Alvarez, P. M. Stefani, *Bioresources* **2011**, 6, 14.
- [74] T. M. Wood, in *Methods in Enzymology*, Vol. 160, Academic Press, **1988**, pp. 19-25.
- [75] G. Brunner, in *Supercritical Fluid Science and Technology*, Vol. 5 (Ed.: G. Brunner), Elsevier, **2014**, pp. 395-509.
- [76] a) W. Zhu, H. Theliander, *Bioresources* **2015**, 10, 19; b) M. A. Gilarranz, F. Rodriguez, M. Oliet, J. A. Revenga, *Sep. Sci. Technol.* **1998**, 33, 1359-1377.
- [77] a) K. M. Holtman, N. Chen, M. A. Chappell, J. F. Kadla, L. Xu, J. Mao, *J. Agric. Food Chem.* **2010**, 58, 9882-9892; b) Y. Lu, Y.-C. Lu, H.-Q. Hu, F.-J. Xie, X.-Y. Wei, X. Fan, *J. Spectrosc.* **2017**, 2017.
- [78] W. Cao, Z. Wang, Q. Zeng, C. Shen, *Appl. Surf. Sci.* **2016**, 389, 404-410.
- [79] a) H. Kono, T. Erata, M. Takai, *Macromolecules* **2003**, 36, 5131-5138; b) H. Yamamoto, F. Horii, *Macromolecules* **1993**, 26, 1313-1317; c) E. Rodriguez Alonso, C. Dupont, L. Heux, D. Da Silva Perez, J.-M. Commandré, C. Gourdon, *Energy* **2016**, 97, 381-390; d) S. Park, J. O. Baker, M. E. Himmel, P. A. Parilla, D. K. Johnson, *Biotechnol. Biofuels* **2010**, 3, 10-10.
- [80] a) E. Abraham, D. B. L. Pothan, S. Thomas, M. John, R. Anandjiwala, U. Cvelbar, *Carbohydr. Polym.* **2011**, 86, 1468-1475; b) S. Sen, J. D. Martin, D. S. Argyropoulos, *ACS Sustain. Chem. Eng.* **2013**, 1, 858-870.
- [81] X. Chen, J. Yu, Z. Zhang, C. Lu, *Carbohydr. Polym.* **2011**, 85, 245-250.
- [82] a) D. Watkins, M. Nuruddin, M. Hosur, A. Tcherbi-Narteh, S. Jeelani, *J. Mater. Res. Technol.* **2015**, 4, 26-32; b) F. Xu, J.-X. Sun, R. Sun, P. Fowler, M. S. Baird, *Ind. Crops Prod.* **2006**, 23, 180-193.
- [83] M. K. Mohamad Haafiz, S. J. Eichhorn, A. Hassan, M. Jawaid, *Carbohydr. Polym.* **2013**, 93, 628-634.

- [84] M. Ago, T. Endo, K. Okajima, *Polym. J.* **2007**, *39*, 435-441.
- [85] L. Segal, J. J. Creely, A. E. Martin, C. M. Conrad, *Text. Res. J.* **1959**, *29*, 786-794.
- [86] J. S. Moulthrop, R. P. Swatloski, G. Moyna, R. D. Rogers, *ChemComm.* **2005**, 1557-1559.
- [87] J.-M. Andanson, E. Bordes, J. Devémy, F. Leroux, A. A. H. Pádua, M. F. C. Gomes, *Green Chem.* **2014**, *16*, 2528-2538.
- [88] S. Shimamoto, H. Ohno, *Vol. US 9217043 B2*, Daicel Corporation, Japan, **2014**, p. 13pp.
- [89] a) J.-M. Andanson, E. Bordes, J. Devémy, F. Leroux, A. A. H. Pádua, M. F. C. Gomes, *Green Chem.* **2014**, *16*, 2528-2538; b) D. L. Minnick, R. A. Flores, M. R. DeStefano, A. M. Scurto, *J. Phys. Chem. B* **2016**, *120*, 7906-7919.
- [90] K. M. Gupta, Z. Hu, J. Jiang, *RSC Adv.* **2013**, *3*, 12794-12801.
- [91] a) H. Zhang, J. Wu, J. Zhang, J. He, *Macromolecules* **2005**, *38*, 8272-8277; b) L. K. J. Hauru, M. Hummel, A. W. T. King, I. Kilpeläinen, H. Sixta, *Biomacromolecules* **2012**, *13*, 2896-2905.
- [92] F. Elhia, T. Aidb, M. Koelc, *Mater. Sci.* **2016**, *65*, 255-266.
- [93] Z. Papanyan, C. Roth, K. Wittler, S. Reimann, R. Ludwig, *Chemphyschem* **2013**, *14*, 3667-3671.
- [94] D. Ozokwelu, S. Zhang, O. C. Okafor, W. Cheng, N. Litombe, in *Novel Catalytic and Separation Processes Based on Ionic Liquids* (Eds.: D. Ozokwelu, S. Zhang, O. C. Okafor, W. Cheng, N. Litombe), Elsevier, Amsterdam, **2017**, pp. 203-220.
- [95] a) Z.-D. Ding, Z. Chi, W.-X. Gu, S.-M. Gu, J.-H. Liu, H.-J. Wang, *Carbohydr. Polym.* **2012**, *89*, 7-16; b) Y. Yao, Y. Li, X. Liu, X. Zhang, J. Wang, X. Yao, S. Zhang, *Chin. J. Chem. Eng.* **2015**, *23*, 1894-1906.
- [96] J. Zhang, L. Xu, J. Yu, J. Wu, X. Zhang, J. He, J. Zhang, *Sci. China Chem.* **2016**, *59*, 1421-1429.
- [97] Z. Papanyan, C. Roth, D. Paschek, R. Ludwig, *ChemPhysChem* **2011**, *12*, 2400-2404.
- [98] Å. Östlund, D. Lundberg, L. Nordstierna, K. Holmberg, M. Nydén, *Biomacromolecules* **2009**, *10*, 2401-2407.
- [99] H. Ohno, K. Fujita, Y. Kohno, *Phys. Chem. Chem. Phys.* **2015**, *17*, 14454-14460.
- [100] J. Jacquemin, P. Husson, A. A. H. Padua, V. Majer, *Green Chem.* **2006**, *8*, 172-180.
- [101] L. Gentile, U. Olsson, *Cellulose* **2016**, *23*, 2753-2758.
- [102] B. Crawford, A. E. Ismail, *Polymers (Basel)* **2020**, *12*, 627.
- [103] C. Chiappe, D. Pieraccini, *J. Phys. Org. Chem.* **2005**, *18*, 275-297.
- [104] S. Liu, J. Zeng, D. Tao, L. Zhang, *Cellulose* **2010**, *17*, 1159-1169.
- [105] A. Idström, L. Gentile, M. Gubitosi, C. Olsson, B. Stenqvist, M. Lund, K.-E. Bergquist, U. Olsson, T. Köhnke, E. Bialik, *Cellulose* **2017**, *24*, 3645-3657.

- [106] M. A. Rasool, P. P. Pescarmona, I. F. J. Vankelecom, *ACS Sustain. Chem. Eng.* **2019**, *7*, 13774-13785.
- [107] X. Zhang, M. Chen, C. Liu, A. Zhang, R. Sun, *Molecules* **2015**, *20*, 6033-6047.
- [108] P. K. Chatterjee, C. M. Conrad, *J. Polym. Sci.* **1968**, *6*, 3217-3233.
- [109] a) A. Idström, S. Schantz, J. Sundberg, B. F. Chmelka, P. Gatenholm, L. Nordstierna, *Carbohydr. Polym.* **2016**, *151*, 480-487; b) G. Zuckerstätter, N. Terinte, H. Sixta, K. C. Schuster, *Carbohydr. Polym.* **2013**, *93*, 122-128.
- [110] G. Cox, B. Juniper, *J. Microsc.* **1973**, *97*, 343-355.
- [111] C. Yin, S. Wang, Y. Zhang, Z. Chen, Z. Lin, P. Fu, L. Yao, *Environ. Sci.-Wat. Res.* **2017**, *3*, 1037-1041.
- [112] J. K. Lin, M. R. Ladisch, J. A. Patterson, C. H. Noller, *Biotechnol. Bioeng.* **1987**, *29*, 976-981.
- [113] S. Singh, K. C. Khulbe, T. Matsuura, P. Ramamurthy, *J. Membr. Sci.* **1998**, *142*, 111-127.
- [114] A. Hedlund, T. Köhnke, J. Hagman, U. Olsson, H. Theliander, *Cellulose* **2019**, *26*, 1545-1563.
- [115] J. d. S. Macedo, N. B. da Costa Júnior, L. E. Almeida, E. F. d. S. Vieira, A. R. Cestari, I. d. F. Gimenez, N. L. Villarreal Carreño, L. S. Barreto, *J. Colloid Interface Sci.* **2006**, *298*, 515-522.
- [116] Masayuki Umeno, Satoshi Takita, *Vol. 4,761,493* (Ed.: U. S. Patent), Japan, **1987**.
- [117] X. Zhao, N. Sun, S. Wang, F. Li, Y. Wang, *Ind. Eng. Chem. Res.* **2008**, *47*, 1365-1369.
- [118] J. B. Priebe, J. Radnik, A. J. J. Lennox, M.-M. Pohl, M. Karnahl, D. Hollmann, K. Grabow, U. Bentrup, H. Junge, M. Beller, A. Brückner, *ACS Catal.* **2015**, *5*, 2137-2148.
- [119] S. Liu, J. Zeng, D. Tao, L. Zhang, *Cellulose* **2010**, *17*, 1159-1169.

## 7. APPENDIX

### List of Publications, Posters and Presentations

#### 1. Publications

- 1) **Mai N. Nguyen**, Udo Kragl, Dirk Michalik, Ralf Ludwig, Dirk Hollmann. The Effect of Additives on the Viscosity and Dissolution of Cellulose in Tetrabutylphosphonium Hydroxide. *ChemSusChem* **12**, 3458-3462 (2019).
- 2) **Mai N. Nguyen**, Udo Kragl, Ingo Barke, Regina Lange, Henrik Lund, Marcus Frank, Armin Springer, Victoria Aladin, Björn Corzilius, Dirk Hollmann. Coagulation using organic carbonates opens up a sustainable route towards regenerated cellulose films. *Communications Chemistry* **3**, 116 (2020).
- 3) **Mai N. Nguyen**, Udo Kragl, Victoria Aladin, Dirk Hollmann. Isolation and characterization of cellulose from rice straw to produce regenerated cellulose films. *Cellulose* (to be submitted).
- 4) Luong T. Duong, **Mai N. Nguyen**, Duong T. T Nguyen, Amitava Acharjya, Arne Thomas, Dirk Hollmann. New Preparation Methodology of Cellulose - Photocatalyst Composites for Photocatalytic Membrane Reactors. *Catalyst* (to be submitted).

#### 2. Patents

- 1) Nguyen. N. Mai, Dirk Hollmann, Udo Kragl. Herstellen von regenerierten Polysacchariden. *U. o. Rostock* DE 10 2020 103 195.5, (2020), 07.02.2020.

#### 3. Posters

- 1) "Recovery of carbohydrates from crop residues with ionic liquids" in the *Workshop of Department Life, Light and Material, Faculty for Interdisciplinary Research*, June 2018. Rostock, Germany.
- 2) "Recovery of cellulose from rice straw with an electrolyte solution and its application" in the *Rohan evaluation*, January 2019. Rostock, Germany.
- 3) "Recovery of cellulose from rice straw with an electrolyte solution and its application" in the *JCF Poster party*, June 2019. Rostock, Germany.

#### 4. Presentations

- 1) Oral presentation with title: "Study on the Dissolution of Cellulose in Tetrabutylphosphonium Hydroxide - Influence of Additives on the Viscosity". *4<sup>th</sup> Green & Sustainable Chemistry Conference*. Dresden, Germany. 05.05 - 08.05.2019.
- 2) Oral presentation with title: "The Effect of Additives on the Viscosity and Dissolution of Cellulose in Tetrabutylphosphonium Hydroxide". *3<sup>rd</sup> RoHan DAAD SDG Summer school 2019*. Hanoi, Vietnam. 09.09 - 22.09.2019.



# CURRICULUM VITAE



Full name: **NGUYEN-NGOC MAI**

Date of birth: 23.11.1985

Place of birth: Hanoi, Vietnam

Gender: Female

Marital status: Married

Phone number: +49-(0)381-498-8992

Email: [nnmai.edu@gmail.com](mailto:nnmai.edu@gmail.com);

Address: Room 247, Department Life, Light & Matter

Faculty for Interdisciplinary Research, University of Rostock

Albert-Einstein-Straße 25, 18059 Rostock, Germany

Website: <https://www.kragl.chemie.uni-rostock.de/team/>

## EDUCATION

---

- **2018 – Now:** PhD student of Chemistry, University of Rostock, Rostock, Germany
- **2009 – 2011:** Master's degree of Chemical Engineering, Hanoi University of Science and Technology (HUST), Hanoi, Vietnam  
*Grade: Excellent; GPA: 3.81 on a 4.0 scale*
- **2004 - 2009:** Bachelor's degree of Chemical Process Equipment, Hanoi University of Science and Technology (HUST), Hanoi, Vietnam  
*Grade: Good; GPA: 7.87 on a 10.0 scale; Order: 1/18*
- **2000 – 2003:** High school diploma, Viet Duc high school, Hanoi, Vietnam

## PROFESSIONAL EXPERIENCE

---

- **2018 – Now:** PhD student in the field "Green chemistry"
- **2009 – 2017:** Lecturer at the School of Chemical Engineering, Hanoi University of Science and Technology, Vietnam
- **2004 – 2009:**  
2008: Technical internship in Lam Thao Fertilizers and Chemical Company  
2007: Technical internship in Ha Bac nitrogen Fertilizers and Chemical Company  
2006: Technical internship in Hanoi Liquor Company

## AWARDS, FELLOWSHIPS AND GRANTS

---

- **10.2017:** Rohan scholarship for 3 years PhD from 01/2018 to 12/2020 in Rostock, Germany
- **02.2009:** Yamaha Scholarship for the best student in Hanoi University of Science and Technology
- **09.2008:** Schlumberger scholarship for Female in Oil and Gas industry
- **08.2008:** Scholarships of HUST for the best student in Chemical Engineering
- **06.2008:** The English training programme at Language Link sponsored by Petronas
- **08.2007:** Scholarships of HUST for the best student in Chemical Engineering
- **08.2006:** Scholarships of HUST for the best student in Chemical Engineering
- **08.2005:** Scholarships of HUST for the best student in Chemical Engineering

## SCIENTIFIC PUBLICATIONS, PATENTS AND RESEARCH PROJECTS

---

- **Mai N. Nguyen**, Udo Kragl, Ingo Barke, Regina Lange, Henrik Lund, Marcus Frank, Armin Springer, Victoria Aladin, Björn Corzilius, Dirk Hollmann. Coagulation using organic carbonates opens up a sustainable route towards regenerated cellulose films. *Communications Chemistry* **3**, 116 (2020).
- **Nguyen. N. Mai**, Dirk Hollmann, Udo Kragl. Herstellen von regenerierten Polysacchariden. *U. o. Rostock* DE 10 2020 103 195.5, (2020), 07.02.2020.
- **M. N. Nguyen**, U. Kragl, D. Michalik, R. Ludwig, D. Hollmann, The Effect of Additives on the Viscosity and Dissolution of Cellulose in Tetrabutylphosphonium Hydroxide. *ChemSusChem* **12**, 3458-3462 (2019).
- **Nguyen Ngoc Mai**, Vu Dinh Tien, Investigation and simulation of Glucose-Fructose separation process using preparative chromatography. *Journal of science and technology* **82**, 6-10 (2011).
- Nguyen Dang Binh Thanh, Nguyen Trung Dung, Ta Hong Duc, **Nguyen Ngoc Mai**, Kinetics and modeling of oil extraction from Vietnam lemongrass by steam distillation. *Journal of science and technology* **47** (2017).
- **Nguyen Ngoc Mai**, Study on kinetics of anthracite coal gasification by steam – Project T2012 – 60, 2012.
- **Nguyen Ngoc Mai**, Investigation and simulation of Glucose and Fructose separation process using preparative chromatography – Project T2010 – 26, 2010.